Technical University of Denmark

DTU

Micromechanical resonators as a tool for polymer characterization

Bose-Goswami, Sanjukta; Almdal, Kristoffer; Boisen, Anja; Keller, Stephan Sylvest

Publication date:
2014

Document Version
Publisher's PDF, also known as Version of record

Link back to DTU Orbit

Citation (APA):
Bose, S., Almdal, K., Boisen, A., & Keller, S. S. (2014). Micromechanical resonators as a tool for polymer characterization. DTU Nanotech.

DTU Library
Technical Information Center of Denmark

Micromechanical resonators as a tool for polymer characterization

Sanjukta Bose
PhD Thesis September 2014

DTU Nanotech
Department of Micro- and Nanotechnology

Micromechanical resonators as a tool for polymer characterization

Sanjukta Bose

Ph.D. Thesis

September 2014

Preface

This Ph.D. thesis was written as a partial fulfillment of the requirements for obtaining the Ph.D. degree at the Technical University of Denmark (DTU). The Ph.D. project was carried out at the Department of Micro- and Nanotechnology (DTU Nanotech) during the period from the 1st of September 2011 to the 31th of August 2014. This Ph.D. project is part of NAMEC, a VKR Center of Excellence which has been financed by the Villum Kann Rasmussen foundation. This Ph.D. project was supervised by:

Main supervisor: **Professor Kristoffer Almdal**

Co-supervisor: **Professor Anja Boisen**

Co-supervisor**: Senior Researcher Stephan Sylvest Keller**

I would like to express my sincere gratitude to all my supervisors; their guidance was invaluable for completing this thesis. I have always returned from our supervisor meetings highly motivated and encouraged after the inspiring discussions!

I would like to thank Kristoffer Almdal for believing in me and giving me an opportunity to work here. You have been a great supervisor supporting me in every possible way and constantly backing my ideas. I am grateful to Anja Boisen for her constant encouragement. Thanks for providing all the positive energy and a simulating work environment. I would like to give special thanks to Stephan Sylvest Keller for his immense help, patience and endless motivations. A 2 minutes visit to your office most of the time has easily extended to 20 minutes on fruitful discussions!

I am indebted to Assistant Professor Silvan Schmid for his valuable ideas and help for the string experiments. Thanks to Tom Larsen for his assistance and helpful discussions with the string experiments. I would like to thank Tommy Sonne Alstrøm for his invaluable help in all the statistical analysis. Thanks to Professor Peter Sommer-Larsen for let me conduct the dielectric analysis in his laboratory. I would like to thank Filippo Bosco for his help with the DVD experiments.

Thanks to Katharina Nilson, Tage A. Larsen, Søren M. B. Petersen, Majken Becker and Jens Hemmingsen from DTU Danchip for their ready help whenever needed.

I am indebted to all the past and present members of Amphiphilic Polymers in Biological Sensing group and Nanoprobes group for a lot of assistance and helpful discussions in our group meetings. It was a real pleasure working with you all. Thanks to all the members of the NAMEC project for providing new ideas and excellent feedback during our meetings.

In particular I would like to thank Rikke Kragh Lauridsen for her caring attitude and helping me in my initial days in Denmark, Ritika Singh Petersen for being a lovely friend and keeping my Hindi alive, Shoko Yamada and Xueling Quan for being great companions. Special thanks goes to my office mates Paolo Marizza and Alberto Cagliani for their helpful discussions about the project and all the good times we spent over discussing Indian and Italian food, culture, language, politics and travel destinations! Thanks to Letizia Amato for being a caring friend and for those lovely cappuccinos and cakes from "Café Leti". I am thankful to Olga Mednova, Simon Levinsen and Saif Ullah for their assistance whenever needed.

Outside DTU, I would like to thank all my friends of BID specially Saswati Chakladar and Krishnendu Mukherjee for providing all the support and the feeling of home away home. Very special thanks goes to Susanta Mitra for showing me the path to Denmark and all the motivating emails to stay focused in work all through these years.

Finally I would like to thank my family, my parents Buddhadev Bose and Kalpana Bose and my parents in-law Gautam Goswami and Bharati Goswami for their endless support, unconditional love and constant encouragement. A very special thanks goes to my husband Kaustav Goswami for being with me for the past 10 years in all the joys and woes that life has offered. Thank you!

Sanjukta Bose

September 5, 2014

DTU Nanotech

Technical University of Denmark

v

Abstract

The aim of this Ph.D. project was the evaluation of micromechanical resonators like cantilevers and strings as analytical tools for characterization of polymers.

Spray coating was used as the technique to coat one side of the micromechanical resonators with polymer. Process optimization of different spray coating parameters was carried out with two polymer-solvent systems to obtain homogeneous films with uniform thickness and low roughness. Full factorial experimental design was employed to identify the most important parameter among the crucial parameters of spray coating such as nozzle-substrate distance, the temperature of the substrate and the speed of the spraying nozzle.

Micromechanical string resonators were successfully developed as an analytical tool for sensitive and fast thermal characterization of polymers with only a few nanograms of sample. Both the glass transition (T_g) and sub-T_g transition of different polymers were detected and confirmed by conventional thermal polymer characterization techniques. An analytical model was derived to validate the resonance frequency response of the polymer coated microstrings during heating cycles. The resonance frequency change provided the quasi-static T_g of polymers while the quality factor change provided the frequency dependent shift of T_g to higher temperature.

Microcantilevers were successfully employed as a platform for fast estimation of polymer degradation rate with minute amount of sample compared to conventional techniques. A detailed investigation of enzymatic degradation of poly (D, L-lactide) was done in buffered proteinase K solution. The influence of concentration of the enzyme solution, pre-hydration in buffer, surface morphology and adsorption time of enzymes on the rate of degradation was studied. The bulk degradation rate estimated from the experimental results and model simulation of multilayered cantilever structures matched well with values reported in literature.

The basic understanding of the spray coating process and the newly developed approaches of microstrings and microcantilevers as analytical tools show promising potential for investigation of different polymers and pharmaceutical systems.

Danske Resumé

Formålet med dette phd-projekt er at evaluere mikromekaniske resonatorer - bjælker og strenge – som analytiske værktøjer til karakterisering af polymerer.

Sprøjtebelægning (spray coating) blev anvendt til at deponere polymer på den ene side af de mikromekaniske resonatorer. For at opnå en homogen film, med ensartet tykkelse og lav ruhed, blev der udført procesoptimeringer af forskellige sprøjtebelægnings parametre, med to forskellige polymer/opløsningsmiddel systemer. Blandt de vigtigste parametre for sprøjtebelægning, så som dyse-substrat afstand, substrat temperatur og sprøjtedysehastighed, blev den mest betydende parameter identificeret ved hjælp af en total faktoranalyse af det eksperimentelle design.

De mikromekaniske streng resonatorer er med stor succes blevet udviklet til et følsomt analytisk redskab til hurtig termisk karakterisering af nanogram-prøver af polymer. Både den formelle glasovergangstemperatur (T_g), samt den underliggende T_g overgang, blev påvist i forskellige polymerer og bekræftet ved konventionelle teknikker til termisk karakterisering af polymerer. En analytisk model blev udledt til at validere ændringer i resonansfrekvensen af de polymerbelagte mikrostrenge under opvarmningscykler. Ændringen i resonansfrekvensen giver en kvasi-statisk T_g bestemmelse for polymerer mens ændringer i kvalitetsfaktoren (Q faktorer) giver det frekvensafhængige skift af T_g til højere temperatur.

Ydermere er det lykkedes at bruge mikrobjælker som en platform til hurtig estimering af nedbrydningshastigheder i polymerer, og med anvendelse af minimal prøvemængde sammenlignet med konventionelle teknikker. En detaljeret undersøgelse blev gennemført af den enzymatiske nedbrydning af poly (D, L-lactid) i bufferet proteinase K-opløsning. Indflydelsen på nedbrydningshastigheden blev undersøgt ved hjælp af: koncentrationen af enzymopløsningen, prehydrering i buffer, overflademorfologi og enzymadsorptionstid,. Ud fra de eksperimentelle resultater, samt en modelsimulering af flerlags bjælkestrukturer, blev nedbrydningstiden estimeret, og viste sig at have god overensstemmelse med værdier tidligere rapporteret i litteraturen.

Den grundlæggende forståelse af sprøjtebelægningsprocessen, samt de nyudviklede tilgange til brug af mikrobjælker og -strenge som analytiske værktøjer, har meget lovende potentiale indenfor undersøgelse af forskellige polymerer og farmaceutiske systemer.

x

List of publications

- **Paper I**

Process Optimization of Ultrasonic Spray Coating of Polymer Films

Sanjukta Bose, Stephan S. Keller, Tommy S. Alstrøm, Anja Boisen and Kristoffer Almdal

- **Paper II**

Micromechanical String Resonators: Analytical Tool for Thermal Characterization of Polymer

Sanjukta Bose, Silvan Schmid, Tom Larsen, Stephan S. Keller, Peter Sommer-Larsen, Anja Boisen and Kristoffer Almdal

- **Paper III**

Micromechanical Fast Quasi-Static Detection of α- and β-Relaxations with Nanograms of Polymer

Sanjukta Bose, Silvan Schmid, Tom Larsen, Stephan S. Keller, Anja Boisen and Kristoffer Almdal

- **Paper IV**

Microcantilever Sensors for Fast Analysis of Enzymatic Degradation of Poly (D, L-lactide)

Sanjukta Bose, Stephan S. Keller, Anja Boisen and Kristoffer Almdal

My Contribution to the Papers

Paper I. I took part in planning and performed all the experiments for the optimization of the spray coating process. I participated in discussion of the results and had a major contribution in writing the manuscript.

Paper II. I did most of the planning and executed the spray coating on microstrings with different polymers. I did the measurements of the resonance frequency of the microstrings, differential scanning calorimetry and dielectric spectroscopy studies.I took part in evaluation of the results and wrote the manuscript.

Paper III. I planned and executed all the experiments. I had a major contribution in evaluation of the results and writing the manuscript.

Paper IV. I participated in planning of the experiments. I spray coated on the microcantilevers and performed all the degradation experiments. I participated in discussion of the results, did the finite element simulation and had a major contribution in writing the manuscript.

Table of Contents

List of figures

Introduction

Chapter 1

1.1 Introduction

The recent advances in polymer science have integrated the presence of polymers in our everyday lives. The advent of biopolymers based on natural resources or biodegradable polymers having the capability to degrade in a natural environment or possessing biological compatibility make them even more interesting from an ecological and application point of view. It is essential to characterize polymers for acquiring considerable knowledge about their material properties which is very important to determine their final applications. A true workhorse for polymer characterization is thermal analysis[1] which is an ideal technique in defining the temperature dependent compositional and structural changes of the polymers during their production, processing and applications[2]. Glass transition temperature (T_g), often called the α relaxation, is the characteristic temperature of the polymer where there is an onset of coordinated molecular motion in the polymer chain which leads to a transition from a hard glassy state to a soft rubbery state[3]. The importance of the glass transition in polymer science was stated by Eisenberg[3, 4] who declared the glass transition as perhaps the most important single parameter that determines the application of many non-crystalline polymers now available. Differential scanning calorimetry (DSC) is the most frequently employed technique for determining T_g followed by several other widely used methods such as thermomechanical analysis (TMA), dynamic mechanical analysis (DMA) and dielectric spectroscopy (DES)[2]. DMA and DES can reveal more subtle temperature dependent transitions such as sub-T_g transitions or β relaxations as they affect the mechanical modulus and dielectric properties of materials. However, all these different techniques have their own advantages and disadvantages which leave a need for a platform where most of the advantages of these conventional techniques could be combined for a fast and reliable analysis of samples.

As already mentioned, the advent of biocompatible and biodegradable polymers has given a new direction to research in biomedical fields because of their broad application area ranging from surgical sutures, biocompatible stents, scaffolds for tissue engineering, surgical implants to drug carriers for targeted delivery[5–7]. Poly (lactide) (PLA) has gained a lot of attention among the existing biodegradable polymers such as poly(glycolic acid) (PGA), poly(lactide-co-glycolides) (PLGA), polyhydroxyalkanoates (PHAs), poly(caprolactone) (PCL), poly(butylene succinate)

(PBS) etc. due to the efficient production of its raw material lactic acid from sugars and starchy materials[8, 9]. Over the years a lot of research has focused on PLA based biomedical applications with particular focus on the degradation behavior of PLA films which is of prime importance in determining the stability of scaffolds or devices for site specific drug delivery[10]. Due to the presence of hydrolytically labile ester bonds on the PLA backbone hydrolytic degradation studies of PLA have been executed in presence of acids, alkalis, salts or enzymes as catalysts[10–13]. Generally speaking, degradation studies require a long time[14–16] ranging from several hours to a few months and often need chemical or thermal acceleration in the form of high/low pH or elevated temperatures respectively[17]. This shows the demand for a system which can provide fast and sensitive measurement of degradation of polymer films.

On the other hand advances in micro- and nano- fabrication technologies enabled the fabrication of micromechanical sensors such as microcantilevers (singly clamped beams) and microstrings (doubly clamped tensile pre-stressed beams) which can be used as highly sensitive tools for the detection of mass, chemicals, humidity, temperature and other physico-chemical changes[18–26]. Moreover, these sensors possess the prospect of measuring very small quantities of samples and subtle phenomena that are otherwise difficult to accomplish by existing methods and they are therefore considered as very interesting fundamental research tools[20]. In this Ph.D. project, the potential of micromechanical resonators like cantilevers and strings are investigated in fast and sensitive characterization of minute quantities of polymers.

This chapter aims at providing the background and motivations for the work presented in this thesis. A discussion on the advantages and disadvantages of the state of the art thermal characterization techniques of polymers is given in section 1.2 and the recent approaches undertaken for detecting thermal transitions of polymers by micromechanical sensors is discussed in section 1.3. Section 1.4 provides studies on degradation behavior of PLA and its stereo forms poly (L-lactide) (PLLA), poly(D-lactide) (PDLA) and poly(DL-lactide) (PDLLA) with particular focus on the enzymatic degradation by conventional approaches followed by recent approaches developed to detect biodegradation of PLA in micro scale in section 1.5. Section 1.6 provides the project framework with a brief overview of the work done so far. The objective of this Ph.D. project is presented in section 1.7 and the thesis structure is outlined in section 1.8.

1.2 Thermal characterization of polymers: conventional approaches

As mentioned in section 1.1 the glass transition or α relaxation of polymers is a crucial parameter as it determines the material properties with respect to the end-use temperature of the material. Like in the case of a rigid plastic the upper use temperature depends on T_g which determines its softening or deformation. In the case of a soft rubber, the higher the T_g the more it will be brittle at temperature lower than T_g. During the glass to rubber transition, changes in several material properties occur for example specific heat capacity (measured by DSC), coefficient of thermal expansion (CTE) (measured by TMA), mechanical modulus or energy loss (measured by DMA) and change in permittivity or dielectric loss (measured by DES)[2]. Due to the increase in heat capacity, T_g resembles a second order thermodynamic transition. However since this change in heat capacity takes place over a temperature range, it is not fulfilling the condition of equilibrium thermodynamics and hence the glass transition is a kinetically controlled second order process[2, 3]. When the glass transition is measured by the change in relaxation processes by DMA or DES it is defined as the α relaxation and the major sub-T_g transition is defined the β relaxation. The β relaxation or the secondary relaxation process is often termed as a precursor to the primary or α relaxation[27] where local chain motions exist in the form of conformational changes in the side groups or hindered bond rotations[2, 28]. It is reported that the flexibility signaled by secondary chain motions in β relaxations impart toughness in some rigid polymers by responding to the applied stress[3, 29]. However due to the similarities in the activation energies of β relaxations with flow or creep, acoustic damping, physical aging changes or diffusion of gas in polymers, Bershtein[27] considered this sub-T_g transition as the "activation barrier" for solid-phase reactions. Apart from polymers, detection of α and β relaxations are also crucial for amorphous pharmaceutical solids since molecular mobilities associated with these relaxation processes determines their physical and chemical stabilities[30, 31].

DSC is by far the most common technique used for measuring glass transitions of polymers by the change in the heat flow rate to or from a sample as it is subjected to controlled temperature ramps. For subtle transitions like β transitions or for glass transitions of some pharmaceutical drugs or proteins[30] where the associated heat capacity change is negligible DSC is not appropriate. Moreover, in general the sample requirement for DSC experiments is 3-10 mg[2] which is considered a lot in some cases. The commonly used heating rate is 5-10 °C/min[2] and the heating rate is a very important factor which is related to the total experimental time requirement. The faster

the rate of heating, the lower is the experimental time. However, the glass transition being a kinetic phenomenon; it is a function of both time and temperature so T_g will shift to a higher temperature when heated at a higher rate. Though the instrument sensitivity increases at a higher heating rate, the shape of the DSC curve broadens and temperature resolution decreases due to the thermal lag produced by the temperature gradient in the sample[2, 32] as seen in Figure 1.1.
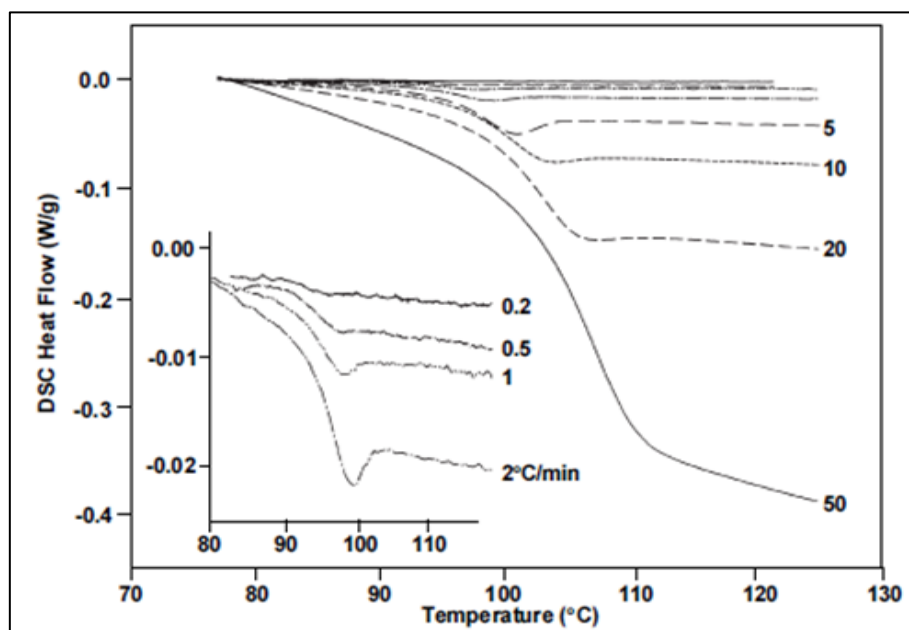
Figure 1.1: *A typical DSC curve showing endothermic shift in the baseline due to glass transition of the polymer at different heating rates. Figure adapted from[32].*

Thus a better alternative tool will be a system which allows higher heating rates with a very small amount of sample and suitable for detection of both major and subtle phase transitions.

Figure 1.2 shows a schematic of a typical TMA plot for determining the glass transition temperature.
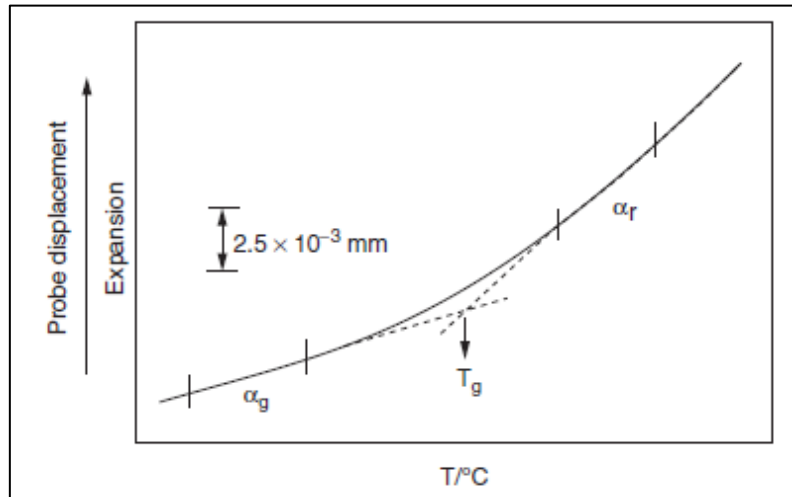
Figure 1.2: *A typical TMA experiment for determination of T_g of a polymer. α_g and α_r are CTEs of glassy and rubbery state of the polymer. Figure adapted from[2].*

As seen from Figure 1.2, T_g of a polymer is determined as an abrupt change of the slope in the thermal expansion curve due to the expansion of the free volume above the glass transition which allows greater chain mobility. In another approach, TMA measures the glass transition temperature as a change in sample dimensions usually with a static load applied by a probe in a controlled temperature programme[2]. The probe penetrates into the sample when the polymer transits from a rigid glass to the soft rubbery regime indicating the dimensional change in the material. However the probe loading conditions may give rise to inconsistencies in the result and TMA, though suitable for detecting glass transition, is not recommended for β transitions[32]. A slow heating rate of 1-5°C/min should be maintained with a minimum sample thickness of 0.5mm[2] which means long experimental time and substantial sample requirements.

DMA on the other hand is suitable for measuring both α and β relaxations of polymers since it measures the change in the mechanical properties of materials with time, temperature or frequency when a periodically oscillating force is applied to it. The elastic modulus of the material is measured as the storage modulus (E′) and the loss modulus (E″) from where the loss factor or the damping coefficient (tan δ) is deduced as the ratio of E″/ E′. Typically the peak values of the E″ or the tan δ is used to detect the transition temperatures. Since mechanical relaxations are a kinetic phenomenon they change with the applied mechanical frequency. This is well known from the time-temperature superposition where time and temperature can be mathematically interchanged at certain conditions[3]. If the measurement is done at a higher frequency, a higher temperature is

needed to reach the same mechanical state obtained at a lower frequency. Figure 1.3 represents a typical effect of increase in oscillation frequency in determining mechanical relaxations by DMA.
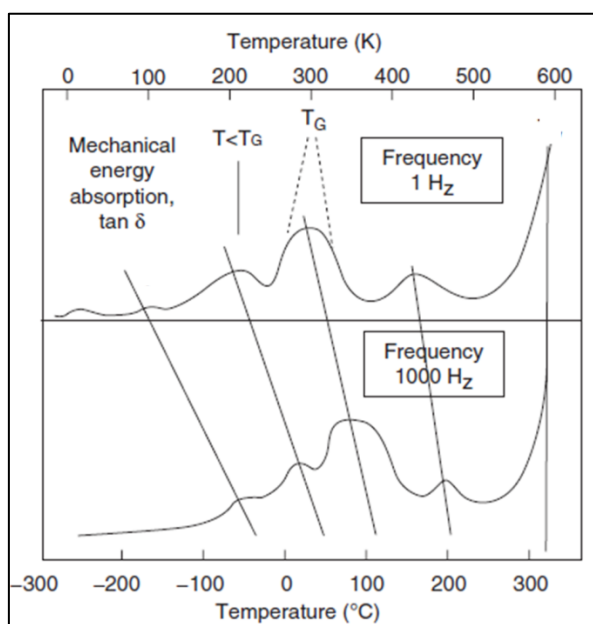
Figure 1.3: *Effect of changes in frequency on an idealized dynamic mechanical temperature scan. The loss peaks for various transitions shift to higher temperatures with increasing frequency. Figure modified from[2].*

It is seen from Figure 1.3 that better resolution of the transitions is favored at lower oscillation frequencies. Due to the difference in activation energies the shifts in T_g and sub-T_g transitions are different. This observation in shifting of transition temperatures is also true when measuring with DES where the shift depends on the frequency of the alternating current. In DES, the transition temperatures are obtained from the peak of the imaginary permittivity (ε'') or a ratio of the imaginary to real permittivity (ε') known as tan δ (i.e., $\varepsilon''/\varepsilon'$) when subjected to a field of alternating current. For determining α and β transitions DES is often preferred due to its high sensitivity and wide dynamic range[33, 34] provided the sample possesses considerable polarizibility[2]. However β relaxations are normally determined in experiments executed at lower frequencies as they become less pronounced when measurement is done at higher frequencies[35, 36]. Figure 1.4 shows a standard behavior of the temperature dependence of permittivity components (ε' and ε'') for an amorphous polymer with considerable polarizability. The α and β relaxation peaks will shift to a higher or lower temperature depending on the frequency of the applied current.
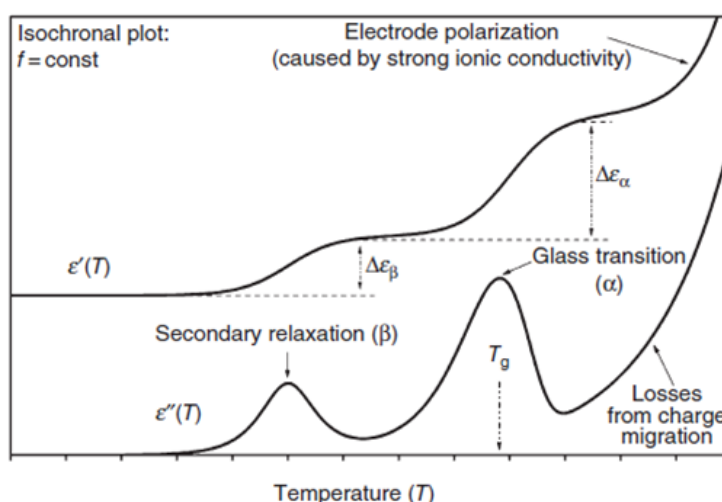
Figure 1.4: *Plot of permittivity components (ε ', ε ") versus temperature for an amorphous polymer showing the α and β relaxation temperatures at a fixed frequency of alternating current. Figure modified from[2].*

Thus to compare transition values from other thermal methods and for estimation of sensitive transitions DMA and DES are often run at lower frequencies (~1 Hz) and lower heating rates (2-5 °C/min) which in turn adds on to the total experimental time [2, 32, 36]. Moreover the need for preparation of bulk samples increases the total amount of analyte required to execute the experiments.

In summary, from the discussion of the possibilities and limitations of the state of the art thermal analysis techniques it can be deduced that there is a need for a new analytical tool which can do fast measurements of both α and β relaxations of polymers with a very small sample volume without frequency effects like in DSC but high sensitivities like DMA or DES. Such a method could also be applied for thermal analysis of drugs and proteins.

1.3 Thermal characterization of polymers: recent approaches

In recent years, technological advancement in micro- and nano thermal analysis allows detection of thermal transitions with minute quantity of sample and mapping of "localized" variations in properties or compositions of heterogeneous samples at the microscopic level [2, 37]. For instance atomic force microscopy (AFM) in non-contact mode has been used as a dynamic mechanical analyzer to measure thermal transitions on a micrometer scale[38]. Another approach is based on cantilever like micromechanical sensors which has been successfully used to determine various

polymer properties with nanograms to picograms of samples [22, 39]. Jeon *et al.* used microcantilevers to detect glass transition temperatures of polystyrene (PS), polyvinyl acetate (PVAc), blends and diblock copolymer of PS with polymethylmethacrylate (PMMA)[40–42]. The cantilevers were coated on one side with polymer by inkjet printing. Both static deflection and resonance frequency change of the polymer coated cantilevers were monitored when subjected to temperature cycles as shown in Figure 1.5. T_g was determined from the deflection induced by the change in volume and elastic properties of the polymer when heated. Temperature dependency of the effective Young's modulus of PVAc was investigated by vibrating the polymer coated cantilever at its resonance frequency[41].
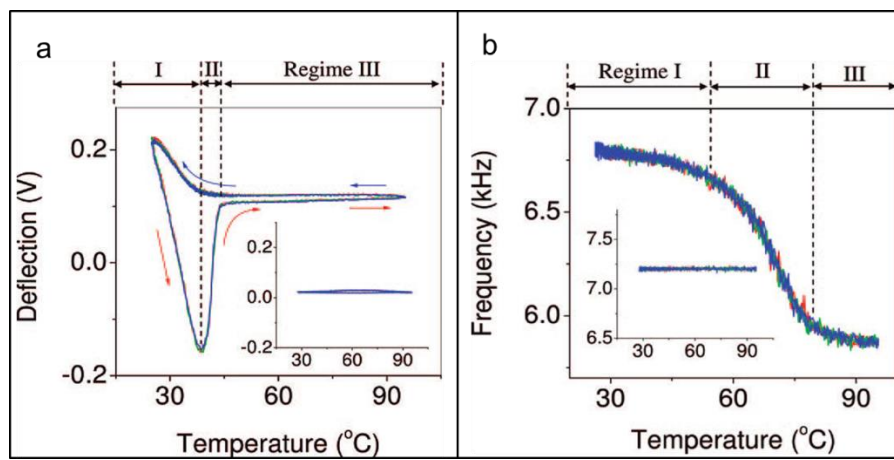
Figure 1.5: *Plots of variation with temperature in (a) the deflection and (b) the resonance frequency of a PVAc-coated cantilever during three thermal cycles (red, first; green, second; blue, third). The inset shows the variation with temperature in the deflection of an uncoated silicon cantilever. Figure adapted from[41].*

Non-uniformity of the polymer film was however identified as an issue in proper estimation of the Young's modulus. Homogeneous films prepared from monolayer of colloidal PS on the other hand allowed a precise measurement of the Young's modulus along with frequency dependent glass transitions of PS by microcantilevers as reported by Berger *et al.*[43]. Ayela *et al.* analyzed viscoelastic properties, more specifically viscous losses of thin polyisobutylene (PIB) films by microcantilevers[44]. Microelectromechanical systems (MEMS) based thin-film differential scanning calorimetry device was developed by Allen *et al.* which showed potential for studies of glass transition for polymer films with nanometer-range thickness. To prepare the calorimetric cell a silicon nitride (SiN_x) membrane was integrated into a sensor with a silicon (Si) substrate. An

electrical circuit was formed by placing a thin platinum layer directly on the membrane which functioned both as a heater and a thermometer[45, 46]. Nevertheless to the best of our knowledge, none of the existing micromechanical systems discussed above can provide a fast analysis of both T_g and sub-T_g transitions of polymers. This was the motivation to investigate the potential of double clamped tensile pre-stressed SiN_x microstrings as a new analytical tool for fast detection of both α and β relaxations of nanograms of polymer. These SiN_x microstring resonators being double clamped on a Si substrate were expected to eliminate issues with the initial out-of-plane deflection often experienced with coated microcantilevers which impedes the optical read out of mechanical motion.

1.4 Degradation studies of biodegradable polymers: conventional approaches

As mentioned in section 1.1, PLLA, PDLLA, PDLA and their copolymers, blends and composites have found wide applications in the biomedical industry because of their good biocompatibility and tailorable biodegradability along with good mechanical properties and processability[5, 6, 10]. Degradation of these polymers is a desired process for bioabsorbable surgical sutures[5], for tissue engineering scaffolds where a second surgical intervention to remove the scaffold could be avoided[47, 48] and for controlled drug delivery where the release kinetics of the therapeutic agent can be designed depending on the degradation behavior of the polymer employed[49, 50]. Thus, over the years, a lot of research has focused on catalyzed hydrolytic degradation studies of PLA based polymers. The rate of degradation depends on many material factors like molecular weight (MW) and distribution, crystallinity, dimensions and morphology, surface treatment and coating and media related factors like temperature, pH, concentrations and kinds of solutes or enzymes present in the media[5, 10]. Ikada *et al*. observed degradation of PLLA for 175 days in 0.01 N NaOH solution (pH 12) at 37 °C and reported a constant rate of mass loss for 100 days followed by a decrease in the rate of mass loss[15]. Peroxide modification of PLLA increased the weight loss compared to unmodified specimen by 7 % due to change in surface morphology during immersion for 20 weeks in Tris-buffer solution (pH 7.4) at 37 °C[14]. An increase in crystallinity was observed over 150 days, when 50 µm thick PLLA film was subjected to alkaline degradation in pH 12 solution at 37 °C due to preferential degradation of the amorphous part of the polymer[16]. Ikada *et al.*also reported an increase in crystallinity on hydrolysis of high molecular weight PLLA in phosphate buffered solution at 37°C as shown in Figure 1.6.
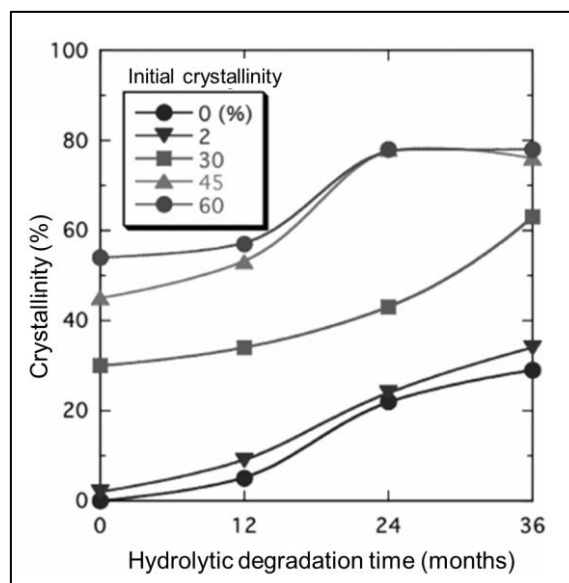
Figure 1.6: *Crystallinity change of PLLA films having different initial crystallinity values during hydrolytic degradation in a phosphate-buffered solution. Figure modified from[51].*

William first reported hydrolytic degradation of PLLA by the enzyme proteinase K from *Tritirachium album*[52] followed by Ashley and McGinity who confirmed enzymatic degradation of PDLLA[53]. Proteinase K has exhibited strong acceleration in the rate of degradation of PLLA when compared to several other enzymes like esterases, pronese and bromelain[54]. Proteinase K degradation of PLA stereo forms revealed a preference towards degrading L-lactyl units over D-lactyl [10, 54, 55]. Moreover a decrease in the rate of degradation was also observed with the increase in crystallinity of PLLA since proteinase K preferentially hydrolyses amorphous regions[56]. The investigation of the effect of temperature and acidic media on enzymatic degradation of PDLLA revealed that at 60 °C and pH 7.4 around 90% weight loss was observed in 21 days compared to around 85 days when experiments were conducted at 37 °C and pH 3.7 due to heterogeneous degradation over the sample thickness[57]. All of the above mentioned degradation studies be it alkaline, acidic or enzymatic degradation of PLA have used conventional characterization techniques like gravimetric analysis for weight loss determination, size exclusion chromatography (SEC) to measure change in molecular weight and molecular weight distribution, DSC for thermal characterization, X-ray diffraction (XRD) and DSC to measure change in crystallinity and tensile testing for mechanical characterization[58]. For most of the studies the total degradation time ranged from hours to several weeks with acceleration at extreme pH or elevated temperatures. Due to the increased use of biodegradable polymers in clinical and pharmaceutical

10

applications there is a growing need to establish a system for rapid degradation analysis of biodegradable polymer films.

1.5 Degradation studies of biodegradable polymers: recent approaches

Recent approaches for measuring degradation of biodegradable polymer films in micro scale includes AFM[10, 59, 60] and quartz crystal microbalance (QCM)[10, 48] which can characterize films with thicknesses below 1 µm down to a few nanometers. AFM is a widely used tool for characterization of polymer surface morphologies and also allows *in situ* observation of crystal structures. The crystalline morphologies of thin PLLA films (thickness 100 nm) were characterized by using AFM and the degradation behavior in presence of proteinase K at 37 °C was observed *in situ*[60]. As observed by others[56] preferential degradation of amorphous regions compared to crystal structures was confirmed. While AFM provides microscopic static information when monitoring enzymatic degradation, QCM offers a macroscopic dynamic analysis of the same. A combination of these two characterization tools (Figure 1.7) were used by Yamashita *et al.* to observe enzyme adsorption and degradation characteristics of amorphous PLLA at the molecular level[48]. QCM is a sensitive instrument which detects the change of mass with nanogram precision by measuring the change in resonance frequency of the quartz electrode. Degradation rate was detected on the basis of the irreversible adsorption of the proteinase K enzyme on the 100 nm thick PLLA film.
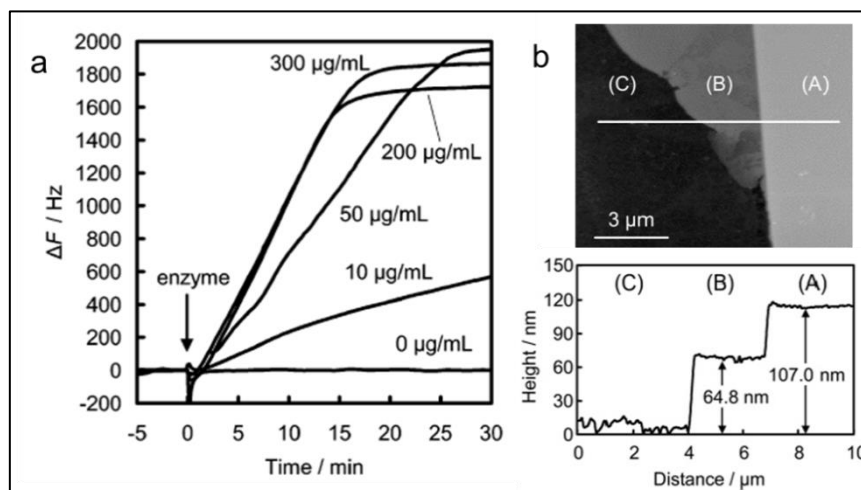
Figure 1.7: *(a) Frequency changes (ΔF) observed by QCM during enzymatic degradation of the PLLA amorphous films at different concentrations of proteinase K and (b) AFM height image of the PLLA film after stepwise enzymatic degradation at concentration 250 g/mL in (A) 0, (B) 7, and (C) 14 min, at 25 °C. Figure adapted from[48].*

Complete removal of the thin film in 20 minutes was observed for a concentration of enzyme greater than 100 µg/ml. Keller et al. pioneered the use of SU-8 microcantilevers in measuring enzymatic degradation of PLLA from the change in resonance frequency of these micro resonators in a principle similar to that of QCM[61]. Typically thin[48, 62, 63] (thickness less than 1µm) and homogeneous[64] polymer films are required for analysis by QCM whereas microcantilevers are capable of characterizing polymer films with thicknesses of several microns and varied surface morphologies. This should allow probing of macroscopic properties on a microscopic platform.

The results obtained from the initial studies of biodegradation of polymers[61] were motivations for a detailed study on fast analysis of enzymatic degradation of amorphous PDLLA on silicon microcantilevers. Here, the vision was that the miniaturized system will be highly sensitive towards detecting biodegradation of minute amount of polymers without the need of experiments at elevated temperature or with chemical acceleration.

1.6 *The NAMEC project : framework and funding*

This Ph.D. project is carried out as part of a strategic research centre called NAMEC– NanoMEChanical sensor and actuators, fundamentals and new directions – a VKR Centre of Excellence financed by the Villum Kann Rasmussen Foundation. The NAMEC project started in 2009 and will run until the end of 2014 as a collaboration between four partners: the Department of Micro- and Nanotechnology, the Department of Electrical Engineering, the Department of Applied Mathematics and Computer Science from the Technical University of Denmark (DTU) and the Department of Pharmacy from the University of Copenhagen (KU Pharma). The overall goal of NAMEC is to develop new micromechanical sensors and oral drug delivery systems. In realization of the goal, the NAMEC project is broadly divided into two parallel activities (a) Sensors and (b) Drug delivery.

The 'Sensors' part of the project is based on the need to develop new sensors which could exhibit fast and reliable investigation of small amount of analytes with specific focus on pharmaceutical research. With respect to that, microcantilevers were developed as a combined platform for electrochemical and surface stress sensing[65] and as mass sensors with integrated microfluidic channels[66]. Micromechanical string resonators were developed as ultrasensitive temperature sensor and photothermal spectrometer for micro- and nano- particle detection[67].

The 'Drug delivery' part of the project on the other hand is based on the need for precise and reliable oral delivery of pharmaceutical drugs with poor solubility and low membrane permeability.

In respect to that new approaches to form stable drug formulations by preparing solid dispersions of drug and polymer like hydroxypropyl methyl cellulose (HPMC) were investigated[68]. Fabrication of microcontainers for oral drug delivery with biodegradable polymers such as PLLA and PCL by means of hot embossing was achieved[69]. Possible drug loading techniques for efficient drug delivery were studied which include impregnation of drug in polyvinylpyrollidone (PVP) by super critical carbon dioxide and preparation of drug loaded micro patterned PVP hydrogels[70]. Enteric coatings with pH responsive polymer namely Eudragit L 100 can be successfully used to form a lid on the micro containers. The lid protects the drug from undesirable degradation and can trigger drug release at a specific region of the gastrointestinal tract.

This Ph.D. thesis is trying to bridge between the two parallel activities in the NAMEC project. Here the goal was to apply the micromechanical resonators used in the 'Sensor' part for characterization of different polymers used in the 'Drug delivery' part of the project.

1.7 Objective of thesis

The objective of this Ph.D. project is to use micromechanical resonators such as cantilevers and strings as analytical tools for characterization of polymers.

To achieve the project objective, the research has been focused on the following areas:

- Optimization of spray coating as a method for preparing polymer films (Paper I).
- Evaluation of micromechanical string resonators for detection of T_g or α-relaxations and sub-T_g transition or β-relaxations of polymers (Paper II and Paper III).
- Evaluation of microcantilevers for fast analysis of enzymatic degradation of biodegradable polymer (Paper IV).

1.8 Thesis Outline

Chapter 2: This chapter contains the presentation of the read-out principles and the basic theories of microcantilevers and microstring resonators.

Chapter 3: This chapter contains description of spray coating for preparation of polymer films on the micro resonators along with different techniques used for preparing selectively coated cantilevers by shadow masking. Furthermore, the description and working principle of different characterization methods like optical profilometer, Laser Doppler vibrometer, differential scanning calorimetry and dielectric spectroscopy used in this project are briefly presented. The chapter also

includes a discussion on the Finite Element Method (FEM) simulations used to build a model of multilayered singly clamped beam structure for estimation of the enzymatic degradation rate of the biodegradable polymer used in this project.

Chapter 4: This chapter contains summary of the published papers and the prepared manuscripts on the research done in this Ph.D. thesis.

Chapter 5: This chapter contains concluding remarks and a discussion about the future prospective based on the work conducted in this thesis.

Basic Theory of Micromechanical Resonators

Chapter 2

2.1 Principle of operation of cantilever like sensors

Cantilever sensing has been investigated in two fundamentally different working modes, the static mode and the dynamic (resonant mode) as schematically represented in Figure 2.1.
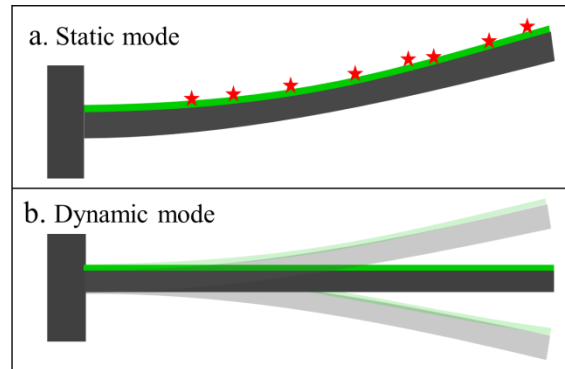
Figure 2.1: Schematic representation of the two working modes of cantilever like sensors: (a) static mode (b) dynamic mode.

In static mode (Figure 2.1a), the stress induced bending of a cantilever is measured. This deflection can be caused by surface stress or an internal stress gradient [20] and is promising for a wide number of applications for example, in chemical sensing, temperature sensing, in detection of biomarkers or specific DNA sequences and material characterization [20, 23, 26, 71–74]. In dynamic mode (Figure 2.1b), the cantilever is actuated into vibration and the resonance frequency of the vibrating cantilever is measured which has been successfully used for example as mass sensor, for determining viscosity, mass density and mechanical properties of materials [20, 21, 66, 75–77]. This Ph.D. thesis has focused on characterizing polymers based on the change of resonance frequencies of the polymer coated micromechanical sensors so unless otherwise stated all the measurements presented here use the dynamic mode of operation.

2.1 Micromechanical resonators

A micromechanical resonator is a micro meter sized mechanical structure or device vibrating at resonance. The resonance frequency (f_r) is the natural oscillation frequency, where the vibrational amplitude reaches its maximum. The quality factor (Q) determines the sharpness of the resonance peak i.e. provides information about the damping or energy loss of the system.[67] The principle of

sensing with micromechanical resonators is that the measured quantity modifies some oscillation characteristics of the mechanical resonators. The characteristics of the resonance, such as the resonance frequency or the quality factor are affected by addition of mass, alteration in damping, changes in material properties or resonator geometries, alteration of stress in the system or changes in the amplitude of actuation driving the system[78]. In this thesis two different kinds of micromechanical resonators have been used, i) singly clamped beams or cantilevers and ii) doubly clamped tensile pre-stressed beams or strings. Understanding the resonating behavior of these microbeams is thus essential when using them as tools for thermal and degradation analysis of polymers. This chapter aims at providing the basic theory of microcantilevers in section 2.2 and of microstring resonators in section 2.3.

2.2 Basic theory of cantilevers[1]

2.2.1 Resonance frequency of cantilever like single clamped beam

Figure 2.2 shows a thin beam of length (L), width (w) and thickness (h) with the aspect ratio (L/h) > 10.
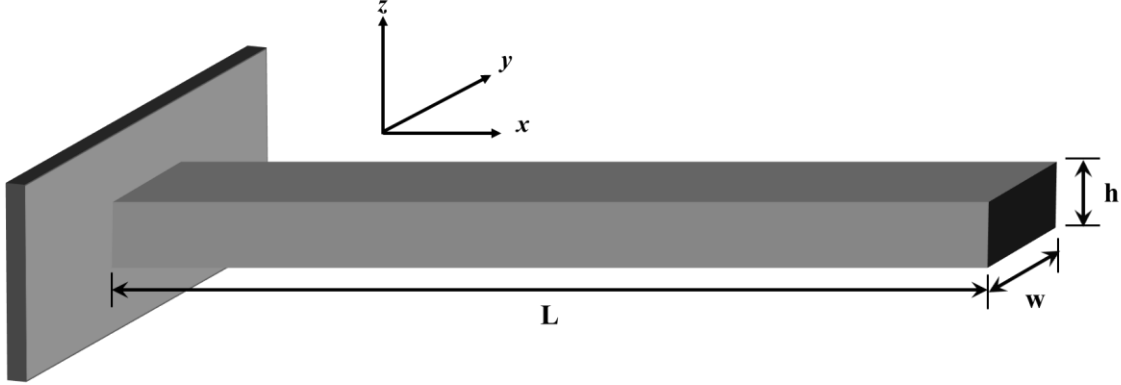
Figure 2.2: *Schematic of a cantilever: single beam clamped at one end*

The equation of motion of a thin beam can be derived by means of the equilibrium of forces for an infinitesimal piece of beam. Assuming a linear elastic material and small deflections, the equation of motion of a thin beam is given the Euler-Bernoulli beam equation[79, 80]

$$EI \frac{\partial^4 U(x,t)}{\partial x^4} + \rho A \frac{\partial^2 U(x,t)}{\partial t^2} = 0 \qquad (2.1)$$

---

[1] This chapter is based on the materials found in [20, 67, 79, 82–84, 86]

where $U(x, t)$ is the displacement of the beam as a function of the position along the beam and time. E is the Young's modulus, I is the area moment of inertia, ρ is the mass density and A is the cross sectional area of the beam. The rotational inertia and shear deformation is neglected in this case due to the large aspect ratio. Solutions to this differential equation can be found by using the separation of variable approach. The displacement function can then be written as a product of a spatial varying function and a time varying function[20, 67]:

$$U(x,t) = \phi(x)exp(i\omega_n t) \tag{2.2}$$

where ω_n is the frequency of motion and n is the modal number. By inserting (2.2) into (2.1), it can be rewritten as

$$\frac{\partial^4 U(x)}{\partial x^4} = c_n^4 U(x) \tag{2.3}$$

where the wave number c_n is given by

$$c_n^4 = \frac{\omega_n^2 \rho A}{EI} \tag{2.4}$$

The displacement functions for this simplified beam equation can be written as:

$$U_n(x) = A_n \cos(c_n x) + B_n \cosh(c_n x) + C_n \sin(c_n x) + D_n \sinh(c_n x) \tag{2.5}$$

The unknown coefficients A_n, B_n, C_n and D_n can be found out by means of the specific boundary conditions. The beam equation (2.5) is solved with the boundary conditions of a single clamped beam at x=0 and a free end at x=L:

$$\left. \begin{aligned} u(0) = 0 \ \text{ and } \ \left.\frac{\partial u}{\partial x}\right|_{x=0} = 0 \\ \left.\frac{\partial^2 u}{\partial x^2}\right|_{x=L} = 0 \ \text{ and } \ \left.\frac{\partial^3 u}{\partial x^3}\right|_{x=L} = 0 \end{aligned} \right\} \tag{2.6}$$

Applying the boundary conditions yields the characteristic equation for the allowed wavenumbers as:

$$\cos(c_n L).\cosh(c_n L) + 1 = 0 \tag{2.7}$$

which is solved as

$$\lambda_n = c_n L = 1.875, 4.694, 7.855, ...; n = 1, 2, 3, ... \tag{2.8}$$

where the solution represents different resonant modes and the fundamental mode is n=1. From (2.5) it is clear that a beam will vibrate in certain vibrational modes each with a distinct spatial shape described by the following equation[81, 82]:

$$U_n(x) = \sin(\frac{\lambda_n}{L} x) - \sinh(\frac{\lambda_n}{L} x) + \frac{\sin(\frac{\lambda_n}{L} x) + \sinh(\frac{\lambda_n}{L} x)}{\cos(\frac{\lambda_n}{L} x) + \cosh(\frac{\lambda_n}{L} x)} \left[\cosh(\frac{\lambda_n}{L} x) - \cos(\frac{\lambda_n}{L} x) \right] \tag{2.9}$$

Figure 2.3 shows the side-view schematics of the first four bending modes of a cantilever.
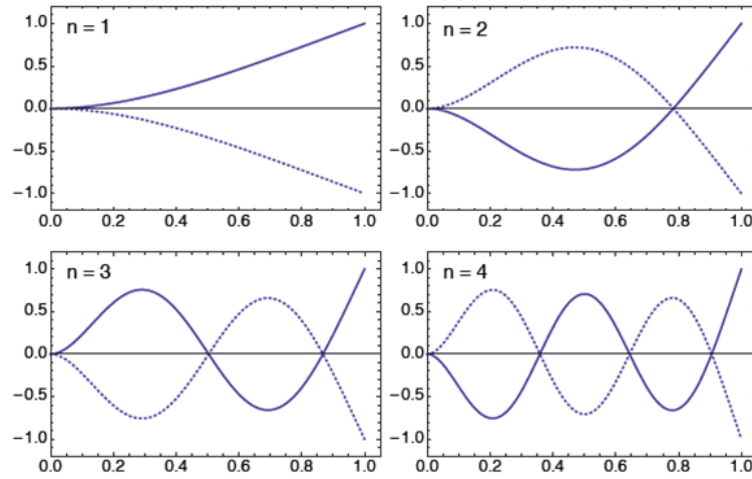
Figure 2.3: *First four bending modes (n=1, 2, 3 and 4) of a cantilever seen from the side. The y-axis corresponds to the amplitude and x- axis the position where 0 indicates the base of the cantilever. The figure is adapted from[79].*

The eigenfrequency of a bending beam is then given by:

$$\omega_n = \lambda_n^2 \sqrt{\frac{EI}{A\rho}} \frac{1}{L^2} = \lambda_n^2 \frac{h}{L^2} \sqrt{\frac{E}{12\rho}}, n = 1, 2, ... \tag{2.10}$$

where, $I = \frac{wh^3}{12}$ and $A = wh$.

The eigenfrequency of the system at n'th mode in hertz (Hz) in then given by dividing (2.10) by 2π as:

21

$$f_n = \frac{\lambda_n^2}{2\pi}\sqrt{\frac{EI}{A\rho}}\frac{1}{L^2} = \frac{\lambda_n^2}{2\pi}\frac{h}{L^2}\sqrt{\frac{E}{12\rho}}, n = 1, 2, \ldots \quad (2.11)$$

Simplifying the beam-dynamics of an individual resonance mode with that of a harmonic oscillator the eigenfrequency can generally be expressed as [20]

$$f_n = \frac{1}{2\pi}\sqrt{\frac{k_{eff}}{m_{eff}}} \quad (2.12)$$

Where, k_{eff} is the effective spring constant and m_{eff} is the effective mass of the cantilever beam.

Now, the effective mass of a resonating cantilever beam can be calculated though equating the kinetic spring energy of the resonator to the kinetic energy along the beam[82]:

$$\frac{1}{2}m_{eff}\omega_n^2 U_n(L)^2 = \frac{1}{2}\frac{m_0}{L}\omega_n^2\int_0^L U_n(x)^2 dx \quad (2.13)$$

Where m_0 is the true mass of the cantilever given by $m_0 = \rho whL$. Applying (2.9) into (2.13) the effective mass is found to be a quarter of the total cantilever mass, independent of the mode number

$$m_{eff} = \frac{m_0}{4} \quad (2.14)$$

Based on Hooke's law, the static spring constant k_{static} of a cantilever beam can be derived from the static deflection for an applied force at the cantilever tip:

$$k_{static} = \frac{3EI}{L^3} = \frac{Eh^3 w}{4L^3} \quad (2.15)$$

The effective spring constant can then be obtained as by using (2.11)(2.12)(2.14) and (2.15) as

$$k_{eff} = \frac{\lambda_n^4}{12}k_{static} \quad (2.16)$$

2.2.2 Multilayer cantilever theory

The theory of multilayered cantilever becomes important when a polymer layer is deposited on one side of the cantilever which causes a shift in the resonance frequency. From (2.12) it is clear that this additional polymer layer on the existing singly clamped beam can cause an increase or decrease

of the resonance frequency due to the change in k_{eff}/m_{eff} ratio. Thus the expression for k_{eff} and m_{eff} for a multilayered cantilever have to be found to obtain the expression of the eigenfrequency. The neutral plane of the cantilever is the plane with zero strain which retains its original length during bending of a multilayered cantilever. The position of this plane is denoted as z_N from the bottom surface of the cantilever as shown in Figure 2.4 and expressed as:

$$z_N = \frac{\sum_i E_i h_i z_i}{\sum_i E_i h_i}$$ (2.17)

where, E_i is the Young's modulus for the i'th layer, h_i is the thickness and z_i is the position of the i'th layer as shown in Figure 2.4
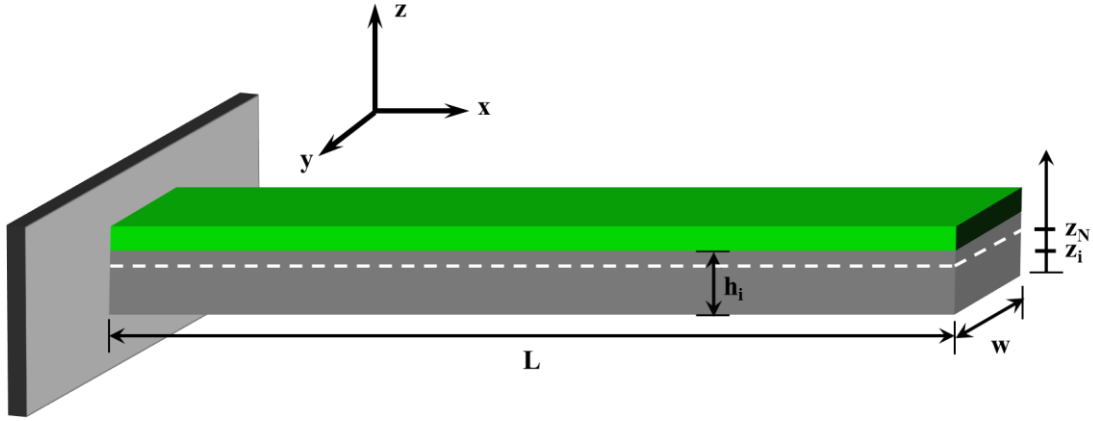
Figure 2.4: A multilayer cantilever, with layers of thickness h_i and neutral plane at z_N.

EI$_{eff}$ for a multilayered cantilever is found by:

$$EI_{eff} = \sum_i E_i I_i$$ (2.18)

The area moment of inertia for the i'th layer, I_i can be calculated using the position of the neutral plane and the parallel axis theorem with the central plane of the cantilever layer displaced a distance r from the neutral plane of the cantilever. The area moment of inertia for a rectangular area A in general is given by:

$$I_r = I + Ar^2$$ (2.19)

Where I_r is the area moment of inertia for an area displaced with the distance *r and I* is the area moment of inertia of the rectangular area *A* when it is not displaced relative to its centroid. From the expression in (2.19) the area moment of inertia for each layer of cantilever can be calculated. The area moment of inertia for a beam with rectangular cross section is $I = \dfrac{wh^3}{12}$. The distance *r* in the case of a multilayered cantilever is the distance between the neutral plane and the central plane of the *i*'th layer $z_N - z_i$. From (2.19) the general area moment of inertia for the *i*'th layer in the cantilever is given by:

$$I_i = \frac{wh^3}{12} + wh_i \left(z_N - z_i \right)^2 \tag{2.20}$$

From (2.16) the effective spring constant for multilayered cantilever can be re-written as

$$k_{eff} = \frac{\lambda_n^4 \sum_i E_i I_i}{4L^3} \tag{2.21}$$

And from (2.14) the effective mass for multilayered cantilever can be re-written as

$$m_{eff} = \frac{Lw \sum_i \rho_i h_i}{4} \tag{2.22}$$

where ρ_i is the density of the *i*'th layer.

From (2.12) the general equation for eigenfrequency of multilayered cantilever becomes

$$f_n = \frac{\lambda_n^2}{2\pi L^2} \sqrt{\frac{\sum_i E_i I_i}{w \sum_i \rho_i h_i}} \tag{2.23}$$

2.2.3 Quality factor of singly clamped beam

For any mechanical resonator the quality factor *Q* is defined as:

$$Q = \frac{\Delta f}{f_r} \tag{2.24}$$

where f_r is the resonance frequency and Δf is the bandwidth at the 3dB amplitude point or the half power point as shown in Figure 2.5.
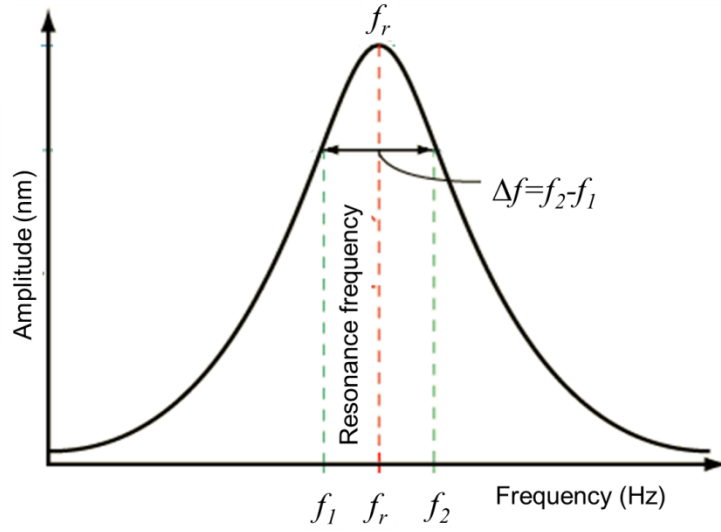
Figure 2.5: *Amplitude response of vibrating cantilever around resonance peak at f_r, as a function of oscillation frequency.*

Q factor is related to the detection sensitivity and resolution when the resonance frequency is measured[83]. Thus a high Q indicates a sharp resonance peak while when the vibration is damped by air, liquid or added material, the peak broadens and a decrease in Q is observed. For reliable measurement care should be taken to keep the Q factor as high as possible where a distinct displacement of the resonance peak can be detected. The theoretical eigenfreqeuncy (f_n) can be related to the measured resonance frequency (f_r) for a damped resonator as[83]:

$$f_r = f_n \sqrt{1 - 2\zeta^2} \tag{2.25}$$

where ζ is the damping coefficient related to Q by:

$$Q = \frac{1}{2\zeta} \tag{2.26}$$

However for slightly damped system with $Q \geq 100$, ζ is negligible and the resonance frequency of a damped resonator can be assumed to be equal to the eigenfrequency of an undamped resonator to a good approximation shown as:

$$f_r \cong f_n \tag{2.27}$$

2.3 Basic theory of strings

2.3.1 Resonance frequency of string like double clamped pre-stressed beam

Strings are doubly clamped beams with built in tensile pre-stress. Figure 2.6 shows a schematic representation of a vibrating string on its fundamental mode with length *L*, width *w* and thickness *h*. Like above for the cantilevers, the common assumption is to consider a very long and very thin beam where (L/h) >> 10[67].
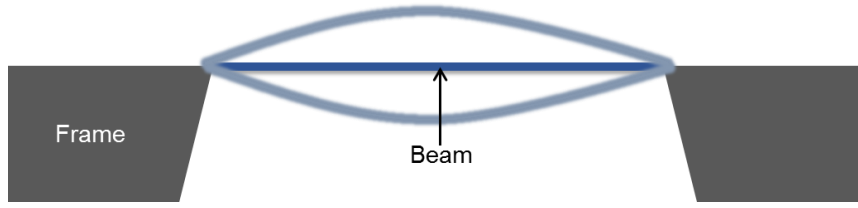
Figure 2.6: *Schematic of a vibrating string: pre-stressed single beam clamped at both ends.*

A tensile stress σ increases the eigenfrequency and has to be taken into account by adding a term for the tensile force $N = \sigma A$ to(2.1). The equation of motion is modified to[20, 67]:

$$EI \frac{\partial^4 U(x,t)}{\partial x^4} - N \frac{\partial^2 U(x,t)}{\partial x^2} + \rho A \frac{\partial^2 U(x,t)}{\partial t^2} = 0 \tag{2.28}$$

The shape functions are now dependent on the tensile force and the conditions that have to be fulfilled are more complex than for the stress free single clamped beam. Equation (2.28) can only be solved analytically when the following boundary conditions are fulfilled:

$$\left. \begin{array}{l} u(0) = 0 \ \ \text{and} \ \ u(L) = 0 \\ \left. \frac{\partial^2 u}{\partial x^2} \right|_{x=0} = 0 \ \ \text{and} \ \ \left. \frac{\partial^2 u}{\partial x^2} \right|_{x=L} = 0 \end{array} \right\} \tag{2.29}$$

The eigenfrequency of a doubly clamped bending beam with a tensile force is then given by:

$$\omega_n = \frac{\lambda_n^2}{2\pi L^2} \sqrt{\frac{EI}{\rho A}} \sqrt{1 + \frac{\sigma A L^2}{\lambda_n^2 EI}} \tag{2.30}$$

where $\lambda_n = n\pi$ are solutions to the characteristic equation. When the tensile stress becomes sufficiently high, $12\sigma L^2 \gg (n\pi)^2 Eh^2$, the flexural rigidity can be neglected and the dynamic behavior becomes string-like. In this case (2.30) reduces to:

$$\omega_n = \frac{n\pi}{L}\sqrt{\frac{\sigma}{\rho}} \tag{2.31}$$

and the displacement function is

$$U_n(x) = a_n \sin\left(\frac{n\pi}{L}x\right) \tag{2.32}$$

Figure 2.7 shows the side-view schematics of the first four bending modes of a doubly clamped string like structure.
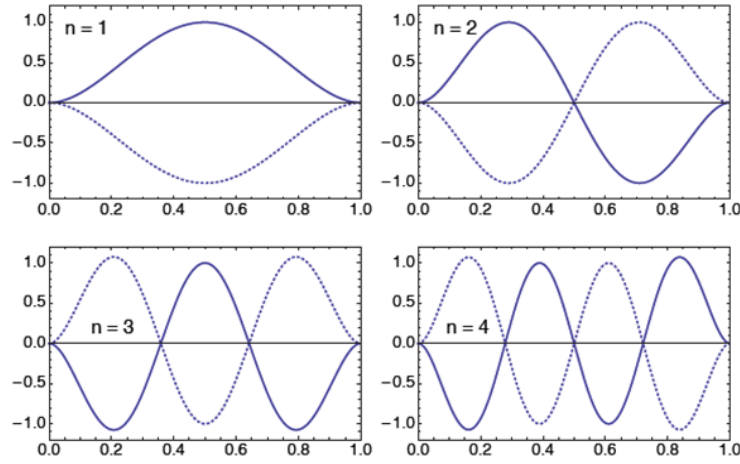
Figure 2.7: *First four bending modes (n=1, 2, 3 and 4) of a doubly clamped beam seen from the side. The y-axis corresponds to the amplitude and x- axis the position where 0 and 1 indicate the clamped ends of the beam. The figure is adapted from*[79]*.*

2.3.2 Temperature dependency of string resonator

As seen from (2.31) the eigenfrequency of string resonator is dependent on the length, mass density and tensile stress in the beam. When the beam and the support frame (Figure 2.6) are of different materials, the differential thermal expansion of the beam and the frame will influence the strain in the beam. This will result in a temperature dependent tensile stress in the beam and as a consequence the eigenfrequency of the string will also become temperature dependent. If the string and the frame expand linearly with temperature the temperature dependent strain is given as[67]:

$$\varepsilon(T) = \varepsilon_0 - (\alpha_S - \alpha_F)(T - T_0) \tag{2.33}$$

where ε_0 is the strain at temperature T_0, T the temperature, α_S the coefficient of thermal expansion of the string (S) and α_F the coefficient of thermal expansion of the frame (F). Stress and strain are related to each other via Hooke's laws. If the string is made of a linear elastic material and the strain does not exceed the elastic limit, the temperature dependent stress can be defined as

$$\begin{aligned}
\sigma &= E\varepsilon(T) \\
\sigma &= E\left(\varepsilon_0 - (\alpha_S - \alpha_F)(T - T_0)\right) \\
\sigma &= \sigma_0 - E(\alpha_S - \alpha_F)(T - T_0)
\end{aligned} \tag{2.34}$$

Inserting (2.34) in (2.31), the eigenfrequency in Hz is given by

$$f_n = \frac{\omega_n}{2\pi} = \frac{n}{2L}\sqrt{\frac{\sigma_0 - E(\alpha_S - \alpha_F)(T - T_0)}{\rho}} \tag{2.35}$$

When a polymer layer of thickness h_P, coefficient of thermal expansion α_P, mass density ρ_P and Young's modulus E_P is added on top of the string as shown in Figure 2.8, the resonance frequency of the multilayered string resonator is derived as (shown in paper II):

$$f_n = \frac{n}{2L}\sqrt{\frac{\left(h_S\left[\sigma_{0,S} + (\alpha_F - \alpha_S)E_S\right] + h_P\left[\sigma_{0,P} + (\alpha_F - \alpha_P)E_P\right]\right)(T - T_0)}{h_S\,\rho_S + h_P\,\rho_P}} \tag{2.36}$$
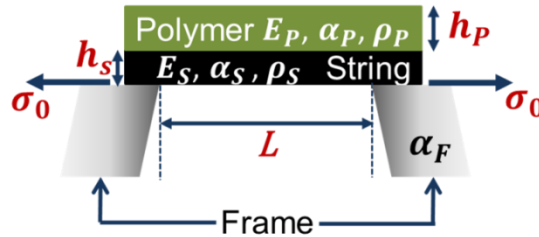
Figure 2.8: *Schematic representation of a multilayered string resonator with the material properties of both layers*

2.3.3 Quality factor of string resonator

In a pre-stressed beam or string the quality factor is highly dependent on the residual stress in the beam. As seen in section 2.2.3, the quality factor is defined as the ratio of the frequency bandwidth of the resonance peak and the resonance frequency as shown in (2.24). The Q of a mechanical

resonator is also defined as the ratio of stored energy (W) versus lost energy (ΔW) during one cycle of oscillation. Like above for the cantilevers, a higher Q is equal to a sharper resonance peak. Combining both definitions one obtains [84]

$$Q = \frac{\Delta f}{f_r} = 2\pi \frac{W}{\Delta W} \qquad (2.37)$$

The tensile stress increases the resonance frequency (which is equal to the stored energy) without significantly influencing the peak width (which is equal to the damping or energy lost). When a viscoelastic polymer layer is added on top of the silicon nitride string used in this study it becomes important to identify the relation between the material damping and quality factor.

When an oscillatory stress σ(t) is applied to a polymer, the accompanying strain ε(t) lags behind the stress by the phase angle δ due to the viscoelastic nature of the material [84, 85].

The loss tangent $\tan \delta$ or the damping of the material is given by the ratio of the loss modulus E'' to the storage modulus E' of the system:

$$\frac{E''}{E'} = \tan \delta \qquad (2.38)$$

.Q for the intrinsic material loss then can be related as:

$$Q_{mat} = \frac{E'}{E''} = \frac{1}{\tan \delta} \qquad (2.39)$$

Taking into account the different factors contributing to the damping of a micromechanical string resonator, Q_{string} can be written as[84, 86]:

$$Q_{string} = \left(\frac{(n\pi)^2}{12} \frac{E}{\sigma} \left(\frac{h}{L} \right)^2 + \frac{1}{\sqrt{3}} \sqrt{\frac{E}{\sigma}} \right)^{-1} Q_{mat} \qquad (2.40)$$

Thus from (2.39) and (2.40) it can be seen that there exist a linear relation between the Q factor of the string and the intrinsic material damping of the polymer which can be given by:

$$Q_{string} \propto Q_{mat} \propto \left(\tan \delta \right)^{-1} \qquad (2.41)$$

This relation has been used in paper II to estimate the influence of frequency on T_g from Q factor determination.

Experimental Methods

Chapter 3

This chapter aims at providing an overview of the methods and characterization tools used during this Ph.D. project. Section 3.1 contains a description of the spray coating process which has been used to deposit polymers on micromechanical resonators. A unique method of shadow masking to produce selectively coated cantilevers is also discussed. Section 3.2 contains an overview of the working principle of a stylus profilometer used for surface analysis of the spray coated films in terms of their thickness and roughness. The description and principle of operation of a Laser Doppler vibrometer is explained in Section 3.3 which has been used for monitoring the resonance frequencies of the micromechanical resonators. The characterization techniques employed for detecting the glass transition temperatures of the polymers used in this project are described in section 3.4 (Differential Scanning Calorimetry) and in section 3.5 (Dielectric spectroscopy). The final section of this chapter, section 3.6 contains a description of the Finite Element Method (FEM) simulation of polymer coated singly clamped beams for iterative analysis of the thickness of the polymer layer to estimate degradation rate.

3.1 Spray Coating
3.1.1 Working Principle

Spray coating in general includes the atomization of the coating solution in the spray nozzle to form minute droplets, deposition of the atomized droplets on a substrate and coalescence of the droplets to form a film after the solvent has been evaporated from the solution. In this work ultrasonic atomization of the spray solution has been employed instead of the more commonly used pneumatic technique[87]. The ultrasonic spray nozzle produces high frequency sound vibration on the atomizing surface and the spray solution forms a mist of small spray droplets with diameter in micrometer range[88] after reaching the atomizing surface as schematically shown in Figure 3.1. Compressed nitrogen is introduced in the nozzle shroud producing a uniform air flow around the nozzle tip and entrains the generated spray droplets thereby shaping the spray beam and focusing it on the substrate kept below the spray nozzle.
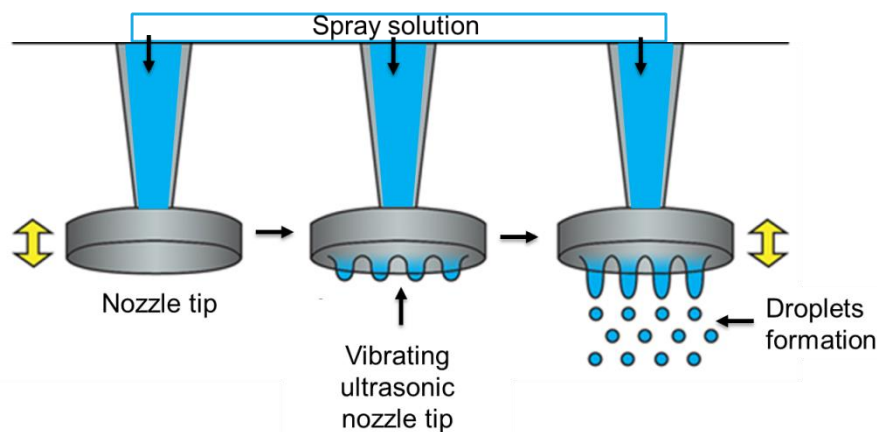
Figure 3.1*: Schematic representation of ultrasonic atomization of spray solution. Figure is modified from[88].*

An Exacta Coat Ultrasonic Spraying System (Sonotek, USA) equipped with an Accumist nozzle has been used in this study as shown in Figure 3.2.
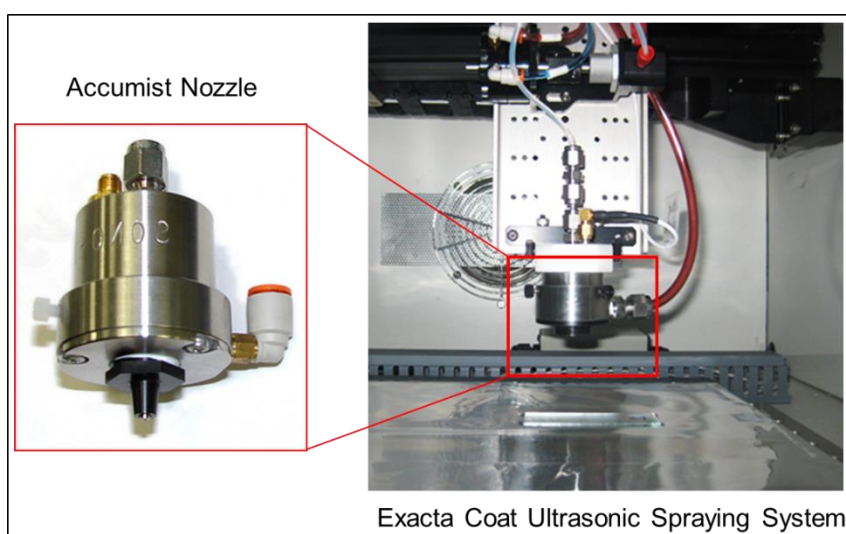
Figure 3.2: *Spray Coating setup at DTU Nanotech. The inset shows the Accumist nozzle used [88].*

A detailed description of the spray coating process and the optimization of the spraying parameters to achieve uniform polymer films form the basis of the paper I. Spray coating has been used in all the other papers (II, III and IV) for coating microcantilevers and microstrings.

3.1.2 Selective coating on cantilevers

Spray coating has been used to completely or selectively coat one side of the microcantilevers with polymer. Microcantilevers are clamped tightly onto a holder fitted with a screw as shown in the

inset of Figure 3.3 before being spray coated with polymer. A cantilever chip contains an array of eight cantilevers. In experimental studies, it is often an advantage to have blank reference cantilevers and polymer coated cantilevers on the same chip. This configuration ensures that both types of cantilevers are subjected to exactly the same experimental condition. For measurement in dynamic mode as in this project, initial experiments were carried out with selectively-coated cantilever chips where two cantilevers were kept blank and the remaining six were coated to see the effect of polymer coating and subsequently the effect of degradation conditions on the resonance frequency of silicon cantilevers.
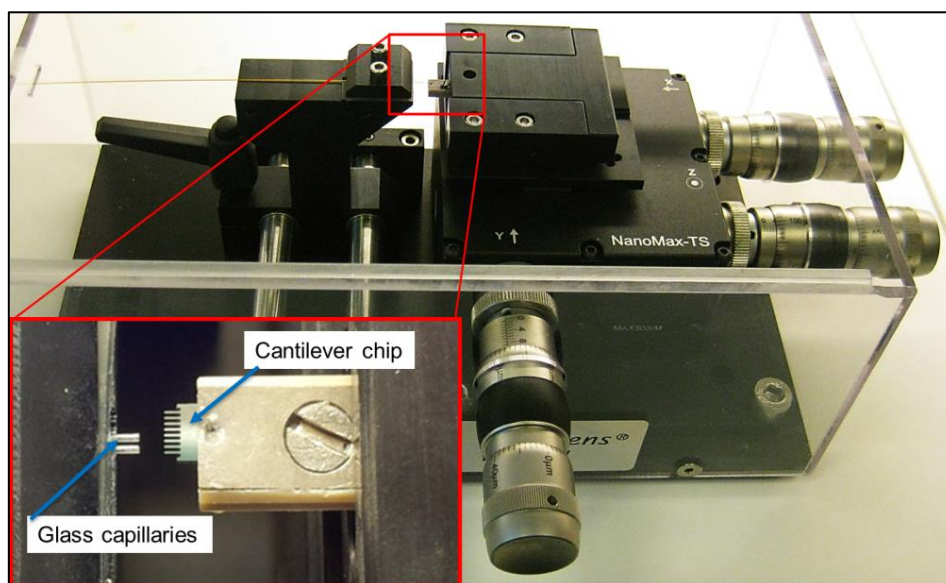
*Figure 3.3:**Functionalization unit Cantisens FU-40 at DTU Nanotech. The inset shows a cantilever chip mounted onto the holder to be inserted into glass capillaries.*

Only after it was confirmed that there is no effect of degradation conditions on a blank reference cantilever, all the experiments shown in paper IV have been executed with eight completely coated cantilevers on a chip. The functionalization unit Cantisens FU-401(Concentris, Switzerland) is a commercially available device which can selectively functionalize individual cantilevers in an array[89] by inserting them into glass capillaries using a precision micromanipulator as shown in Figure 3.3. In this project, these glass capillaries have been used as a shadow mask to prevent spraying on all the cantilevers as shown in Figure 3.4.
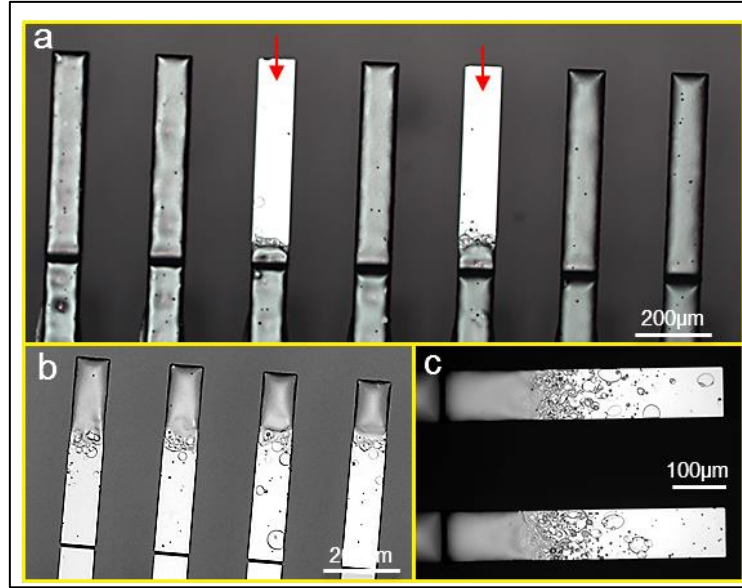
Figure 3.4:*a) Selectively coated (masked cantilevers shown by red arrow), b) tip coated and c) base coated cantilevers*

Two cantilevers (marked with arrows in Figure 3.4a) were inserted inside the glass capillaries before spray coating. These cantilevers can be used as blank references while the other cantilevers in the array are coated with polymers. In another configuration, the cantilever holder cover (Figure 3.3inset) was used as a shadow mask to prepare cantilevers only coated at the tip as shown in Figure **3.4**b. Alternatively, the cantilevers were not completely inserted into the glass capillaries. A gap between the capillaries and the base of the cantilevers limited polymer deposition only to that unmasked area resulting in beams only coated at the base as shown in Figure 3.4c. Localized coatings on cantilever surface like the ones at the tip or at the base as shown in Figure 3.4 influence the ratio of k_{eff}/m_{eff} (as discussed in section 2.2.2) differently and can thus be used for decoupling stiffness and mass effect from a multilayered cantilever. Mass effect is more prominent when there is an addition of mass at the tip of the cantilever (Figure 3.4 b) which results in a decrease in resonance frequency[26] as seen in case of the tip coated cantilever (Figure 3.5). Stiffness effect is more prominent when there is an addition of mass at the base of the cantilever (Figure 3.4 c) which results in an increase in resonance frequency[26] as seen in case of the base coated cantilever (Figure 3.5).
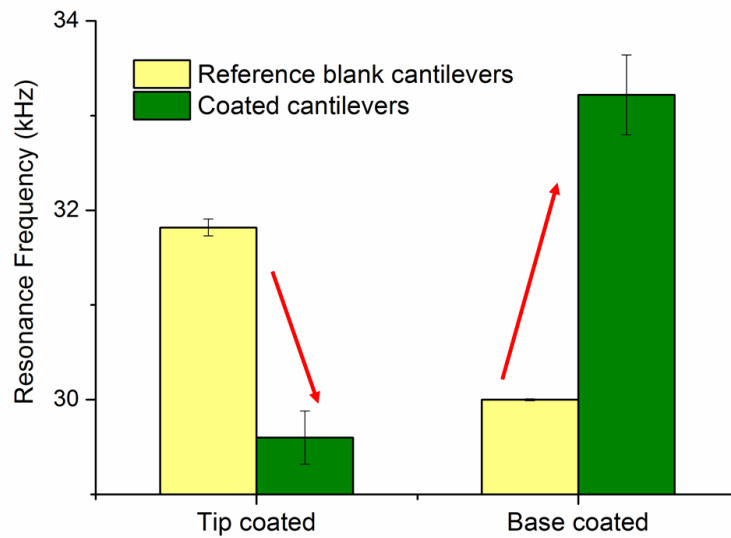
Figure 3.5: *Resonance frequency change of the cantilevers due to tip coating and base coating.*

3.2 Profilometer

A profilometer is an instrument which can be used to study surface topography. There are different kinds of profilometer available based on contact or non-contact working modes[90]. In this project a contact mode based stylus profilometer Dektak 8 (Veeco, USA) has been used. A stylus profilometer can measure film thickness (by scanning step heights and trench depths) as well as surface roughness. The sample is placed on a vacuum chuck to avoid sample displacement during measurement. The diamond tipped stylus which is mechanically coupled to the core of a LVDT (Linear Variable Differential Transformer) is placed vertically in contact with the sample with a specified contact force[91]. The scan stage on which the vacuum chuck is placed then moves for a specified distance as shown schematically is Figure 3.6.
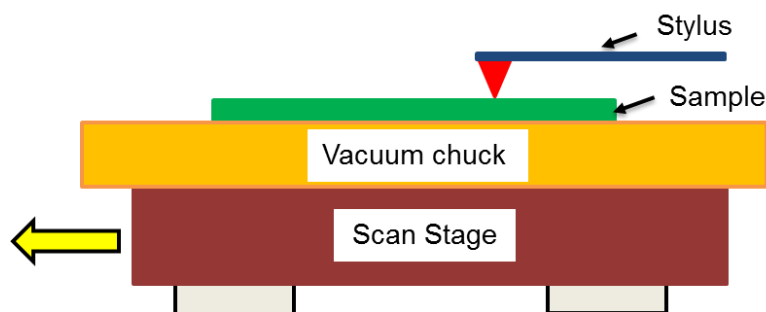
Figure 3.6: *Schematic representation of the contact mode based stylus profilometer.*

The surface topography can be determined from the output of the analog signal generated by the height position of the stylus which is converted into a digital signal, stored, analyzed and displayed[90]. Figure 3.7 shows a profilometer scan of a spray coated film of PDLLA on a glass substrate. Procedure for measuring average roughness (R_a) and thickness (t) is shown in Figure 3.7.

$$R_a = \frac{1}{L} \int_{x=0}^{x=L} |y|\, dx$$
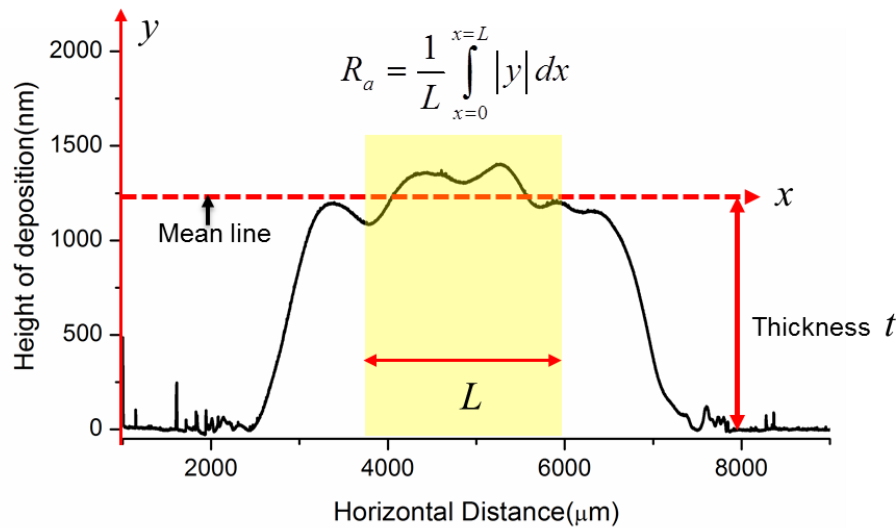
Figure 3.7:A profilometer scan of a spray coated film of PDLLA showing thickness (t) and average roughness (Rₐ)

The height difference between the flat baseline and the top of the rough coating gives the thickness (t) of the film whereas the average roughness R_a is the arithmetic average deviation from the mean line within the scan length (L) as shown in Figure 3.7[91]. Stylus profilometry has been used to measure the thickness and the average roughness of spray coated polymer films on flat substrates as discussed in paper I.

3.3 Laser Doppler Vibrometer

A Laser Doppler vibrometer (LDV) is an instrument that is used to measure out-of-plane vibrations of a surface in non-contact mode. The vibration amplitude and frequency due to motion of the surface can be extracted from the Doppler shift of the reflected laser beam when the laser beam from the LDV is focused on the surface[92]. The working principle of a LDV is explained by the schematic in Figure 3.8.
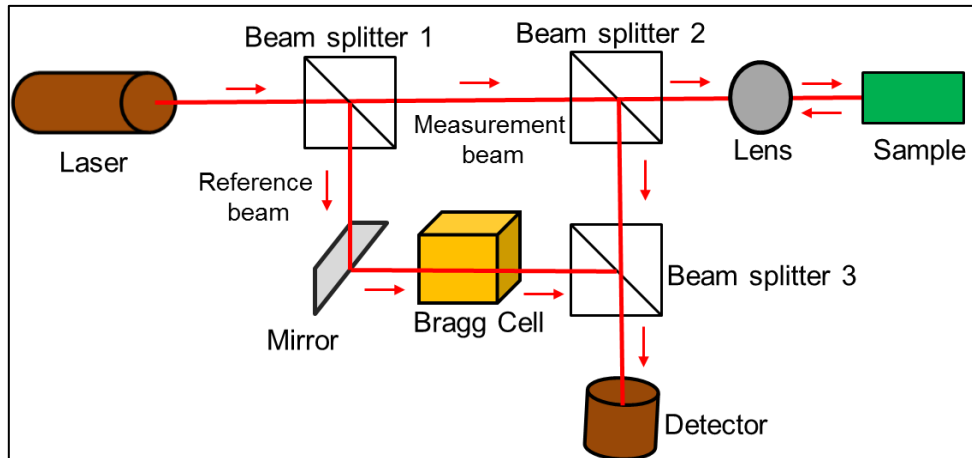
Figure 3.8:*Working principle of a Laser Doppler vibrometer*

If light is scattered from a moving object there is a shift in its frequency. This minute frequency shift of the back scattered light can be detected with a vibrometer by the principle of interferometry. A helium neon laser beam is splitted into measurement beam and reference beam by beam splitter 1. The measurement beam after passing through the beam splitter 2 is directed onto the sample where the beam is scattered due to a moving sample surface. Depending on the velocity and the displacement of the sample, the frequency and the phase of the back scattered light is changed. The characteristics of the motion are completely contained in this backscattered light which is now deflected by the beam splitter 2 towards the beam splitter 3. The reference beam on the other hand is reflected by a mirror towards an acousto-optic modulator (Bragg cell) and ultimately reaches beam splitter 3. The superposition of the reference and the measurement beams in beam splitter 3 creates a modulated output signal reaching the photodetector and revealing the Doppler shift in the frequency. Finally, the signal processing and analysis provides the vibrational velocity and displacement of the test sample[93]. In this project a Laser Doppler vibrometer (MSA-500 from Polytech GmbH, Germany) has been used as shown in Figure 3.9.
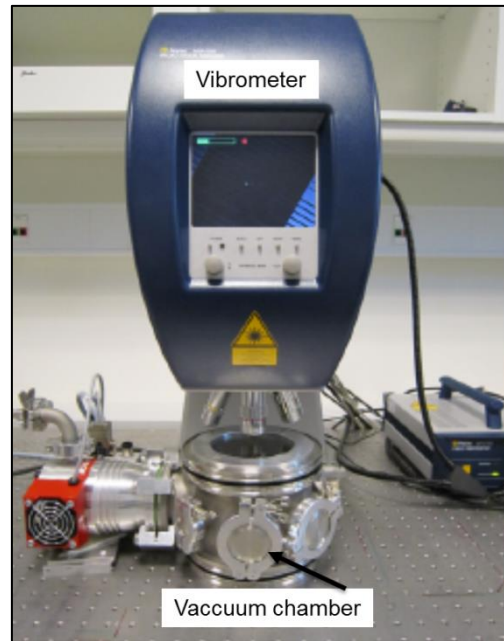
Figure 3.9:*Vibrometer setup at DTU Nanotech. This digital picture is modified from[67].*

The micromechamical resonators are placed in a vacuum chamber under a pressure of 3×10^{-5} mbar established using a turbo pump (HiPace 80, Pfeiffer Vacuum) and a membrane pump (PJ 15347-813.4, Leybold AG) placed in series. The pressure is measured using a MKS 972 DualMag pressure gauge and a MKS PDR900-1 vacuum gauge controller[67]. The Laser Doppler vibrometer has been used to measure resonance frequency and quality factor of microcantilevers and microstrings as shown in paper II, III and IV.

3.4 Differential Scanning Calorimetry (DSC)

DSC measures heat flow differences between a sample and a reference. More precisely, DSC measures the energy necessary to keep the sample and the reference at the same temperature when both of them are subjected to an identical temperature gradient. There are two working modes for DSC: power-compensation and heat-flux[2]. In power compensation DSC, the sample and the reference are kept in separate furnaces and identical temperatures are maintained in both by varying the power input to the two furnaces. The energy required to do this is the measure of the enthalpy or heat capacity changes in the sample relative to the reference[94]. In heat-flux DSC as shown schematically in Figure 3.10, both the sample and the reference are kept in the same furnace connected by a low-resistance heat-flow path to measure the heat exchange. Thermocouples at the base of each platform (Figure 3.10) are used to measure the temperature of the sample and the reference. A third detector (T_0) is used to measure the temperature of the sensor base. The

differential behavior of the sample and the reference is used to measure the material phase transitions as a function of time and temperature[95].
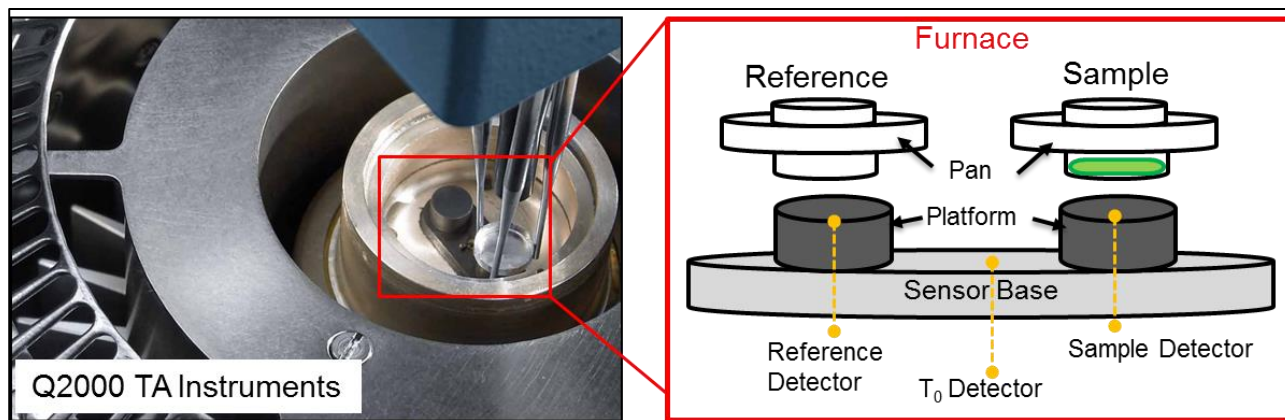
Figure 3.10:*DSC Q2000 from TA instruments and schematic of DSC cell cross-section modified from[95].*

Some of the physical phenomena studied with a DSC are glass transitions (T_g), melting, heats of fusion, crystallinity, oxidative stability or decomposition, curing kinetics etc. [95] as shown by an idealized DSC plot in Figure 3.11.
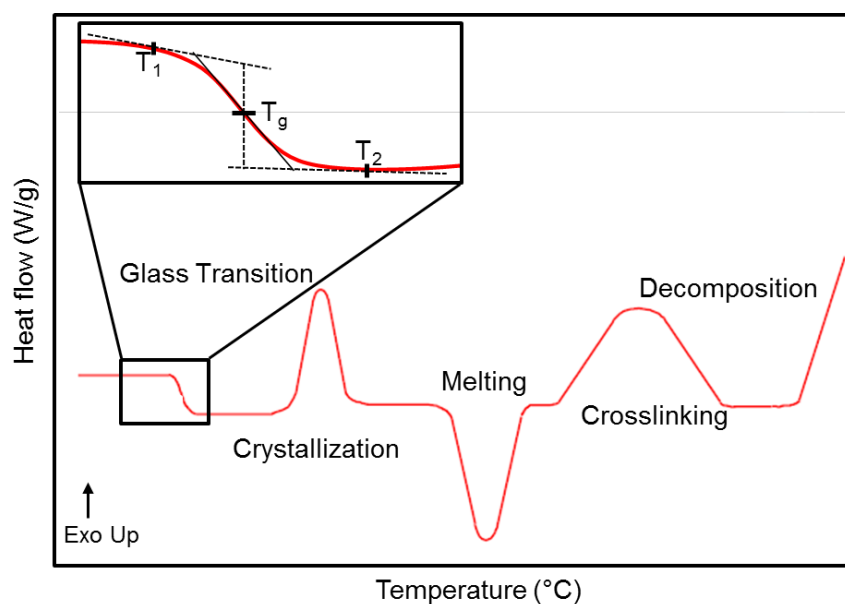
Figure 3.11:*Schematic of a typical DSC curve. The inset shows the detection of glass transition temperature.*

For an exothermic transition (such as crystallization) heat is released from the sample while for endothermic transition (such as melting) more heat is to be supplied to the sample with respect to the reference. In this project DSC has been used to detect the glass transition temperatures of different polymers as shown in paper II and paper III. As seen from Figure 3.11, glass transition is observed as an endothermic shift in the baseline (heat flow signal) due to an increase in the specific-heat capacity of the polymer. Generally T_g is determined from the middle point of the heat flow change plot. Two temperatures, T_1 and T_2 (Figure 3.11 inset) are selected in the linear region of the heat flow curve before and after the transition respectively from where two straight lines are drawn. The mid-point of the tangent to the heat flow change line touching the above drawn lines through T_1 and T_2 marks the glass transition temperature. T_g can also be taken as the inflection point corresponding to the peak in the derivative of the heat flow or heat capacity versus temperature curve[2].

3.5 Dielectric Spectroscopy(DES)

Dielectric spectroscopy measures the ability of dipoles present in a material to align with an oscillating electric field. Since the development of Debye's dipole relaxation theory, DES has been widely used to study conformation, structure and dynamics of polymer systems[96]. The complex dielectric function is given as[96]:

$$\varepsilon^*(\omega) = \varepsilon'(\omega) + i\varepsilon''(\omega) \tag{3.1}$$

where, $i^2 = -1$ and ω is the angular frequency of the alternating current. ε' is the reversible energy stored in the material whereas ε'' is the energy dissipated per cycle of oscillation. The absorption maxima given by the loss tangent $\tan\delta$ or ε'' in a dielectric spectroscopy curve can be evaluated to detect the different relaxations of the polymeric sample (Figure 1.4) when it is placed in between parallel plate capacitors in an alternating electric field[3] as shown in the schematic representation of the DES set up in Figure 3.12. In particular, dielectric analysis provides the most sensitive method to probe local motions along the polymer chain with polar groups, since polar bonds (such as >C=O, ≡C-OH, and >N-H) are directly affected by the electric stimulus. Furthermore DES has a wide range of application frequencies (10µHz-100GHz) which allows it to measure transitions even at higher applied frequencies[2]. DES has been used in this project to find the glass transition temperature of polymers at an applied frequency in the range of $\sim10^5$ Hz as shown in paper II whereas literature values of DES data of β relaxation has been shown to agree well with experimental results in paper III.
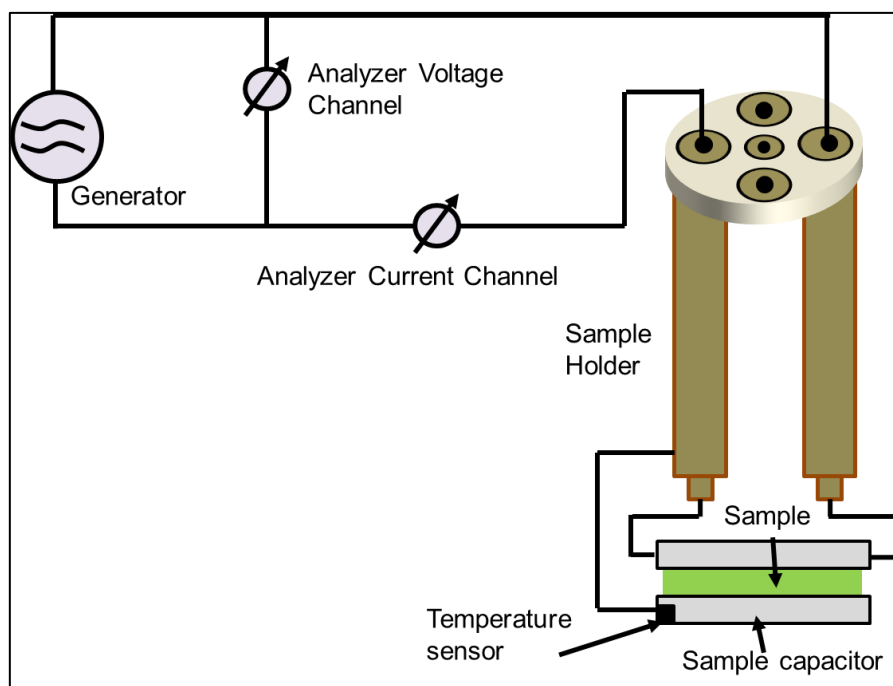
Figure 3.12:*Schematic of DES set up modified from[97]*

3.6 Finite Element Method (FEM)

FEM simulation was performed for the degradation study summarized in paper IV in order to find the change in thickness of the polymer coating on the microcantilever. With the progress of degradation the dimensions of the polymer layer on the cantilever were changing such as the length, width and thickness of the coating. Therefore, it was decided so used FEM simulation using COMSOL 4.4 to determine the degradation rate instead of the analytical model described in section 2.2.2. Image Analysis software was used to measure the lengths and widths of the cantilevers and the polymer coating on the cantilevers during degradation. The thickness of the polymer coatings on the microcantilevers was then calculated with an iterative finite element method[83].

For this purpose, the cantilever has been modelled as a perfectly rectangular structure, rigidly clamped in one end. For the coated cantilevers, another block with different material properties was added on top of the cantilever block. The material data considered are as follows: mass densities and Young's modulus of silicon and polymer are considered to be 2329 Kg/m^3, 1240 Kg/m^3 (taken from manufacturer's data sheet) and 170 GPa, 3.2 GPa[10] respectively. It was assumed that both the modulus and the densities remain constant throughout the experiment. Figure 3.13 shows the simulated first mode of vibration of a singly clamped cantilever beam.
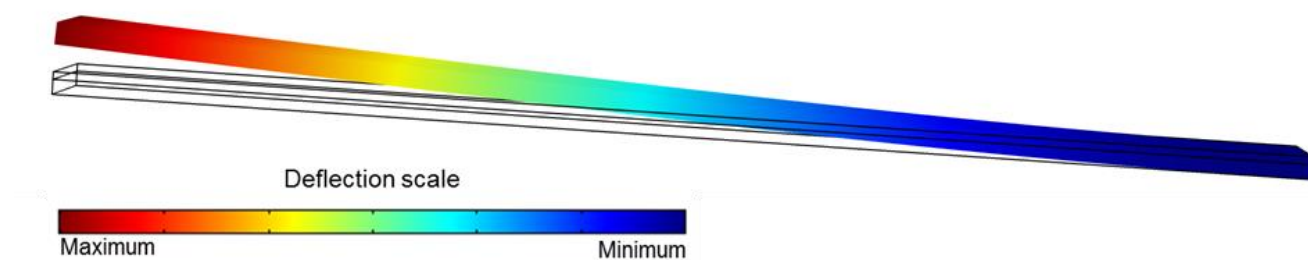
Figure 3.13:Simulated displacement of the first vibrational mode of a singly clamped cantilever beam, red color indicates a point with a maximum deflection.

Furthermore, it was assumed that the polymer layer on top of the cantilever is a uniform, continuous rectangular block as shown in Figure 3.14.
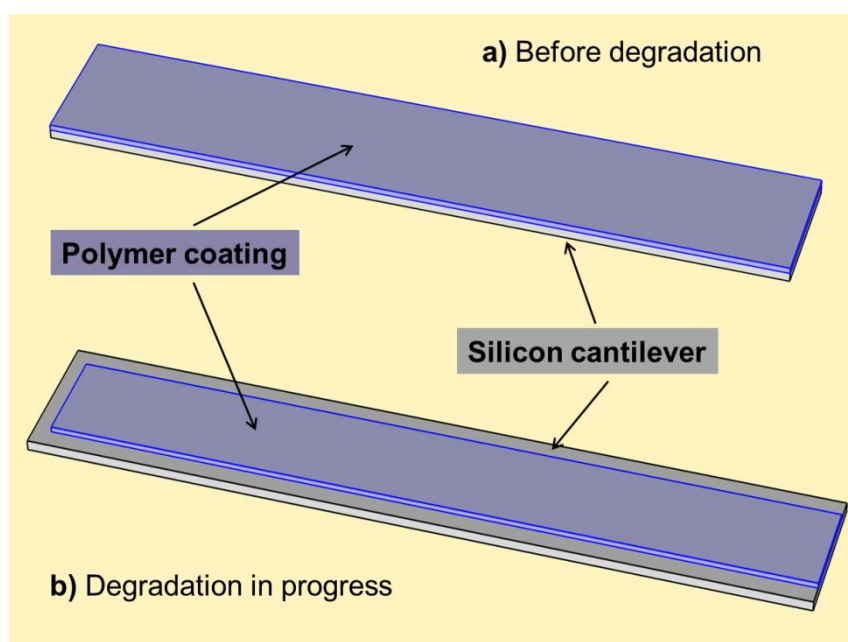
Figure 3.14:Model of polymer coated cantilever (a) before degradation and (b) degradation in progress.

The eigenfrequency of a silicon cantilever with a polymer layer on the top surface was simulated for an estimated thickness of the polymer film. The obtained eigenfrequency was then compared to the measured resonance frequency and the thickness of the polymer coating was iteratively adjusted until the difference of the computed and measured frequency values were below 0.1% of the measured frequency. The change in width and thickness was then used to determine the degradation rates of enzymatic degradation of polymer for a particular degradation condition.

Summary of papers

Chapter 4

Paper I is based on the process optimization of ultrasonic spray coating of polymer films. A detailed study was done on the influence of various spray coating parameters in producing polymer films of uniform thickness (500nm-1μm) and low roughness. Spray coating of polyvinylpyrrolidone (PVP) was used to do a full factorial design of experiments with selected process parameters such as temperature, distance between spraying nozzle and substrate and speed of the spraying nozzle. The distance between spraying nozzle and substrate was found to be the most crucial parameter. Two distinct spray regimes were identified and termed as "wet" and "dry". The optimized condition lies in a narrow window between these two regimes. The processing knowledge obtained with PVP was then applied to spray coat uniform films of PDLLA.

Paper II is based on the development of micromechanical string resonators as an analytical tool for thermal characterization of polymers with only few nanograms of sample. The glass transition temperatures of PDLLA and PLLA were investigated after spray coating on one side of SiN_x microstrings. When subjected to temperature cycles, the change in resonance frequency and Q factor of the spray coated microstrings yield the "static" T_g and the "dynamic" T_g of the polymers simultaneously. The frequency response of the microstring is validated with a derived analytical model. The detected static T_g was confirmed with DSC analysis and the dynamic T_g with DES at $\sim 10^5$ Hz.

Paper III is based on the detection of α- and β-relaxation of polymers by microstrings. The successful detection of the glass transition or α-relaxation of polymers in paper II lead to the investigation of microstring's potential to detect more subtle sub-T_g transitions like the β-relaxation. Polystyrene (PS) and poly (methylmethacrylate) (PMMA) were used for the studies and were spray coated on one side of the microstrings. The change in slope of the resonance frequency curve directly relates to the change in mechanical contribution of the polymer on the static tensile stress of the microstring. From the peaks in the derivative plots of the resonance frequency, both α and β relaxation temperatures were estimated and confirmed by DSC and literature values respectively.

Paper IV is based on the use of microcantilevers as a tool to study enzymatic degradation of PDLLA. PDLLA was spray coated on the microcantilevers and then subjected to buffered proteinase K enzyme solution. The influence of concentration of enzyme solution, pre-hydration in

46

buffer, surface morphology and adsorption time of enzymes on the rate of degradation has been investigated. The degradation rate of the polymer has been estimated by model simulation of multilayered cantilever. The miniaturized cantilever system allows fast analysis of polymer degradation rate which was found to be matching well with the bulk degradation rate of PDLLA reported in literature.

Conclusions and Outlook

Chapter 5

5.1 Conclusions

The aim of this Ph.D. project has been the evaluation of micromechanical resonators like cantilevers and strings as analytical tools for characterization of polymers. Spray coating was used to coat one side of these micro resonators with polymer. Microstrings were used for thermal characterization of polymers and microcantilevers for the analysis of enzymatic degradation of biodegradable polymers.

Process optimization of different spray coating parameters was carried out with two sets of polymer-solvent systems to obtain homogeneous films with uniform thickness and low roughness. Analysis of the full factorial experimental design identified the nozzle-substrate distance as the most important parameter among the crucial parameters of spray coating which also include the temperature of the substrate and the speed of the spraying nozzle. Low spraying speed at room temperature was found to be ideal for formation of continuous uniform film. Two broad regimes of film deposition were detected: "dry" and "wet" depending on the drying and coalescence of the spray drops after reaching the substrate. The limitation of the wet regime was the formation of edge peaks and the one of the dry regime was very rough surface. An optimized condition was identified in a narrow window between these two regimes where a uniform film with low roughness and no edge peaks was obtained.

Thermal characterizations of polymers were successfully executed by using micromechanical string resonators. Silicon nitride microstrings were spray coated with polymers and subjected to heating cycles and the change in resonance frequency and Q factor was simultaneously observed. Both α- and β-relaxation temperatures of different polymers were detected and confirmed by DSC, DES and literature values. The microstrings facilitated fast, sensitive and quasi-static measurements on reduced sample size (few nanograms) compared to conventional polymer characterization by thermal techniques. An analytical model was derived to understand the resonance frequency change of the polymer coated microstrings during heating below and above glass transition. From the resonance frequency change the quasi-static glass transition temperature of polymers was observed while the Q factor change provided the frequency dependent shift of glass transition to higher temperature.

Microcantilevers were successfully employed for detailed investigation of enzymatic degradation of the biodegradable polymer PDLLA. The resonance frequencies of the cantilevers were measured before and after spray coating with PDLLA and at regular intervals during the degradation process. From the relative shift in the resonance frequency compared to the initially blank cantilever, progress of degradation was monitored. A bulk degradation rate of 0.24 µg mm^{-2} hour^{-1} was estimated from experimental results and model simulation of multilayered cantilever structures which matches well with literature values where the study was done on larger sample size and for significantly longer time. Thus microcantilevers provide a platform for fast estimation of degradation rate of polymer with minute amount of sample compared to conventional techniques. The study showed that surface morphology plays a pivotal role in determining degradation rate. A threshold time of around 3 hours is essential for enzyme adsorption on the polymer coating after which degradation can proceed even in the absence of enzyme in the solution.

In conclusion, through this Ph.D. project a successful bridge between the parallel activities in NAMEC has been established where the micromechanical resonators from the "Sensor" part were used for characterization of different polymers used in the "Drug delivery" part. The basic understanding of the spray coating process and new approaches developed through the evaluation of microstrings and microcantilevers as analytical tools can in future be applied to different polymers and pharmaceutical systems.

5.2 Outlook

In the future, the application of microstrings can be extended beyond polymers to proteins and pharmaceutical drugs which do not show significant change in heat capacity during transitions and are not suitable for detection by conventional DSC[30]. Since the molecular mobility determines the physical and chemical stability of the drugs, the knowledge of mechanical relaxation temperatures of such samples is crucial to identify their proper storage conditions. Due to the sufficiency of low sample volumes for thermal characterization by microstrings, novel synthesized precious polymers or blends can also be evaluated.

The biodegradation study performed in this thesis has used the dynamic mode for cantilevers where the resonance frequency has been measured to estimate degradation rate. Some initial studies have been performed with the same PDLLA-proteinase K system but using the static mode of operation

of microcantilevers. A DVD-ROM based high-throughput cantilever sensing platform was used for this purpose[98]. The optics and mechanics from a DVD player were used to handle liquid samples and for simultaneous monitoring of cantilever deflection and optical roughness of the polymer coated cantilever surface during degradation. Selectively coated cantilevers (where two cantilevers were blank while the others were coated with PDLLA) were loaded into reservoirs made on the DVD disc-like substrate. Below the disc, DVD-ROM optical pickup heads provide the read-out system. The disc is rotated and the DVD laser beam is focused on the cantilevers. The deflection profiles are measured using the astigmatic detection mechanism embedded in the DVD-ROM system[99]. Differential deflection between the blank reference cantilever and the coated cantilevers can be recorded when enzyme solution is passed through the reservoir at a fixed flow rate. However, the data obtained from the initial experiments revealed that further optimization of the experimental set up and the data analysis is required to detect polymer deflection and change in roughness due to degradation by the DVD-ROM system.

The characterization of degradation of polymers on microcantilevers can not only be extended to other polymers that are used for biomedical or drug delivery purposes but also to non-biodegradable conventional polymers which are used in several other applications. Studies on the influence of a variety of degradation media such as gastrointestinal fluid will be interesting for *in vitro* estimation of *in vivo* degradation rates for biodegradable polymers used in biomedical field. This new approach will also allow fast analysis of the influence of temperature and chemicals on conventional polymers for specific applications.

Bibliography

1. Polymer Characterization. http://en.wikipedia.org/wiki/Polymer_characterization. Accessed 29 Aug 2014

2. Chartoff, R. P.; Menczel, J. D.; Dillman SH (2009) Thermal Analysis of Polymer Fundamental and Applications. John Wiley & Sons, Inc., New Jersey, USA

3. Sperling LH (2005) Introduction to Physical Polymer Science, Fourth. John Wiley & Sons, Inc., New Jersey, USA

4. Mark J (ed) (2007) Physical properties of polymers handbook, Second. Springer, New York, USA

5. Hayashi T (1994) Biodegradable polymers for biomedical uses. Prog Polym Sci 19:663–702

6. Ulery BD, Nair LS, Laurencin CT (2011) Biomedical Applications of Biodegradable Polymers. J Polym Sci B Polym Phys 49:832–864

7. Lin YM, Boccaccini a R, Polak JM, Bishop a E, Maquet V (2006) Biocompatibility of poly-DL-lactic acid (PDLLA) for lung tissue engineering. J Biomater Appl 21:109–118

8. Tokiwa Y, Calabia BP (2006) Biodegradability and biodegradation of poly(lactide). Appl Microbiol Biotechnol 72:244–251

9. Datta R, Henry M (2006) Lactic acid: recent advances in products, processes and technologies — a review. J Chem Technol Biotechnol 81:1119–1129

10. Auras R, Lim L, Selke S, Tsuji H (2011) Poly (lactic acid): synthesis, structures, properties, processing, and applications. John Wiley & Sons, Inc., New Jersey, USA

11. Tsuji H, Ogiwara M, Saha SK, Sakaki T (2006) Enzymatic, alkaline, and autocatalytic degradation of poly(L-lactic acid): effects of biaxial orientation. Biomacromolecules 7:380–387

12. Zeng J, Chen X, Liang Q, Xu X, Jing X (2004) Enzymatic degradation of poly(L-lactide) and poly(epsilon-caprolactone) electrospun fibers. Macromol Biosci 4:1118–1125

13. Shih C (1995) Chain-end scission in acid catalyzed hydrolysis of poly (d,l-lactide) in solution. J Control Release 34:9–15

14. Södergård A, Selin J-F, Näsman JH (1996) Hydrolytic degradation of peroxide modified poly(L-lactide). Polym Degrad Stab 51:351–359

15. Cam D, Hyon S, Ikada Y (1995) Degradation of high molecular weight poly(l-lactide) in alkaline medium. Biomaterials 16:833–843

16. Tsuji H, Ikada Y (1998) Properties and morphology of poly(L-lactide). II. hydrolysis in alkaline solution. J Polym Sci Part A Polym Chem 36:59–66

17. Xu L, Crawford K, Gorman CB (2011) Effects of Temperature and pH on the Degradation of Poly(lactic acid) Brushes. Macromolecules 44:4777–4782

18. Larsen T, Schmid S, Grönberg L, Niskanen a. O, Hassel J, Dohn S, Boisen A (2011) Ultrasensitive string-based temperature sensors. Appl Phys Lett 98:121901

19. Schmid S, Wägli P, Hierold C (2008) All-Polymer Microstring Resonant Humidity Sensor with Enhanced Sensitivity due to Change of Intrinsic Stress. Proc. EUROSENSORS XXII Conf. pp 697–700

20. Boisen A, Dohn S, Keller SS, Schmid S, Tenje M (2011) Cantilever-like micromechanical sensors. Reports Prog Phys 74:036101

21. Schmid S, Dohn S, Boisen A (2010) Real-time particle mass spectrometry based on resonant micro strings. Sensors 10:8092–8100

22. Chen GY, Thundat T, Wachter E a., Warmack RJ (1995) Adsorption-induced surface stress and its effects on resonance frequency of microcantilevers. J Appl Phys 77:3618–3622

23. Yun M, Yim C, Jung N, Kim S, Thundat T, Jeon S (2011) Nanomechanical Thermal Analysis of Photosensitive Polymers. Macromolecules 44:9661–9665

24. Yun M, Yim C, Jung N, Kim S, Thundat T, Jeon S (2011) Nanomechanical Thermal Analysis of Photosensitive Polymers. Macromolecules 44:9661–9665

25. Lochon F, Fadel L, Dufour I, Rebière D, Pistré J (2006) Silicon made resonant microcantilever: Dependence of the chemical sensing performances on the sensitive coating thickness. Mat Sci Eng C 26:348–353

26. Tamayo J, Kosaka PM, Ruz JJ, San Paulo Á, Calleja M (2013) Biosensors based on nanomechanical systems. Chem Soc Rev 42:1287–1311

27. Bershtein VA, Egorov VM, Egorova LM, Ryzhov VA (1994) The role of thermal analysis in revealing the common molecular nature of transitions in polymers. Thermochim Acta 238:41–73

28. Yano O, Wada Y (1971) Dynamic mechanical and dielectric relaxations of polystyrene below the glass temperature. J Polym Sci Part A-2 Polym Phys 9:669–686

29. Krevelen D Van, Nijenhuis K Te (2009) Properties of polymers: their correlation with chemical structure; their numerical estimation and prediction from additive group contributions, Fourth. Elsevier B.V., Amsterdam, The Nederlands

30. Reddy R, Chang L' L', Luthra S, Collins G, Lopez C, Shamblin SL, Pikal MJ, Gatlin LA, Shalaev EY (2009) The glass transition and sub-T(g)-relaxation in pharmaceutical powders and dried proteins by thermally stimulated current. J Pharm Sci 98:81–93

31. Yoshioka S, Aso Y (2005) Glass transition-related changes in molecular mobility below glass transition temperature of freeze-dried formulations, as measured by dielectric spectroscopy and solid state nuclear magnetic resonance. J Pharm Sci 94:275–287

32. Foreman J, Sauerbrunn S, Marcozzi C (2006) Exploring the sensitivity of thermal analysis techniques to the glass transition Document reference: TA082. In: TA Instruments Therm. Anal. Rheol. http://www.tainst.com. Accessed 20 Aug 2014

33. Sengers WGF, van den Berg O, Wübbenhorst M, Gotsis a. D, Picken SJ (2005) Dielectric spectroscopy using dielectric probes: a new approach to study glass transition dynamics in immiscible apolar polymer blends. Polymer 46:6064–6074

34. Jakobsen B, Niss K, Maggi C, Olsen NB, Christensen T, Dyre JC (2011) Beta relaxation in the shear mechanics of viscous liquids: Phenomenology and network modeling of the alpha-beta merging region. J Non Cryst Solids 357:267–273

35. Pathmanathan K, Johari GP, Faivre JP, Monnerie L (1986) A dielectric study of secondary relaxations and the "memory effect" in two compatible polystyrene blends. J Polym Sci Part B Polym Phys 24:1587–1595

36. McCrum N, Read B, Williams G (1991) Anelastic and dielectric effects in polymeric solids. Dover Publications, New York

37. Pollock HM, Hammiche A (2001) Micro-thermal analysis: techniques and applications. J Phys D Appl Phys 34:R23–R53

38. Meincken M, Graef S, Mueller-Nedebock K, Sanderson RD (2002) Thermal transitions of polymers measured by atomic force microscopy. Appl Phys A Mater Sci Process 74:371–375

39. Thundat T, Sharp SL, Fisher WG, Warmack RJ, Wachter EA (1995) Micromechanical radiation dosimeter. Appl Phys Lett 66:1563–1565

40. Yun M, Jung N, Yim C, Jeon S (2011) Nanomechanical thermal analysis of the effects of physical aging on glass transitions in PS/PMMA blend and PS-PMMA diblock copolymers. Polymer 52:4136–4140

41. Jung N, Jeon S (2008) Nanomechanical Thermal Analysis with Silicon Cantilevers of the Mechanical Properties of Poly(vinyl acetate) near the Glass Transition Temperature. Macromolecules 41:9819–9822

42. Jung N, Seo H, Lee D, Ryu CY, Jeon S (2008) Nanomechanical Thermal Analysis of the Glass Transition of Polystyrene Using Silicon Cantilevers. Macromolecules 41:6873–6875

43. Liu T, Pihan S, Roth M, Retsch M, Jonas U, Gutmann JS, Koynov K, Butt H-J, Berger R (2012) Frequency Response of Polymer Films Made from a Precursor Colloidal Monolayer on a Nanomechanical Cantilever. Macromolecules 45:862–871

44. Ayela C, Heinrich SM, Josse F, Dufour I (2011) Resonant Microcantilevers for the Determination of the Loss Modulus of Thin Polymer Films. J Microelectromechanical Syst 20:788–790

45. Olson E a., Efremov MY, Allen LH (2003) The design and operation of a mems differential scanning nanocalorimeter for high-speed heat capacity measurements of ultrathin films. J Microelectromechanical Syst 12:355–364

46. Efremov MY, Warren JT, Olson EA, Zhang M, Kwan AT, Allen LH (2002) Thin-Film Differential Scanning Calorimetry: A New Probe for Assignment of the Glass Transition of Ultrathin Polymer Films. Macromolecules 35:1481–1483

47. Chen Q-Z, Harding SE, Ali NN, Lyon AR, Boccaccini AR (2008) Biomaterials in cardiac tissue engineering: Ten years of research survey. Mater Sci Eng R Reports 59:1–37

48. Yamashita K, Kikkawa Y, Kurokawa K, Doi Y (2005) Enzymatic degradation of poly(L-lactide) film by proteinase K: quartz crystal microbalance and atomic force microscopy study. Biomacromolecules 6:850–857

49. Dan, Scott Gilead D (ed) (1995) Degradable polymers: principles and applications. Chapman & Hall, London, UK

50. Engineer C, Parikh J, Raval A (2011) Review on hydrolytic degradation behavior of biodegradable polymers from controlled drug delivery system. Trends Biomater Artif Organs 25:79–85

51. Tsuji H, Mizuno A, Ikada Y (2000) Properties and morphology of poly(L-lactide). III. Effects of initial crystallinity on long-termin vitro hydrolysis of high molecular weight poly(L-lactide) film in phosphate-buffered solution. J Appl Polym Sci 77:1452–1464

52. Williams DF (1982) Biodegradation of surgical polymers. J Mater Sci 17:1233–1246

53. Ashley, SL and McGinity J (1989) Enzyme-mediated drug release from poly (d, l-lactide) matrices. Congr Int Technol Pharm 5:195–204

54. Reeve MS, McCarthy SP, Downey MJ, Gross RA (1994) Polylactide stereochemistry: effect on enzymic degradability. Macromolecules 27:825–831

55. Shirahama H, Mizuma K, Umemoto K, Yasuda H (2001) Synthesis of poly(lactide-ran-MOHEL) and its biodegradation with proteinase K. J Polym Sci Part A Polym Chem 39:1374–1381

56. Cai H, Dave V, Gross R a., McCarthy SP (1996) Effects of physical aging, crystallinity, and orientation on the enzymatic degradation of poly(lactic acid). J Polym Sci Part B Polym Phys 34:2701–2708

57. Li S, McCarthy S (1999) Further investigations on the hydrolytic degradation of poly (DL-lactide). Biomaterials 20:35–44

58. Saha SK, Tsuji H (2006) Effects of molecular weight and small amounts of d-lactide units on hydrolytic degradation of poly(l-lactic acid)s. Polym Degrad Stab 91:1665–1673

59. Kikkawa Y, Hirota T, Numata K, Tsuge T, Abe H, Iwata T, Doi Y (2004) In-situ atomic force microscopy observation of enzymatic degradation in poly(hydroxyalkanoic acid) thin films: normal and constrained conditions. Macromol Biosci 4:276–285

60. Kikkawa Y, Abe H, Iwata T, Inoue Y, Doi Y (2002) Crystallization, Stability, and Enzymatic Degradation of Poly(l -lactide) Thin Film. Biomacromolecules 3:350–356

61. Keller SS, Gammelgaard L, Jensen MP, Schmid S, Davis ZJ, Boisen a. (2011) Micromechanical sensors for the measurement of biopolymer degradation. 2011 IEEE 24th Int Conf Micro Electro Mech Syst 457–460

62. Yamashita K, Funato T, Suzuki Y, Teramachi S, Doi Y (2003) Characteristic Interactions between Poly(hydroxybutyrate) Depolymerase and Poly[(R)-3-hydroxybutyrate] Film Studied by a Quartz Crystal Microbalance. Macromol Biosci 3:694–702

63. Wolff O, Seydel E, Johannsmann D (1997) Viscoelastic properties of thin films studied with quartz crystal resonators. Faraday Discuss 107:91–104

64. Vogt BD, Soles CL, Lee H, Lin EK, Wu W (2005) Moisture absorption into ultrathin hydrophilic polymer films on different substrate surfaces. Polymer 46:1635–1642

65. Quan X, Heiskanen A, Sun Y, Labuda A, Wolff A, Jorge Dulanto J, Grutter P, Tenje M, Boisen A (2013) Development of Electrochemical Cantilever Sensors for DNA Applications. ECS Trans 50:77–81

66. Khan MF, Schmid S, Larsen PE, Davis ZJ, Yan W, Stenby EH, Boisen a. (2013) Online measurement of mass density and viscosity of pL fluid samples with suspended microchannel resonator. Sensors Actuators B Chem 185:456–461

67. Larsen T (2012) Micro-Mechanical Temperature Sensors. Technical University of Denmark

68. Nielsen LH, Keller SS, Gordon KC, Boisen A, Rades T, Müllertz A (2012) Spatial confinement can lead to increased stability of amorphous indomethacin. Eur J Pharm Biopharm 81:418–425

69. Nagstrup J (2012) Micro fabrication of biodegradable polymer drug delivery devices. Technical University of Denmark

70. Marizza P, Keller SS, Müllertz A, Boisen A (2014) Polymer-filled microcontainers for oral delivery loaded using supercritical impregnation. J Control Release 173:1–9

71. Lang HP, Hegner M, Gerber C (2005) Cantilever array sensors. Mater Today 8:30–36

72. Quan X (2013) Development of an Electrochemical Cantilever Platform for Bio / Chemical Application. Technical University of Denmark

73. Rasmussen PA (2003) Cantilever-based Sensors for Surface Stress Measurements. Technical University of Denmark

74. Stevenson KA, Mehta A, Sachenko P, Hansen KM, Thundat T (2002) Nanomechanical Effect of Enzymatic Manipulation of DNA on Microcantilever Surfaces. Langmuir 18:8732–8736

75. Maloney N, Lukacs G, Ball SL, Hegner M (2014) Device for filamentous fungi growth monitoring using the multimodal frequency response of cantilevers. Rev Sci Instrum 85:015003

76. Battiston F., Ramseyer J-P, Lang H., Baller M., Gerber C, Gimzewski J., Meyer E, Güntherodt H-J (2001) A chemical sensor based on a microfabricated cantilever array with simultaneous resonance-frequency and bending readout. Sensors Actuators B Chem 77:122–131

77. Kim S, Lee D, Yun M, Jung N, Jeon S, Thundat T (2013) Multi-modal characterization of nanogram amounts of a photosensitive polymer. Appl Phys Lett 102:024103–1–4

78. Brand O, Baltes H (1998) Micromachined Resonant Sensors— an Overview. Sensors Updat 4:3–51

79. Schmid S (2014) Theme M : Nanomechanical Resonators, Lecture Notes Nano-2:Nanosystems Engineering. 1–67

80. Minhang Bao (2005) Analysis and Design Principles of MEMS Devices, First. Elsevier, Amsterdam

81. Tamayo J, Ramos D, Mertens J, Calleja M (2006) Effect of the adsorbate stiffness on the resonance response of microcantilever sensors. Appl Phys Lett 89:224104–1–3

82. Davis Z (2009) NanoElectro Mechanical Systems (NEMS).

83. Schmid S (2009) Electrostatically Actuated All-Polymer Microbeam Resonators - Characterization and Application. Sci reports Micro Nanosyst Vol6 Der Andere Verlag, Zurich, Switzerland

84. Schmid S (2013) Organic Resonant MEMS Devices.

85. Ward I., Sweeny J (2004) An Introduction to the Mechanical Properties of Solid Polymers, 2nd ed. John Wiley & Sons, Inc., West Sussex, England

86. Schmid S, Jensen K, Nielsen K, Boisen A (2011) Damping mechanisms in high-Q micro and nanomechanical string resonators. Phys Rev B 84:1–6

87. Tobiska S, Kleinebudde P (2003) Coating uniformity: influence of atomizing air pressure. Pharm Dev Technol 8:39–46

88. Ultrasonic Nozzle. http://www.sono-tek.com/ultrasonic-nozzle-technology/. Accessed 22 Aug 2014

89. Baller M, Lang H, Fritz J, et al (2000) A cantilever array-based artificial nose. Ultramicroscopy 82:1–9

90. Profilometer. http://en.wikipedia.org/wiki/Profilometer. Accessed 23 Aug 2014

91. Chi T, Ballinger T, Olds R, Zecchino M (2005) Surface texture analysis using dektak stylus profilers. In: Veeco Instruments Appl. http://afsws.rpi.edu/dept/cie/mncr/documents/AN525_Dektak_Surface.pdf. Accessed 27 Aug 2014

92. Laser Doppler Vibrometer. http://en.wikipedia.org/wiki/Laser_Doppler_vibrometer. Accessed 24 Aug 2014

93. Polytec. http://www.polytec.com/us/solutions/vibration-measurement/basic-principles-of-vibrometry. Accessed 24 Aug 2014

94. Bhadeshia HKDH Differential Scanning Calorimetry. http://www.uzaktanegitimplatformu.com/UEP/uep_ylisans/ey2/ey2_download/DSC Thermal2.pdf. Accessed 28 Aug 2014

95. Differential Scanning Calorimetry. http://lipidlibrary.aocs.org/physics/dsc/index.htm. Accessed 25 Aug 2014

96. Schönhals A (1998) Dielectric spectroscopy on the dynamics of amorphous polymeric systems. Novocontrol 1–17

97. Dielectric Spectroscopy. http://centers.njit.edu/mclab/instruments/dielectric-spectrometer.php. Accessed 25 Aug 2014

98. Bosco FG (2011) A DVD-ROM based high-throughput cantilever sensing platform. Technical University of Denmark

99. Hwu E-T, Liao H-S, Bosco FG, Chen C-H, Keller SS, Boisen A, Huang K-Y (2012) An Astigmatic Detection System for Polymeric Cantilever-Based Sensors. J Sensors 2012:1–7

Appendix

Paper I

Process Optimization of Ultrasonic Spray Coating of Polymer Films

Process Optimization of Ultrasonic Spray Coating of Polymer Films

Sanjukta Bose,[†] Stephan S. Keller,*,[†] Tommy S. Alstrøm,[‡] Anja Boisen,[†] and Kristoffer Almdal[†]

[†]Department of Micro- and Nanotechnology, Technical University of Denmark, DK-2800 Kongens Lyngby, Denmark

[‡]Department of Applied Mathematics and Computer Science, Technical University of Denmark, DK-2800 Kongens Lyngby, Denmark

ABSTRACT: In this work we have performed a detailed study of the influence of various parameters on spray coating of polymer films. Our aim is to produce polymer films of uniform thickness (500 nm to 1 μm) and low roughness compared to the film thickness. The coatings are characterized with respect to thickness, roughness (profilometer), and morphology (optical microscopy). Polyvinylpyrrolidone (PVP) is used to do a full factorial design of experiments with selected process parameters such as temperature, distance between spray nozzle and substrate, and speed of the spray nozzle. A mathematical model is developed for statistical analysis which identifies the distance between nozzle and substrate as the most significant parameter. Depending on the drying of the sprayed droplets on the substrate, we define two broad regimes, "dry" and "wet". The optimum condition of spraying lies in a narrow window between these two regimes, where we obtain a film of desired quality. Both with increasing nozzle-substrate distance and temperature, the deposition moves from a wet state to a dry regime. Similar results are also achieved for solvents with low boiling points. Finally, we study film formation during spray coating with poly (D,L-lactide) (PDLLA). The results confirm the processing knowledge obtained with PVP and indicate that the observed trends are identical for spraying of other polymer films.
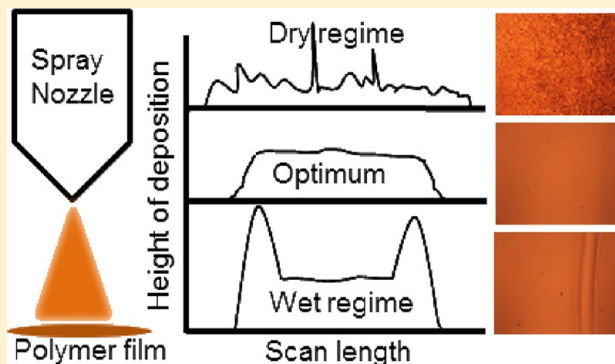
INTRODUCTION

Polymer thin film coatings are the subject of interest for a broad scientific community due to a large number of potential applications. Their use ranges from photovoltaic cells,[1] electrochemical devices,[2] and chemical[3] and biological sensors[4] to biomedical applications like drug delivery, tissue engineering, and biocompatible implants.[5] Among a host of possible polymer film coating techniques, such as spin coating, bar coating, inkjet printing, and screen printing,[6] spray coating has come up with the advantage of being able to coat three-dimensional microstructures like cantilevers,[7] microneedle arrays for drug delivery,[8] and nonplanar surfaces for nano-electromechanical systems (NEMS) and microelectromechanical systems (MEMS) applications.[9,10] Pham et al. have shown the advantage of spray coating photo resist on high topography surfaces for applications in MEMS.[11] Pan et al. have used spray coating to fabricate drug eluting stainless steel stents by coating them with biodegradable polymer acting as drug carrier.[12]

Spray coating in general includes the formation of fine droplets of a coating solution and their deposition and coalescence on a substrate. The liquid to be used for coating breaks up into small droplets by atomization in the spray nozzle. The generated droplets are then deposited on a substrate kept below the spray nozzle where they coalesce to form a coating. Conventionally, air pressure is used for the atomization where the liquid coming through the nozzle is broken down into tiny droplets upon passage through a narrow orifice.[13] Alternatively, the ultrasonic atomization technique, in which high frequency sound vibration generates a fine mist of solution, is used for spray coating and often preferred over pneumatic atomization.[14] Overall, the advantages of ultrasonic spray coating are as follows: simplicity, good transfer efficiency, economical, precise conformal coating on planar and nonplanar surfaces, generation of small droplets in the micrometer range, and good reproducibility.[11,15] Spray coating is associated with many material and process parameters which must be controlled in order to obtain a uniform film. The concentration of the polymer solution, the solvent used, the substrate on which the solution is sprayed, the number of spray passes, the flow rate of the polymer solution, the temperature of the substrate, the distance between the spray nozzle and the substrate, the speed of the moving nozzle during spraying, and the air pressure which transports the sprayed droplets to the substrate are all to be taken into consideration. The large number of parameters indicates the need for systematic process optimization. Perfetti and co-workers[16] and McGrath et al.[8] have investigated the influence of different spraying parameters based on design of experiments (DoE) and subsequent experimental analysis. Perfetti reported the distance between spray nozzle and substrate as one of the main factors affecting film uniformity. McGrath highlighted the physicochemical properties of the coating solution and the substrate

composition as major factors determining the coalescence of droplets after deposition.

Here we report a detailed study of the influence and intercorrelation of various parameters on the quality of the resulting coating. An ultrasonic spray nozzle with programmable $x-y$ motion is used for spraying onto a substrate placed on a stationary temperature-controlled stage. We have used an aqueous solution of the biocompatible polymer polyvinylpyrollidone (PVP) to do a full factorial design of experiments with selected process parameters, such as temperature, distance between spray nozzle and substrate, and speed of the spray nozzle. Statistical analysis is used as a guideline to perform a more in depth study of the most influencing parameters. Our observations lead to the conclusion that the optimum parameter space for spray coating is narrow. To produce a smooth film, one needs to find conditions which are on the border between a dry regime (where dried sprayed drops cover the substrate surface) and a wet regime (which is equivalent to casting of a solution on the surface followed by slow drying). We use a shadow mask (described in detail in the Experimental Section) to prevent some area of the substrate from being coated with the spraying solution. In preliminary experiments, the well-known "coffee-ring effect" has been observed, which is described by Deegan et al. as the result of capillary flow[17] where liquid evaporates faster from the pinned contact line of a deposited solution and is replenished by additional liquid from inside. Accumulation of polymer after solvent evaporation is seen at the edges of the coated areas defined by the shadow mask, as also observed by Dubourg et al.[18] We have named these structures "edge peaks". The aim of our study is to eradicate this edge effect and to have a continuous film of PVP with uniform thickness (500 nm to 1 μm) and minimal roughness compared to the film thickness. In a final study, we utilize and generalize our gained understanding to spray coat a solution of the biodegradable polymer poly (D,L-lactide) (PDLLA) in cyclohexanone.

■ EXPERIMENTAL SECTION

Materials. PVP (K30, M_w 40 000 g/mol) and PDLLA (ester terminated, M_w 16 000 g/mol) were obtained in powder form. Solvents used were cyclohexanone [boiling point (b.p.) 155 °C, density (ρ) 0.947 g/mL at 20 °C], dichloromethane (b.p. 40 °C, ρ 1.33 g/mL at 20 °C), toluene (b.p. 110 °C, ρ 0.86 g/mL at 20 °C) and water. All chemicals were procured from Sigma Aldrich and used as received.

Process optimization was done with solutions of PVP in water and PDLLA in cyclohexanone. Solutions of PVP in dichloromethane and PDLLA in dichloromethane and in toluene were used to compare the effect of the variation of solvent boiling point on film formation. For all experiments, 0.5 wt % of polymer solution was prepared by stirring the solution at room temperature.

Spray Coating. Spray coating was done in an Exacta Coat Ultrasonic Spraying System (Sonotek, U.S.) equipped with an AccuMist nozzle. The main components are illustrated in Figure 1. The polymer solution was placed in a syringe pump connected by tubing to the atomizing nozzle. The pump was programmed to a constant liquid infusion rate of 0.1 mL/min. The tip of the ultrasonic atomizer nozzle was actuated at a frequency of 120 kHz with a generator power of 1.3 W. Compressed nitrogen at 0.03 bar was introduced into the air-focusing shroud. The gas flow and the position of the shroud control the width and shape of the spray coating beam. The movement of the nozzle was controlled by an $x-y-z$ stage, and the nozzle path is shown in Figure 2. The distance between two nozzle paths was kept at 2 mm, which is smaller than the width of the spray (~4 mm). The substrate to be coated was placed on the hot plate, and

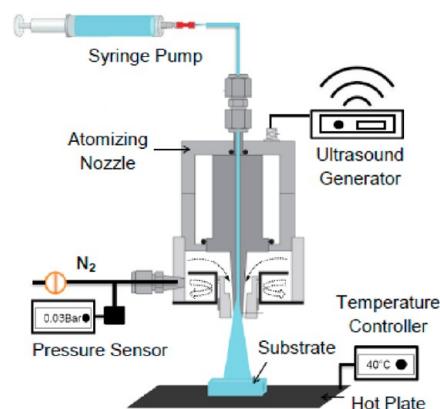**Figure 1.** Schematic representation of setup for spray coating.
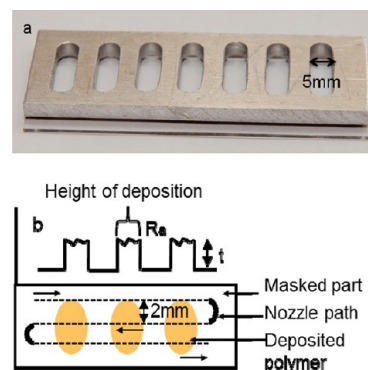

Figure 2. (a) Shadow mask machined from an aluminum block placed on a microscope slide and (b) schematic showing the shadow mask effect on the sprayed polymer with profilometer scan for measuring t and R_a of the deposited film and the spray path of the moving nozzle with a separation of 2 mm.

the temperature was varied according to the experimental design. Microscope glass slides were used as substrates, unless otherwise stated. The number of spray passes was kept constant at 10 for each sample in the study.

Characterization. A shadow mask (Figure 2a) was made by milling holes of 5 mm diameter and 20 mm length in a 76 × 26 × 4 mm³ aluminum block. This mask was placed on the glass slide before deposition to prevent spraying on some of the area. The masked areas acted as a baseline for characterizing the final coating by a surface profilometer Dektak8 (Veeco, U.S.) from which the thickness (t in nm) and the average roughness (R_a in nm) value were calculated as shown schematically in Figure 2b. R_a, also known as the center line average (CLA), is the arithmetic average deviation from the mean line over one sampling length.[19] The stylus tip radius of the profilometer was 5 μm and 3 mg force was applied during scanning with a scan resolution of 0.28 μm. The stylus was moved 10 mm across the sample including masked and deposited part. Within the 5-mm wide deposited section defined by the mask window (Figure 2a), 2 mm in the center were used as reference for calculating t and R_a to avoid influence of edge effects on these values. Each sample was scanned three times, and the average of the data is reported. The surface texture was observed with an optical microscope (OM) (Zeiss, Germany) in bright field mode.

Design of Experiments. Before this optimization, several screening experiments were performed to understand the role of different parameters on the film formation. The parameters tested were liquid infusion rate, generator power, nitrogen pressure in the air focusing shroud, concentration of the polymer solution, temperature of the substrate, the distance between nozzle and substrate, and the speed of the spray nozzle. The infusion rate was kept constant at 0.1 mL/min. At a higher infusion rate, the polymer was seeping below the

shadow mask and the pattern required for further characterization was hampered. For the generator power, a stable spray of the material was obtained at 1.3 W. A lower power did not form a fine mist of spray due to insufficient atomization and a higher power can rip off the liquid causing large chunks of material to be expelled, rather than a spray of droplets. The compressed nitrogen pressure in the air focusing shroud was fixed at 0.03 bar. It was found that a pressure below 0.03 bar was insufficient to focus the entire material coming out of the nozzle onto the substrate. A pressure higher than 0.03 bar put an excess thrust on the focused spray beam reaching the substrate, which led to material deposition below the shadow mask. Experiments were conducted with 0.1, 0.5, and 1 wt % concentration of polymer solution. The 0.1 wt % solution had a very low solid content which was not sufficient for forming a film. Furthermore, the dilute solution was seeping below the shadow mask. The 1 wt % polymer solution formed a film with a thickness higher than desired. Therefore, all of the experiments were performed keeping the concentration of the polymer solution constant at 0.5 wt %. On the basis of the screening experiments, it was concluded that the temperature of the substrate (T), the distance between the nozzle and substrate (N), and the speed of the spray nozzle (S) were the most important operational variables influencing the uniformity of the final film. These three critical process parameters were thus used as factors for DoE. Three values of each variable were selected with T (20 °C, 40 °C, and 60 °C), N (70, 50, and 30 mm) and S (10, 30, and 50 mm/s) for a 3^3 full factorial design. Three center point replicates were performed to improve model adequacy.

In total, 30 experimental runs were performed in random order. MATLAB R2012b software package (Math Work Inc., U.S.) was used to develop mathematical models to determine the influence of the design factors. The responses measured were the appearance of edge peaks, thickness, and roughness of the sprayed films. The appearance of edge peaks was determined by a support vector machine (SVM) with a linear kernel,[20] as we wanted to categorize our observations into two regions; one with the presence of peaks and the other without. SVM is a maximum margin method, so the decision line that is identified by SVM will be placed with equal distance from the peak and nonpeak points that define the support vectors. To improve the accuracy of the model for the other two responses, roughness values higher than 1000 nm were not included in the analysis. These points were identified as outliers. The statistically significant variables, interactions, and second orders on the response roughness and thickness were found. Formally, the following regression model is applied, both to model the roughness and the thickness;

$$Y = \beta + a_1 T + a_2 S + a_3 N + a_4 TS + a_5 TN + a_6 T^2 + a_7 S^2 + a_8 N^2 \tag{1}$$

where Y is either the roughness or the thickness, T is the temperature, S is the speed of spray nozzle, and N is the nozzle-substrate distance. In order to test if a factor is significant, the associated regression coefficient is tested for being different than zero, i.e., if α_1 is significantly different from zero, then the temperature is a significant factor. Hence, the following null hypothesis is employed:

$$H_0: \alpha_i = 0$$
$$H_1: \alpha_i \neq 0 \tag{2}$$

The hypothesis testing is carried out using the t test.

The model specified in eq 1 is fitted using a stepwise approach. Here, the model is created using selection algorithms in order to identify the simplest possible model to explain the observations. The algorithm starts with the full model, and then iteratively removes terms that are found to be insignificant, always choosing the most insignificant term. The term is identified using the F-test with a threshold chosen at $P = 0.1$. The algorithm is implemented in MATLAB R2012b.[21] Based on the results obtained from the analysis of the model, a second set of experiments was done where the nozzle substrate distance was changed in small steps at a fixed speed of spray and temperature. The results from this second set of experiments were not included in the definition of the model.

■ RESULTS AND DISCUSSION

Spray Coating with PVP. *Response Edge Peaks.* First, the appearance of edge peaks is analyzed. Figure 3 shows the
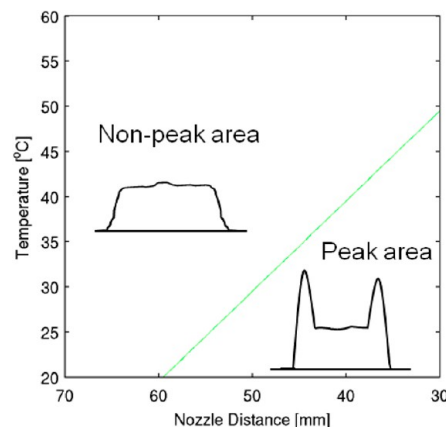
Figure 3. Plot of the decision line separating the peak area with the nonpeak area. Schematics of the deposition profiles in both areas are shown.

decision line predicted by the SVM analysis. It clearly categorizes the whole experimental parameter space into two regions, a peak area and a nonpeak area. As seen from Figure 3, both the temperature of the substrate and the nozzle−substrate distance play an influential role in determining the appearance of edge peaks, whereas the speed of spray has no influence. When the sprayed film dries slowly, accumulation of polymer after solvent evaporation due to the "coffee-ring effect"[17] gives rise to the edge peaks. These peaks are believed to form due to the mobility of the polymer in the wet state. The evaporation of solution is higher at the edge of the coated area, which results in movement of polymer solution from the center to the edge. We define a condition like this as "wet regime" corresponding to the peak area in Figure 3. This phenomenon of edge peak formation has been reported both in the case of spray coating[18,22] and inkjet printing.[23] In the "dry regime" due to the rapid drying of the sprayed droplets peak formation is not observed and hence that corresponds to the nonpeak area in Figure 3. An increase in both temperature and nozzle−substrate distance can pull the system toward the nonpeak region. Increasing the temperature of the substrate induces faster drying of the sprayed droplets on the substrate, while an increase in nozzle−substrate distance results in drier droplets before landing on the substrate. Fine tuning of temperature and nozzle−substrate distance is done in the dry regime or nonpeak area to reach the optimum point in terms of desired thickness with low roughness.

Response Thickness. The P-values predict the terms with most statistical significance, the lower the value the higher is the influence of that factor on that particular response.[24] Here, the factors with P-values lower than 0.1 are considered for the model. For the response thickness, P-values for the factors included in the model are shown in Table 1.

Table 1. Factors Included in the Model and Their Corresponding *P*-Values for Predicting Response Thickness

factors	T	S^2	S	$T \times S$	T^2
P-value	0.010	0.013	0.015	0.054	0.068

Table 1 shows that for response thickness, temperature, and speed of spray are the most significant factors, statistically followed by their interactions. The distance between nozzle and substrate plays no role in determining the thickness of the sprayed film. This is reasonable as the amount of material sprayed remains unchanged with a change in nozzle−substrate distance.

Figure 4 shows the thickness of the sprayed film, as predicted by the model at different speeds of spray and temperature.
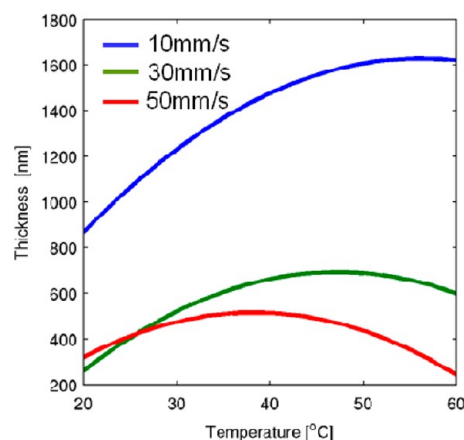
Figure 4. Plot of thickness dependent on temperature at different speeds of spray nozzle predicted by the model.

From Figure 4, it is seen that as the speed of the spray nozzle decreases, the thickness increases due to a higher amount of polymer sprayed on the substrate. However, it is also observed from Figure 4 that the thickness increases with an increase in temperature. This effect is most prominent for the slowest speed of 10 mm/s. In principle, an identical amount of polymer should be deposited independent of temperature. A possible explanation of this observation is given when considering the profilometer scans of two depositions at a speed of 1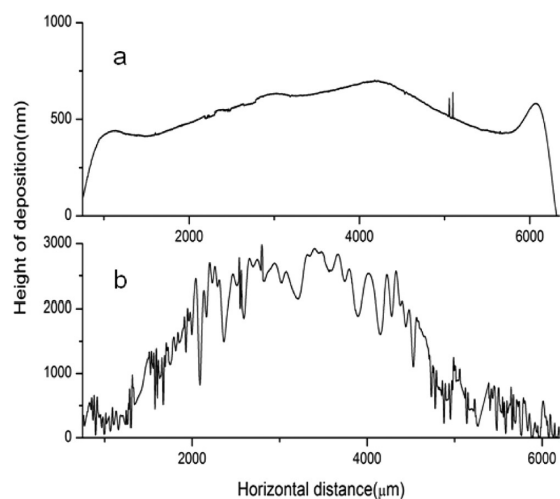0 mm/s and a nozzle substrate distance of 50 mm at 20 °C (Figure 5a) and at 40 °C (Figure 5b). It is observed from Figure 5a that the deposition is more uniformly distributed over the whole surface at 20 °C compared to the one at 40 °C (Figure 5b) where the

Figure 5. Profilometer scan at (a) 20 °C and (b) 40 °C at a nozzle−substrate distance of 50 mm and a speed of spray of 10 mm/s.

surface becomes rough, and the deposition builds up in the middle. At high T, the polymer droplets dry quickly after they land on the substrate. The profile follows a Gaussian distribution due to deposition of polymer on the shadow mask near the edge. At low T, the droplets dry slowly and the polymer has mobility for long time. This potentially allows the droplets to coalesce and form a dense uniform film of low roughness and thickness compared to the one seen at high T.

Response Roughness. For response roughness, the P-values for the factors included in the model are shown in Table 2.

Table 2. Factors Included in the Model and Their Corresponding P-Values for Predicting Response Roughness

factors	N	T	$S \times N$	$T \times S$	T^2	S
P-value	0.00029	0.00048	0.0007	0.008	0.07	0.2456

In Table 2, it is seen that the distance between the nozzle and substrate is the most significant parameter influencing film roughness, as also found by Perfetti et al.,[16] followed by temperature and the interaction between S and N and between T and S. Interestingly, the S is only found statistically significant as an interaction term and not as a single parameter. Although S shows a P-value higher than the threshold value of P defined for the model, it was included in the model due to the interaction terms.

The roughness contours (Figure 6) with the edge peak area from Figure 3 (shaded region) are plotted with T and N as variables with 10 mm/s (Figure 6a), 30 mm/s (Figure 6b) and 50 mm/s (Figure 6c). All of the contours form curved lines due to the $S \times N$ interactions.

The roughness contours in Figure 6 show that with an increase in temperature, the films are getting rougher, irrespective of the speed of spray.

Figure 7 shows the increase of surface roughness of the sprayed film with an increase in the temperature of the substrate. In Figure 7 it is observed that as the temperature of the substrate is raised above 20 °C (Figure 7a), the deposition is moving from the wet regime to the dry regime. Above 30 °C, the surface morphology shows the appearance of dried droplets on the film surface (Figure 7b). The amount of dried droplets increases with an increase in temperature. At 60 °C (Figure 7d), the whole surface is covered with dried droplets. The roughness of the film is seen to depend on the drying of the sprayed droplets on the substrate. Thus the most suitable temperature for spray coating is 20 °C.

Considering the contours as estimated by the model, roughness is lowest in the nonpeak region for a speed of spray of 50 mm/s (Figure 6c). But at this highest speed of spray, it is observed that the film formation is not complete as the amount of deposited material is not sufficient to coalesce and to form a continuous film.

This observation is confirmed by Figure 8, which shows a comparison between three profilometer scans over the identical scan length of 2 mm at a nozzle−substrate separation of 70 mm at 20 °C. The profilometer scan with $S = 50$ mm/s (Figure 8c) is merely a line over a few discontinuous droplets of sprayed polymer rather than a film as it is formed in the case of $S = 10$ mm/s and $S = 30$ mm/s (Figure 8, parts a and b, respectively). Figures 4 and 8 show that the thickness of the film formed at 20 °C with $S = 30$ mm/s and 50 mm/s is below our aim of 500 nm to 1 μm. In order to achieve a continuous film with uniform thickness in the mentioned range and with a low roughness, a
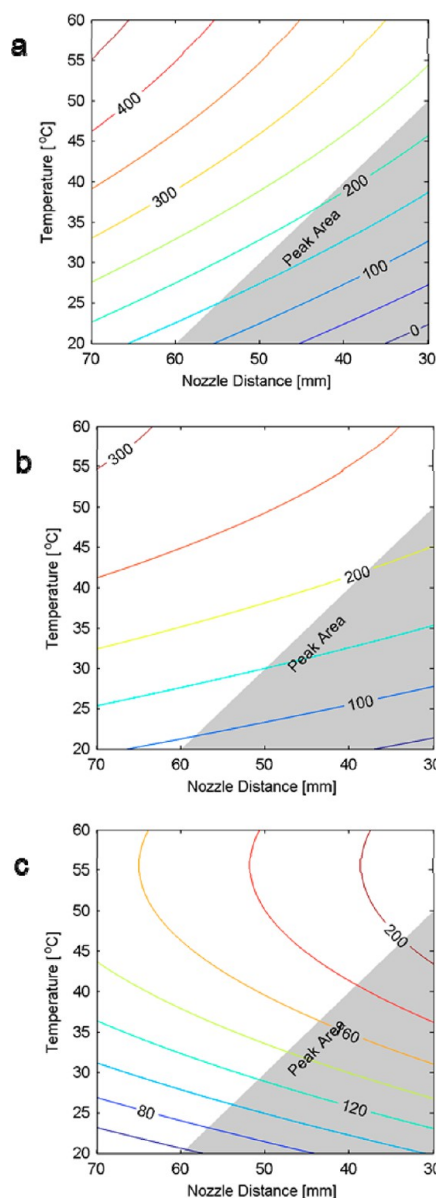
Figure 6. Contour plot of the roughness at speed of spray (a) 10 mm/s, (b) 30 mm/s, and (c) 50 mm/s as predicted by the model. The grey region marks the peak area from Figure 3.
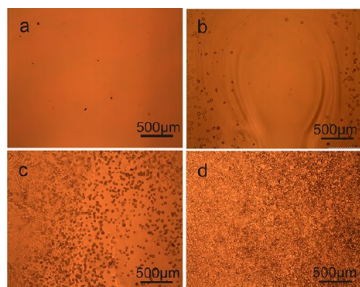
Figure 7. OM images showing the gradual increase in roughness of the spray coated film at a speed of 10 mm/s and 45 mm nozzle−substrate separation at (a) 20 °C, (b) 30 °C, (c) 40 °C, and (d) 60 °C.

second set of experiments was performed with a speed of spray 10 mm/s at 20 °C, changing the nozzle−substrate distance in small steps from $N = 75$ mm to $N = 45$ mm.

Figure 8. Profilometer scan at speed of spray (a) 10 mm/s, (b) 30 mm/s, and (c) 50 mm/s at nozzle−substrate distance 70 mm at 20 °C.
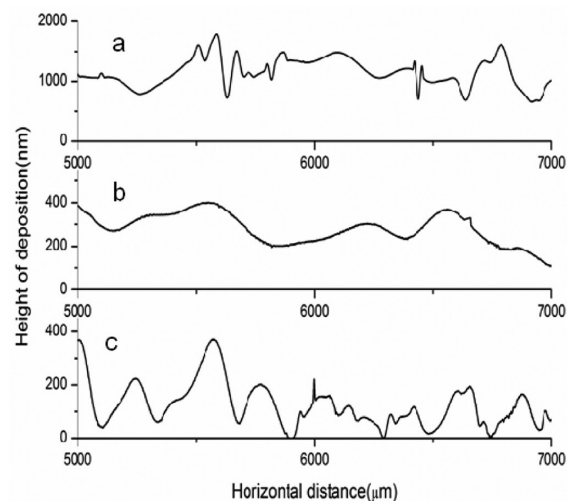
Figure 9 presents the microscopic images and respective profilometer scans at variable nozzle−substrate distances. It is seen that when the distance between nozzle and substrate is high (75 mm and 70 mm, Figure 9, parts a and b, respectively), the surface of the film is dotted with dried droplets which is reflected in a quite high R_a value of 180 nm. When moving close to the substrate the opposite phenomenon is observed. The "coffee-ring effect" starts to appear when $N = 60$ mm ($R_a = 69$ nm in between the peaks, Figure 9d). As the nozzle moves even closer to the substrate ($N = 45$ mm, Figure 9e), the effect becomes more prominent, edge peaks appear at the edge of the coated area, and the film is very uniform in between with $R_a = 22$ nm. At high N, the sprayed droplets are drying on the way to reach the substrate. Here, spray coating is performed in the dry regime. The same effect is observed when the temperature of the substrate is 60 °C (Figure 7d) while spraying and the droplets are drying instantaneously after they reach the substrate. At low N, the polymer is drying slowly which allows it to have enough mobility to form edge peaks at the side of the coated area.

The optimized state at $N = 65$ mm (Figure 9c) lies in the narrow window between these two regimes of dry and wet, where we find a compromise between no edge peaks and a low R_a (76 nm).

Influence of the Substrate. Although we have used microscope glass slides as the substrate for the study, it is interesting to see the effect of substrate on spray coating. The surface energy of the substrate plays an important role in determining the quality of the film formed on it.[8] Different substrate materials frequently used in microfabrication spanning a large range of surface energies were selected. It is seen that uniform films are formed on glass and silicon (Figure 10, parts a and b), whereas the films formed on SU-8, HF etched silicon (hydrophobic silicon) and fluorocarbon coated silicon (Figure 10, parts c, d, and e) are discontinuous. This is explained by the higher surface free energy of glass [water contact angle $(\theta) \approx 27°$][25] and silicon dioxide $(\theta \approx 45°)$[26] compared to SU-8 $(\theta \approx 78°)$,[27] HF etched silicon (hydrophobic silicon) $(\theta \approx 70°)$[26] and fluorocarbon coated silicon $(\theta \approx 106°)$[27] which have low surface energy preventing adequate wetting of the surface.
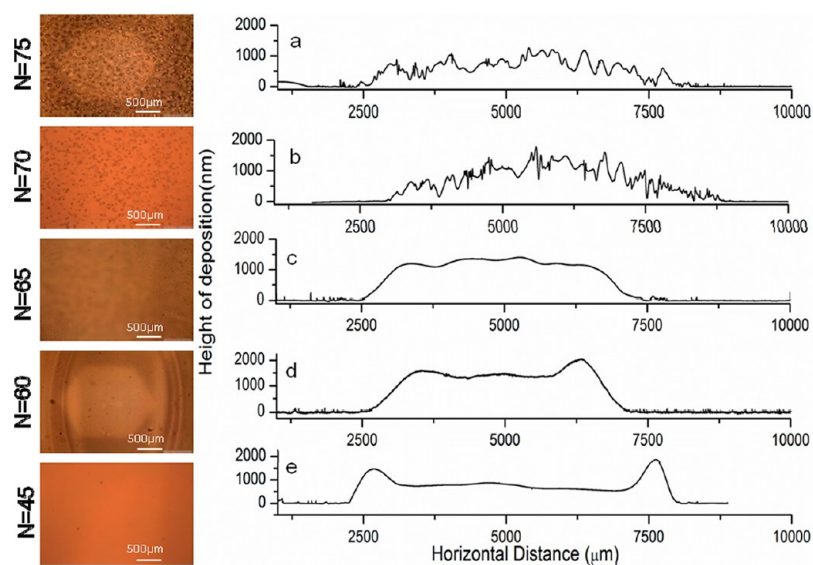
Figure 9. OM image and profilometer scan of PVP showing the effect of the distance between the nozzle and the substrate: (a) 75 mm, (b) 70 mm, (c) 65 mm, (d) 60 mm, and (e) 45 mm at 10 mm/s and 20 °C.
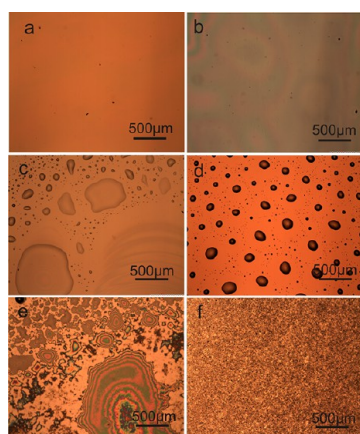

Figure 10. OM image of PVP spray coated from aqueous solution on (a) glass, (b) silicon dioxide, (c) SU-8, (d) HF etched silicon, (e) fluorocarbon coated silicon, and (f) spray coated from dichloromethane solution on glass at T = 20 °C, S = 10 mm/s, and N = 45 mm.

Influence of Solvent. To verify our understanding of the influence of the rapid drying of droplets on surface morphology, a solution of PVP in dichloromethane was prepared and compared to the one obtained with PVP with water as solvent. The parameters for the test were T = 20 °C, N = 45 mm, and S = 10 mm/s. With both solvents, a continuous film is formed, suggesting negligible differences in surface wetting. From Figure 10f, it is concluded that dichloromethane is showing the typical dry regime behavior with R_a = 560 nm and no edge peaks. At the same condition, PVP with water as solvent is forming a uniform film (R_a = 22 nm) but with edge peaks (Figure 10a). Dichloromethane has a low boiling point of 40 °C and hence a higher evaporation rate than water, resulting in a deposition in the dry regime. This demonstrates that in addition to temperature and nozzle−substrate distance, the solvent selected to prepare the solution can also tune the dry and wet regime deposition. For inkjet printing, extensive work has been reported in minimizing the edge peak formation and extension of the narrow regime of uniform film formation by

using cosolvent systems.[28−30] The experiments with different solvents indicate that this also might be applicable for spray coating. However, in this work, we focused mainly on optimization of the processing parameters of spray coating to find the regime of uniform film formation.

Spray Coating with PDLLA. Extensive studies with the PVP−water system have been used to build up knowledge on the role of different spray coating parameters and their inter-relations. A less detailed study with PDLLA in cyclohexanone is performed, and the observations are compared with the ones obtained during the experiments with PVP.

Influence of Solvent. In the case of the PVP, solvent selection plays an important role in final quality of the film. Therefore solutions of PDLLA in cyclohexanone, toluene and dichloromethane were prepared and their film forming behavior at room temperature was compared. It is seen from the OM images in Figure 11 that at identical spraying conditions, the
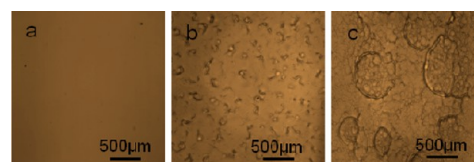
Figure 11. OM images of PDLLA film formed using (a) cyclo-hexanone, (b) toluene, and (c) dichloromethane as solvent for spray coating PDLLA at 20 °C with a speed of 10 mm/s and a nozzle−substrate separation of 45 mm.

film formed with cyclohexanone (Figure 11a) is more uniform than the one formed with toluene (Figure 11b) and dichloromethane (Figure 11c). The observed differences in film morphology could be due to the different evaporation rates or different surface tensions of the three solvents. All of the solutions showed good wetting of the surface forming a continuous film. Therefore, it is assumed that differences in the evaporation rate are the predominant effect. Dichloromethane and toluene evaporated too fast resulting in a rough surface similar to the one observed for PVP deposition with
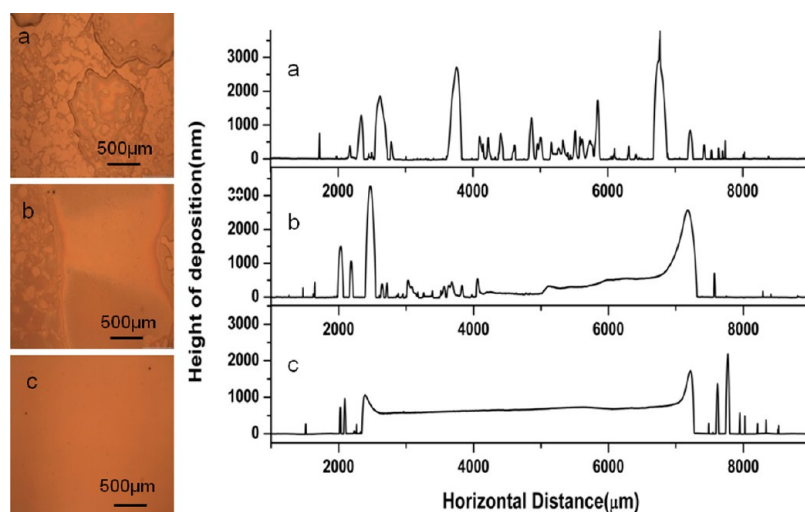
Figure 12. OM image and profilometer scan of PDLLA at nozzle–substrate distance of (a) 75 mm, (b) 60 mm, and (c) 45 mm at 20 °C and a speed of spray of 10 mm/s.
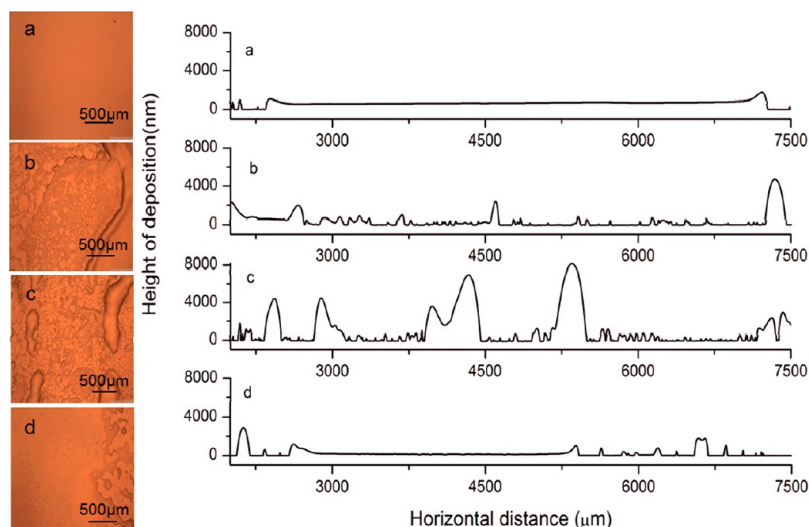
Figure 13. OM image and profilometer scan of PDLLA at (a) 20 °C, (b) 40 °C, (c) 80 °C, when the nozzle–substrate distance is 45 mm and the speed of spray is 10 mm/s, and (d) at a speed of spray of 50 mm/s when the nozzle–substrate distance is 45 mm at 20 °C.

dichloromethane (Figure 10f). Hence, cyclohexanone was selected as the solvent for PDLLA for the study.

Influence of Nozzle–Substrate Distance. Similar to spray coating of PVP, the distance between nozzle and substrate is the most significant parameter influencing the deposition of PDLLA. Figure 12 presents the microscope images and respective profilometer scans at variable nozzle–substrate distances. No true dry regime is observed, but a uniform film formation does not occur (Figure 12, parts a and b) unless an optimum $N = 45$ mm is reached (Figure 12c). Due to the high boiling point of the solvent cyclohexanone, the PDLLA has sufficient mobility after spraying to form puddles of polymer at the edge of the coated areas. This results in the formation of edge peaks. For PDLLA, formation of edge peaks could not be completely avoided. Nevertheless, a satisfying result is achieved as the peaks are narrow in width and the height difference between the center of deposition and the peak is small. Furthermore, the roughness in Figure 12c is very low ($R_a = 21$ nm) for a thickness of 430 nm.

Influence of Temperature and Speed of the Spray Nozzle. The influence of temperature and speed of the spray nozzle on the surface morphology of the sprayed film is quite similar to the PVP–water system. Figure 13 shows the microscope images and respective profilometer scans at variable temperature of the substrate and speed of spray. The film formed at 20 °C with a speed of spray of 10 mm/s (Figure 13a) is uniform compared to the film formed at elevated temperatures (Figure 13, parts b and c) and at a higher speed of 50 mm/s (Figure 13d). Similar to the nozzle–substrate distance, no true dry regime is found but, due to an increase in the rate of drying at higher temperature, nonuniformity in the film is clearly observed both by visual inspection in OM images and their corresponding profilometer scans. (Figure 13, parts b and c). At high speeds of the spray nozzle, the amount of material deposited is not adequate to form a uniform film. The discontinuity of the film can be observed from the OM image and the profilometer scan in Figure 13d. The thickness of the film increases when the speed of spray is decreased from 50 mm/s (Figure 13d) to 10 mm/s (Figure13a).

CONCLUSIONS

This study demonstrates the influence of different factors on homogeneous film formation by spray coating. Here, we found the strength of full factorial experimental design and subsequent analysis in determining the critical parameters of spray operation to achieve a continuous film with uniform thickness and low roughness. Depending on the drying of the sprayed droplets on the substrate, we define two broad regimes, "dry" and "wet". In the wet regime, formation of edge peaks is observed which should be avoided. In the dry regime, no edge peaks are formed, but deposition results in a rough surface. The optimum condition of spraying lies in a narrow window between these two regimes, where we obtain a film of low roughness and with no edge peaks. Thus to move from a wet to a dry regime, three possibilities can be summarized as follows: (1) an increase in temperature to accelerate drying of the droplets deposited on the substrate, (2) the selection of a solvent with higher evaporation rate for spraying, and (3) an increase of the distance between the nozzle and substrate where the drying of the droplets before reaching the substrate is enhanced. For both PVP and PDLLA spray coating, the distance between nozzle and substrate is the most significant parameter. Both a low speed of the spray nozzle and a substrate with a high surface energy result in formation of a continuous film. Even though we are working with two completely different systems, the experiments with PDLLA confirm the observations found for PVP. For both cases, the optimum spraying temperature is 20 °C and the optimal speed of the spray is 10 mm/s. The nozzle−substrate distance is fine-tuned for the respective systems, and the optimum distance is 65 mm for PVP and 45 mm for PDLLA. Continuous film formation occurs on a high surface energy glass surface with the high boiling point solvents being water for PVP and cyclohexanone for PDLLA. The detailed study of the different process parameters with two different polymer−solvent systems improves our understanding of the technique of spray coating. The results can be generalized and other systems can benefit from the conclusions of this work in the future.

AUTHOR INFORMATION

Corresponding Author
* E-mail: Stephan.Keller@nanotech.dtu.dk.

Notes
The authors declare no competing financial interest.

ACKNOWLEDGMENTS

REFERENCES

(1) Krebs, F. C. Fabrication and Processing of Polymer Solar Cells: A Review of Printing and Coating Techniques. *Sol. Energy Mater. Sol. Cells* **2009**, *93*, 394−412.

(2) Lu, W.; Fadeev, A. G.; Qi, B.; Smela, E.; Mattes, B. R.; Ding, J.; Spinks, G. M.; Mazurkiewicz, J.; Zhou, D.; Wallace, G. G.; et al. Use of Ionic Liquids for π-Conjugated Polymer Electrochemical Devices. *Science* **2002**, *297*, 983−987.

(3) Panasyuk, T. L.; Mirsky, V. M.; Piletsky, S. A.; Wolfbeis, O. S. Electropolymerized Molecularly Imprinted Polymers as Receptor Layers in Capacitive Chemical Sensors. *Anal. Chem.* **1999**, *71*, 4609−4613.

(4) Lochon, F.; Fadel, L.; Dufour, I.; Rebière, D.; Pistré, J. Silicon Made Resonant Microcantilever: Dependence of the Chemical Sensing Performances on the Sensitive Coating Thickness. *Mater. Sci. Eng., C* **2006**, *26*, 348−353.

(5) Vendra, V. K.; Wu, L.; Krishnan, S. Polymer Thin Films for Biomedical Applications. In *Nanostructured Thin Films and Surfaces*; Kumar, C. S. S. R., Ed.; Wiley-VCH: Weinheim, 2010; Vol. 5, pp 1−51.

(6) Wang, M.; Yang, G.-Z.; Wang, M.; Liu, T. Effect of Film Thickness Controlled by Ink-Jet Printing Method on the Optical Properties of an Electroluminescent Polymer. *Polym. Adv. Technol.* **2010**, *21*, 381−385.

(7) Keller, S. S.; Gammelgaard, L.; Jensen, M. P.; Schmid, S.; Davis, Z. J.; Boisen, A. Deposition of Biopolymer Films on Micromechanical Sensors. *Microelectron. Eng.* **2011**, *88*, 2297−2299.

(8) McGrath, M. G.; Vrdoljak, A.; O'Mahony, C.; Oliveira, J. C.; Moore, A. C.; Crean, A. M. Determination of Parameters for Successful Spray Coating of Silicon Microneedle Arrays. *Int. J. Pharm.* **2011**, *415*, 140−149.

(9) Linden, J.; Thanner, C.; Schaaf, B.; Wolff, S.; Lägel, B.; Oesterschulze, E. Spray Coating of PMMA for Pattern Transfer via Electron Beam Lithography on Surfaces with High Topography. *Microelectron. Eng.* **2011**, *88*, 2030−2032.

(10) Yu, L.; Lee, Y. Y.; Tay, F. E. H.; Iliescu, C. Spray Coating of Photoresist for 3D Microstructures with Different Geometries. *J. Phys. Chem. Solids* **2006**, *34*, 937−942.

(11) Pham, N. P.; Burghartz, J. N.; Sarro, P. M. Spray Coating of Photoresist for Pattern Transfer on High Topography Surfaces. *J. Micromech. Microeng.* **2005**, *15*, 691−697.

(12) Pan, C. J.; Tang, J. J.; Weng, Y. J.; Wang, J.; Huang, N. Preparation, Characterization and Anticoagulation of Curcumin-Eluting Controlled Biodegradable Coating Stents. *J. Controlled Release* **2006**, *116*, 42−49.

(13) Tobiska, S.; Kleinebudde, P. Coating Uniformity: Influence of Atomizing Air Pressure. *Pharm. Dev. Technol.* **2003**, *8*, 39−46.

(14) Lang, R. J. Ultrasonic Atomization of Liquids. *J. Acoust. Soc. Am.* **1962**, *34*, 6−8.

(15) Pham, N. P.; Boellaard, E.; Burghartz, J. N.; Sarro, P. M. Photoresist Coating Methods for the Integration of Novel 3-D RF Microstructures. *J. Microelectromech. S.* **2004**, *13*, 491−499.

(16) Perfetti, G.; Alphazan, T.; van Hee, P.; Wildeboer, W. J.; Meesters, G. M. H. Relation Between Surface Roughness of Free Films and Process Parameters in Spray Coating. *Eur. J. Pharm Sci.* **2011**, *42*, 262−272.

(17) Deegan, R.; Bakajin, O.; Dupont, T. Capillary Flow as the Cause of Ring Stains from Dried Liquid Drops. *Nature* **1997**, *389*, 827−829.

(18) Dubourg, G.; Fadel-Taris, L.; Dufour, I.; Pellet, C.; Ayela, C. Collective Fabrication of All-organic Microcantilever Chips Based on a Hierarchical Combination of Shadow-Masking and Wafer-Bonding Processing Methods. *J. Micromech. Microeng.* **2011**, *21*, 095021.

(19) Gadelmawla, E. S.; Koura, M. M.; Maksoud, T. M. a.; Elewa, I. M.; Soliman, H. H. Roughness Parameters. *J. Mater. Process. Tech.* **2002**, *123*, 133−145.

(20) http://people.revoledu.com/kardi/tutorial/SVM/What-is-SVM-An-intuitive-introduction.html.

(21) http://www.mathworks.se/help/stats/stepwisefit.html.

(22) Fleury, B.; Dantelle, G.; Darbe, S.; Boilot, J. P.; Gacoin, T. Transparent Coatings Made from Spray Deposited Colloidal Suspensions. *Langmuir* **2012**, *28*, 7639−7645.

(23) Kang, H.; Soltman, D.; Subramanian, V. Hydrostatic Optimization of Inkjet-Printed Films. *Langmuir* **2010**, *26*, 11568−11573.

(24) Wrobel, G. Optimization of High-Density cDNA-Microarray Protocols by "Design of Experiments. *Nucleic Acids Res.* **2003**, *31*, e67.

(25) Canning, J.; Petermann, I.; Cook, K. Surface Treatment of Silicate Based Glass: Base Piranha Treatment versus 193 nm Laser Processing. In *Proc. SPIE*; Canning, J., Peng, G., Eds.; **2012**; Vol. *8351*, pp 83512N−83512N−5.

(26) Franssila, S. *Introduction to Microfabrication*; 2nd ed.; John Wiley & Sons, Ltd: West Sussex, 2010; p 150.

(27) Keller, S.; Haefliger, D.; Boisen, A. Optimized Plasma-deposited Fluorocarbon Coating for Dry Release and Passivation of Thin SU-8 Cantilevers. *J. Vac. Sci. Technol. B* **2007**, *25*, 1903−1908.

(28) Oh, Y.; Kim, J.; Yoon, Y. J.; Kim, H.; Yoon, H. G.; Lee, S.-N.; Kim, J. Inkjet Printing of Al_2O_3 Dots, Lines, and Films: From Uniform Dots to Uniform Films. *Curr. Appl. Phys.* **2011**, *11*, S359−S363.

(29) Teichler, A.; Eckardt, R.; Hoeppener, S.; Friebe, C.; Perelaer, J.; Senes, A.; Morana, M.; Brabec, C. J.; Schubert, U. S. Combinatorial Screening of Polymer:Fullerene Blends for Organic Solar Cells by Inkjet Printing. *Adv. Energy Mater.* **2011**, *1*, 105−114.

(30) Teichler, A.; Perelaer, J.; Schubert, U. S. Screening of Film-Formation Qualities of Various Solvent Systems for π-Conjugated Polymers Via Combinatorial Inkjet Printing. *Macromol. Chem. Phys.* **2013**, *214*, 547−555.

Paper II

Micromechanical String Resonators: Analytical Tool for Thermal Characterization of Polymer

# Micromechanical String Resonators: Analytical Tool for Thermal Characterization of Polymers

Sanjukta Bose,*,[†] Silvan Schmid,[†] Tom Larsen,[†] Stephan S. Keller,[†] Peter Sommer-Larsen,[‡] Anja Boisen,[†] and Kristoffer Almdal[†]

[†]Department of Micro- and Nanotechnology, Technical University of Denmark, DTU Nanotech, DK-2800 Kongens Lyngby, Denmark

[‡]Department of Energy Conversion and Storage, Technical University of Denmark, DTU Energy Conversion, DK-4000 Roskilde, Denmark

Ⓢ *Supporting Information*

ABSTRACT: Resonant microstrings show promise as a new analytical tool for thermal characterization of polymers with only few nanograms of sample. The detection of the glass transition temperature (T_g) of an amorphous poly(D,L-lactide) (PDLLA) and a semicrystalline poly(L-lactide) (PLLA) is investigated. The polymers are spray coated on one side of the resonating microstrings. The resonance frequency and quality factor (Q) are measured simultaneously as a function of temperature. Change in the resonance frequency reflects a change in static tensile stress, which yields information about the Young's modulus of the polymer, and a change in Q reflects the change in damping of the polymer-coated string. The frequency response of the microstring is validated with an analytical model. From the frequency independent tensile stress change, static T_g values of 40.6 and 57.6 °C were measured for PDLLA and PLLA, respectively. The frequency-dependent damping from Q indicates higher T_g values of 62.6 and 88.8 °C for PDLLA and PLLA, respectively, at ~10^5 Hz. Resonant microstrings facilitate thermal analysis of nanogram polymer samples measuring the static and a dynamic glass transition temperature simultaneously.
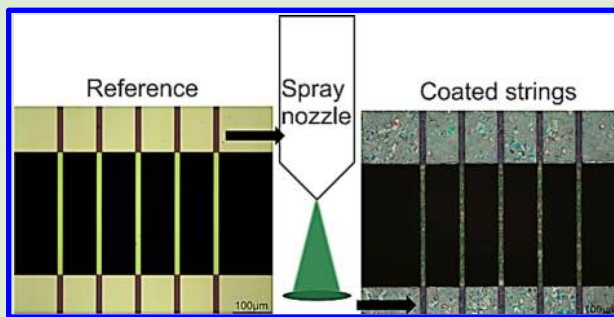
Polymer thin films are widely used in microtechnology[1] and biomedical applications[2] where the knowledge of the exact polymer properties is crucial. Micro- and nanoscale beam resonators have been utilized as highly sensitive sensors for mass,[3] chemicals,[4] humidity,[5] or temperature.[6−8] It has been shown that atomic force microscopy (AFM) can be used in noncontact mode to measure thermal transitions of polymer in micrometer scale.[9] Another approach is based on microcantilevers (singly clamped beams) that have been used efficiently in detecting phase transitions[10,11] and loss modulus of polymers.[12] For detecting glass to rubber transition of polymers, the top surface of a cantilever is coated with a thin film of the polymer. The phase transitions of the polymer can then be detected from the temperature dependent deflection and change in resonance frequency. Microcantilevers coated with polymers often show a large initial deflection due to stress generated during deposition, which impedes the optical readout of the mechanical motion.

In this work we use microstrings (doubly clamped beams with tensile prestress). Strings are clamped on both sides and problems with initial out-of-plane deflection are thus avoided. Microstrings enable the characterization of polymer thin films deposited by arbitrary techniques, such as spray coating, inkjet printing, plasma polymerization, and so on.

The glass transition temperature is an important characteristic temperature of polymers. It is the temperature at which the first long-range segmental motions in the polymer chains occur. The Young's modulus of the material is drastically reduced when the temperature is raised above T_g. Common techniques used to determine T_g are differential scanning calorimetry (DSC), dilatometry, dynamic mechanical analysis (DMA), or dielectric spectroscopy (DES). Here we propose to use microstring resonators for thermal characterization of thin polymer films with a total mass of only a few nanograms. With highly sensitive microstrings, we reduce the material required for a measurement by 6 orders of magnitude compared to DSC. The working principle is demonstrated by first spray coating biodegradable amorphous polymer poly(D,L-lactide) (PDLLA) or semicrystalline poly(L-lactide) (PLLA) on silicon nitride (SiN_x) microstrings. We then monitor the resonance frequency and quality factor of the strings while ramping the temperature up. Temperature-induced changes in both parameters can be correlated to the static and dynamic T_g of the polymers.

The static stress in the microstrings is high, ~190 MPa, and it is a common valid assumption that the deflection-induced

change in tensile stress during vibration is negligible.[13] Thus, the resonance frequency change is a measure of the heating-related static stress change. Hence T_g detected via the resonance frequency corresponds to the static T_g, which is comparable with T_g detected by DSC. Quality factor (Q), on the other hand, is directly related to the viscoelastic material damping, which is frequency-dependent. Thus, T_g measured via Q corresponds to the dynamic T_g, which is comparable with T_g detected by DES at the corresponding frequency.

First we derive a model describing the temperature-induced frequency detuning of a polymer-coated microstring. The total tensile stress σ_S in a simple string as a function of temperature T is given by[6]

$$\sigma_S = \sigma_0 + (\alpha_F - \alpha_S)E(T - T_0) \tag{1}$$

with initial tensile prestress, σ_0, thermal expansion coefficient of the frame and string, α_F and α_S, respectively, Young's modulus of the string, E, and temperature T_0 at which σ_0 is defined. The bimaterial string consists of a SiN$_x$ layer with a thickness h_S and a polymer layer with an effective thickness h_P. In this case, an effective stress σ^* can be defined as

$$
\begin{aligned}
\sigma^* &= \frac{h_S \sigma_S + h_P \sigma_P}{h_S + h_P} \\
&= \{ h_S[\sigma_{0,S} + (\alpha_F - \alpha_S)E_S](T - T_0) \\
&\quad + h_P[\sigma_{0,P} + (\alpha_F - \alpha_P)E_P](T - T_0) \} \\
&\quad / (h_S + h_P)
\end{aligned}
\tag{2}
$$

where the parameters with the subscript S and P belong to the SiN$_x$ and polymer, respectively. The eigenfrequency of the bimaterial string is now given by[6,7]

$$f_0 = \frac{n}{2L}\sqrt{\frac{\sigma^*}{\rho^*}}, \quad n = 1, 2, 3, \ldots \tag{3}$$

where n is the resonant mode number, L is the length of the string, and ρ^* is the effective mass density of the string

$$\rho^* = \frac{h_S \rho_S + h_P \rho_P}{h_S + h_P} \tag{4}$$

The eigenfrequency of the string finally becomes

$$f_0 = \frac{n}{2L}\sqrt{\frac{(h_S[\sigma_{0,S} + (\alpha_F - \alpha_S)E_S] + h_P[\sigma_{0,P} + (\alpha_F - \alpha_P)E_P])(T - T_0)}{h_S \rho_S + h_P \rho_P}} \tag{5}$$

If there is no polymer coating present, eq 5 reduces to

$$f_0 = \frac{n}{2L}\sqrt{\frac{\sigma_{0,S} + (\alpha_F - \alpha_S)E_S(T - T_0)}{\rho_S}} \tag{6}$$

which has been derived and applied in the study reported by Larsen et al.[7] In the case of a high-Q microstring resonator ($Q > 1000$), the eigenfrequency and resonance frequency can be assumed to be equal.

Figures 1 and 2 show the microstring-based thermal analysis of PDLLA and PLLA, respectively, together with respective blank references. The analysis consists of the resonance frequency and Q measured as a function of temperature.

From eq 6 it can be seen that the frequency of a blank SiN$_x$ microstring (α_S = 1.25 ppm/K)[6] on a Si substrate (α_F = 2.6 ppm/K) increases with temperature. This behavior is observed for both reference strings (dotted lines in Figures 1a and 2a).
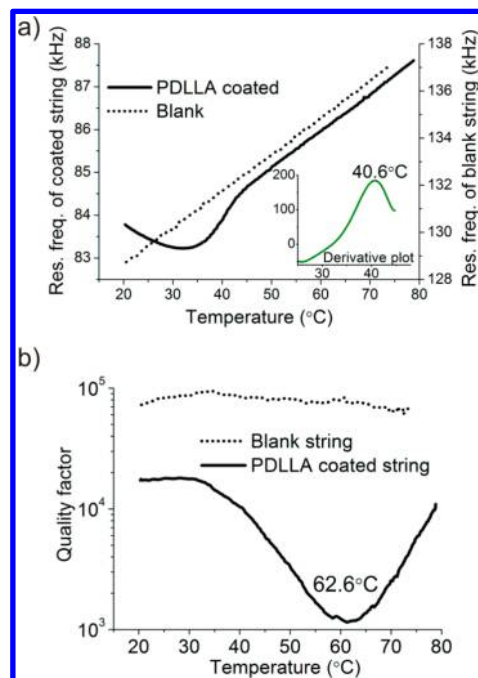
Figure 1. Thermal analysis of PDLLA coated on a 985 μm long, 6 μm wide, and 340 nm thick SiN$_x$ microstring. (a) Resonance frequency change reflecting static stress change; the inset shows the derivative plot indicating the T_g at the peak. (b) Q change as a function of temperature for blank and PDLLA coated strings.
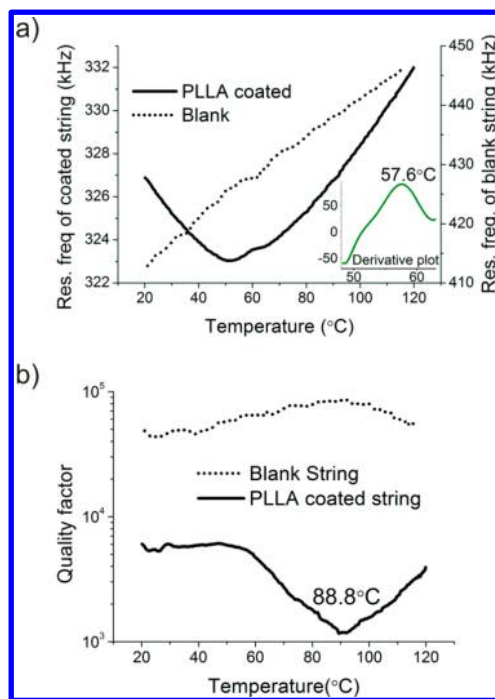
Figure 2. Thermal analysis of PLLA coated on 316 μm long, 14 μm wide, and 340 nm thick SiN$_x$ microstring. (a) Resonance frequency change reflecting static stress change; the inset shows the derivative plot indicating the T_g at the peak. (b) Q change as a function of temperature for blank and PLLA coated strings.

The frame material is expanding more than the string material with increasing temperature. As a consequence of this the tensile stress in the string increases which results in a higher resonance frequency. When a polymer-coated string is heated,

the frequency initially drops (solid lines in Figures 1a and 2a) due to the larger thermal expansion of the polymer (α_P) with respect to the frame (α_F) and string (α_S). After crossing T_g, due to a drastic drop of the Young's modulus of the polymer during the glass−rubber phase transition,[14] the mechanical properties of the string are dominated by the silicon nitride. Above T_g, the numerator in the model of a polymer-coated microstring (eq 5) approaches the numerator in the model for a blank string (eq 6). Hence, after the transition, the resonance frequency increases as a function of temperature as it was observed for the blank strings. The Young's modulus of the SiN$_x$ is considered as 250 GPa for the analytical model. Below T_g, the Young's modulus of the polymer is assumed to be 3.5 GPa, and above T_g, the modulus is assumed to drop 3 orders of magnitude[14,15] to 3.5 MPa. It can be concluded that the maximal change in the slope of the resonance frequency curve thus corresponds to the maximal change in Young's modulus of the polymer. From the frequency slope maximum (inset of Figures 1a and 2a), T_g of PDLLA and PLLA is then determined to be 40.6 and 57.6 °C, respectively. This corresponds well with T_g of 42.7 and 59.9 °C measured by DSC. These experiments were repeated at least three times to confirm the reported results.

In Figure 3 the analytical model (eq 5) is fitted to the experimental data, with α_P, $\sigma_{0,P}$ and h_P as fitting parameters (see
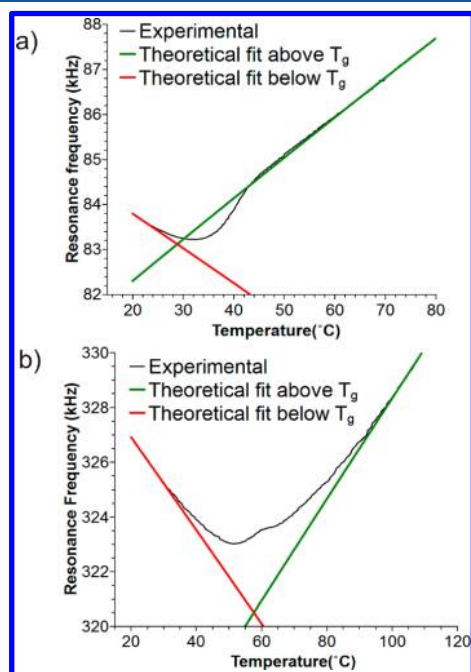
Figure 3. Experimental data and analytical model plotted as a function of temperature for (a) PDLLA and (b) PLLA coated string.

Table 1). The curves below T_g (red line) differ from the fits above T_g (green line) due to a reduced modulus E_P and the tensile prestress in the polymer, $\sigma_{0,P}$. A tensile prestress in the string $\sigma_{0,S}$ of 186 and 197 MPa for PDLLA and PLLA, respectively, was determined before coating at $T_0 = 20$ °C. α_P values obtained from Table 1 are in accordance with the literature values.[16] From the polymer layer thicknesses, a total PDLLA and PLLA mass of 5.9 ng and 6.3 ng, respectively, can be estimated, assuming a mass density of 1248 kg/m³ taken from the polymer data sheet. A thickness of 1.0 μm was measured by white light interferometry for PDLLA deposition

Table 1. Fitting Parameters Obtained from Fitting Eq 5 to Experimental Data (see Figure 3) Measured at $T_0 = 20$ °C

	PDLLA	PLLA
α_P [ppm/K] ($T < T_g$)	80.6	58.4
$\sigma_{0,P}$ [MPa] ($T < T_g$)	−12.4	31.4
α_P [ppm/K] ($T > T_g$)	360.1	299.9
$\sigma_{0,P}$ [MPa] ($T > T_g$)	−14.8	24.1
h_P [μm]	0.78	1.14

on strings. This corresponds well with the effective thickness of ∼0.8 μm extracted from the analytical model.

In a relaxed mechanical resonator, the quality factor (Q) due to intrinsic material damping is equal to the inverse loss tangent.[10] In an unrelaxed resonator such as a string, the tensile stress leads to an enhancement of Q. This results in that Q becoming a linear function of the loss tangent.[17]

$$Q \propto (\tan \delta)^{-1} \tag{7}$$

Thus, T_g of the polymer can be detected at the minimum of the Q versus temperature curve. From Figures 1b and 2b, the frequency dependent glass transitions of PDLLA and PLLA are detected at 62.6 and 88.8 °C, respectively (Figures 1b and 2b, solid line).

As a comparison, the quality factor of the blank reference (Figures 1b and 2b, dotted line) remains unchanged with temperature. Without the dissipative polymer coating, the blank string have significantly higher Q values. Q reaches its minimum at the glass−rubber transition of the polymer where the ratio between the stored elastic energy and that converted to heat during deformation is lowest. Unlike T_g obtained from the resonance frequency (Figures 1a and 2a), T_g determined by means of Q is frequency-dependent. T_g is a kinetic parameter and it is dependent on the mechanical frequency, well-known by the time−temperature superposition where time and temperature can be mathematically interchanged at certain conditions.[18] At a higher frequency, higher temperature is required for a polymer to achieve the equivalent mechanical state that is obtained at a lower frequency. Consequently, the transition shifts to a higher temperature. Since we are performing measurements at a frequency of ∼10⁵ Hz, the observed values for T_g are in well agreement with T_g of PDLLA and PLLA at 59.1 and 80.5 °C, respectively, measured from the loss tangent peak at 10⁵ Hz obtained from dielectric spectroscopy.

In summary, T_g determination of polymer performed by micro string resonators is a new analytical tool. We estimated an error of of ±2 °C for the static and dynamic T_g. This error mainly comes from the uncertainty in the actual temperature of the microstrings. The microstrings facilitate measurements on reduced sample size (5−6 ng) by 6 orders of magnitude compared to 5−10 mg in DSC. Furthermore, the small thermal masses reduce the time to thermal equilibrium significantly making microstrings a fast and highly sensitive tool for measuring phase transitions of polymer samples.

■ EXPERIMENTAL SECTION

SiN$_x$ microstrings were fabricated from low-stress, silicon-rich silicon nitride by standard microfabrication.[3] 0.5 wt % of PDLLA (ester terminated, M_w 16000 g/mol, Sigma Aldrich) solution was prepared with cyclohexanone as solvent and PLLA (M_w 204800 g/mol, NatureWorks PLA polymer 2003D) with dichloromethane as solvent. Both solvents were procured from Sigma Aldrich and used as received.

The polymer solution was sprayed on the strings with an Exacta Coat Ultrasonic Spraying System[19] (Sonotek, U.S.A.). In all our measurements, the coating uniformity has been found to have an insignificant influence on the measurement results.

The resonance frequency was measured with a laser-Doppler vibrometer (MSA-500 from Polytec GmbH) in high vacuum at a pressure below 3×10^{-5} mbar. The quality factor was determined from the -3 dB bandwidth of the resonance curve. A schematic of the experimental setup is shown in Figure 4. The silicon chip comprising
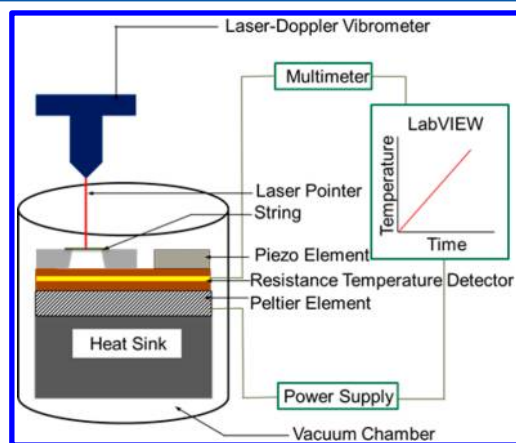

Figure 4. Schematic representation of the experimental set up.

the microstrings was placed on a copper block attached to a Peltier element used for heating and cooling. A resistance temperature detector (RTD; PT-1000) was embedded inside the copper block for measuring the temperature, which was controlled by a LabVIEW based PID controller. Finite Element Method (FEM) simulations (Comsol 4.2) were conducted to investigate the difference in measured temperature and the actual temperature on the strings due to heat loss to the surroundings through radiation in high vacuum. All the temperatures reported are corrected accordingly. For the FEM simulations, thermal conductivities[20,21] of Si, SiN$_x$, and the polymers were considered to be 130, 3.2, and 0.175 W/(m K), respectively. Emissivities[22] of 0.01, 0.95, and 0.7 were assumed for Si, SiN$_x$, and polymers, respectively. The strings were actuated with an external piezo element on the copper block. Temperature was varied from 20 to 80 °C for PDLLA and 20 to 120 °C for PLLA at a heating rate of 15 °C/min. Prior to the each measurement, the polymer coated strings were subjected to repeated heating−cooling cycles in order to remove the thermal history.

DSC reference measurements were performed with a DSC Q1000 from TA Instruments. The sample was subjected to heat−cool−heat cycles from 0 to 200 °C at a heating and cooling rate of 10 °C/min. Temperature-dependent measurements of the complex dielectric function were carried out using a Novocontrol Broadband Dielectric Spectrometer BDS-40. The sample cell consisted of two electrodes, the top electrode was 20 mm and the bottom electrode 30 mm in diameter, and the sample was ∼50 μm thick. The temperature was changed from −100 to 100 °C at a heating rate of 2 °C/min, controlled by a Novocontrol Quattro Cryosystem.

ASSOCIATED CONTENT

S Supporting Information

The optical microscope images of polymer deposition on the microstrings, the calculated relation between and eigenfrequency and resonance frequency of the microstrings, the differential scanning calorimetry curves and the dielectric loss tangent curves of the polymers used in this study, and the estimation of errors in glass transition temperature detection. This material is available free of charge via the Internet at http://pubs.acs.org.

AUTHOR INFORMATION

Corresponding Author
*E-mail: sbos@nanotech.dtu.dk.

Notes
The authors declare no competing financial interest.

REFERENCES

(1) Lochon, F.; Fadel, L.; Dufour, I.; Rebière, D.; Pistré, J. *Mater. Sci. Eng., C* **2006**, *26*, 348−353.
(2) Vendra, V. K.; Wu, L.; Krishnan, S. In *Nanostructured Thin Films and Surfaces*; Kumar, C. S. S. R., Ed.; Wiley-VCH: Weinheim, 2010; Vol. 5, pp 1−51.
(3) Schmid, S.; Dohn, S.; Boisen, A. *Sensors* **2010**, *10*, 8092−8100.
(4) Lang, H. P.; Baller, M. K.; Berger, R.; Gerber, C.; Gimzewski, J. K.; Battiston, F. M.; Fornaro, P.; Ramseyer, J. P.; Meyer, E.; Güntherodt, H. J. *Anal. Chim. Acta* **1999**, *393*, 59−65.
(5) Schmid, S.; Kühne, S.; Hierold, C. *J. Micromech. Microeng.* **2009**, *19*, 065018.
(6) Larsen, T.; Schmid, S.; Grönberg, L.; Niskanen, a. O.; Hassel, J.; Dohn, S.; Boisen, A. *Appl. Phys. Lett.* **2011**, *98*, 121901.
(7) Larsen, T.; Schmid, S.; Boisen, A. *AIP Conf. Proc.* **2013**, *1552*, 931−936.
(8) Larsen, T.; Schmid, S.; Villanueva, L.; Boisen, A. *ACS Nano* **2013**, *7*, 6188−6193.
(9) Meincken, M.; Graef, S.; Sanderson, R. D. *Appl. Phys. A: Mater. Sci. Process.* **2002**, *375*, 371−375.
(10) Jung, N.; Jeon, S. *Macromolecules* **2008**, *41*, 9819−9822.
(11) Jung, N.; Seo, H.; Lee, D.; Ryu, C. Y.; Jeon, S. *Macromolecules* **2008**, *41*, 6873−6875.
(12) Ayela, C.; Heinrich, S. M.; Josse, F.; Dufour, I. *J. Microelectromech. Syst.* **2011**, *20*, 788−790.
(13) Magnus, K., Popp, K. *Schwingungen*; Teubner: Stuttgart, 2005.
(14) Sperling, L. H. *Introduction to Physical Polymer Science*; John Wiley & Sons, Inc.: Hoboken, NJ, 2005.
(15) Henton, D.; Gruber, P.; Lunt, J.; Randall, J. *Nat. Fibers, Biopolym., Biocompos.* **2005**, *527−578*.
(16) Meng, Q. K.; Hetzer, M.; De Kee, D. *J. Compos. Mater.* **2010**, *45*, 1145−1158.
(17) Schmid, S.; Jensen, K.; Nielsen, K.; Boisen, A. *Phys. Rev. B* **2011**, *84*, 1−6.
(18) Chartoff, R. P.; Menczel, J. D.; Dillman, S. H. *Thermal Analysis of Polymer Fundamental and Applications*; John Wiley & Sons, Inc.: Hoboken, NJ, 2009; pp 387−495.
(19) Bose, S.; Keller, S. S.; Alstrøm, T. S.; Boisen, A.; Almdal, K. *Langmuir* **2013**, *29*, 6911−6919.
(20) Sultan, R.; Avery, a. D.; Stiehl, G.; Zink, B. L. *J. Appl. Phys.* **2009**, *105*, 043501.
(21) Kim, H.-S.; Chae, Y. S.; Park, B. H.; Yoon, J.-S.; Kang, M.; Jin, H.-J. *Curr. Appl . Phys.* **2008**, *8*, 803−806.
(22) Ravindra, N. M.; Abedrabbo, S.; Tong, F. M.; Nanda, A. K.; Speranza, A. C. *IEEE Trans. Semicond. Manuf.* **1998**, *11*, 30−39.

Supporting information for

Micromechanical String Resonators: Analytical Tool for Thermal Characterization of Polymers

Sanjukta Bose[1], Silvan Schmid[1], Tom Larsen[1], Stephan S. Keller[1], Peter Sommer-Larsen[2,] Anja Boisen[1] and Kristoffer Almdal[1]*

[1]Department of Micro- and Nanotechnology, Technical University of Denmark, DTU Nanotech, DK-2800 Kongens Lyngby, Denmark

[2]Department of Energy Conversion and Storage, Technical University of Denmark, DTU Energy Conversion DK-4000 Roskilde, Denmark

Polymer deposition on microstrings:

Experiments have been performed on both homogeneous (Fig.S1a) and non-homogeneous (Fig.S1b) polymer coating on microstrings.
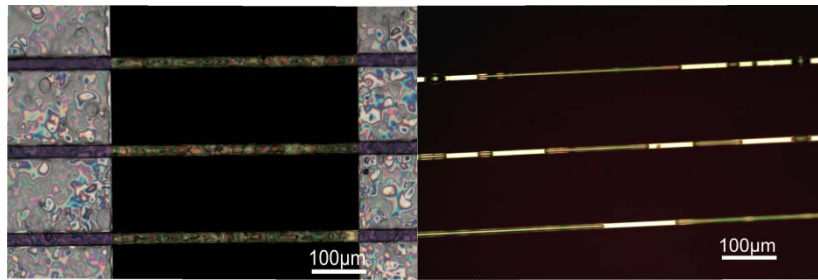

Figure S1: Uniform spray coating of PLLA (a) and non-uniform spray coating of PDLLA (b) on microstrings

In some cases, the coating has been rather inhomogeneous, as can be seen from Fig. S1b. Differences in homogeneity indeed influence the tensile stress of the microstrings but they affect only the absolute value of the resonance frequency of the string and not the relative temperature dependent change, from which T_g is extracted. The measurement has been repeated with multiple strings with different coating homogeneities. No influence of the coating quality on the measured T_g has been observed.

Relation between eigenfrequency and resonance frequency of microstrings:

The strings are microresonators with very high Q-factor. In the experiment the "resonance frequency" of the damped resonator is measured. The resonance and eigen frequencies are in principle not equal. However, the Q of all the measured polymer coated string was always above 1000. Such high Qs of strings, even when coated with a polymer layer, are a result of the large energy stored in the tensile stress (see ref [17] in the manuscript). For such high Qs, the "resonance frequency" of a damped resonator can be assumed to be equal to the "eigenfrequency" of an undamped resonator to a good approximation.

The equation describing the relation between resonance frequency (ω_r) and eigen frequency (ω_0) is given below by eq (1)

$\omega_r = \omega_0\sqrt{1 - 2\xi^2}$ ......(1) where, ξ is the damping coefficient.

For a slightly damped system the relation between Q and ξ is given by eq (2)

$Q = \dfrac{1}{2\xi}$ ....(2)

Assuming Q=1000, from eq (2) we obtain a value of ξ=0.005.

Putting ξ=0.005 in eq (1), $\omega_r = 0.999999\omega_0$ i.e., $\omega_r \cong \omega_0$.

Differential Scanning Calorimetry plots for PDLLA and PLLA

Figure S2: Differential Scanning Calorimetry plot of PDLLA. The sample was subjected to heat-cool-heat cycles from 0 ˚C to 200 ˚C at a heating and cooling rate of 10 ˚C /min. The glass transition temperature was extracted from the second heating cycle.
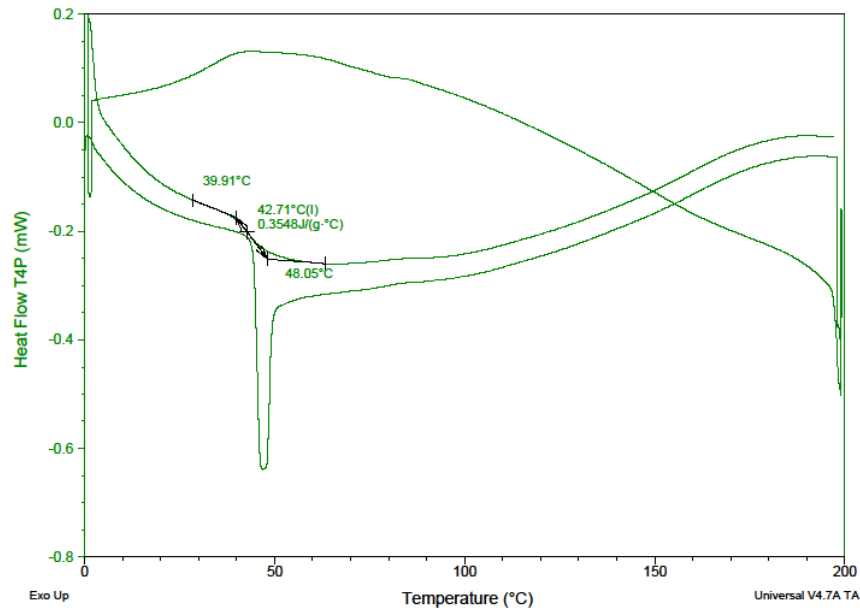
Figure S3: Differential Scanning Calorimetry plot of PLLA. The sample was subjected to heat-cool-heat cycles from 0 ˚C to 200 ˚C at a heating and cooling rate of 10 ˚C /min. The glass transition temperature was extracted from the second heating cycle.
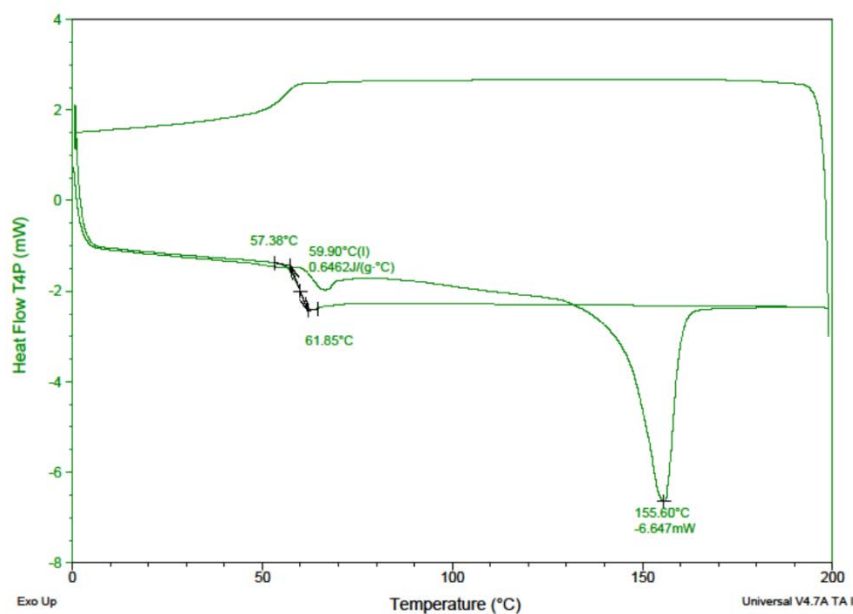
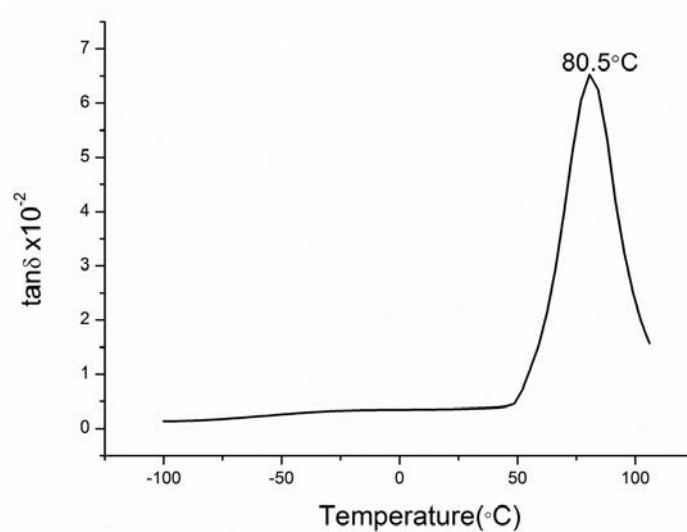**Broadband Dielectric Spectroscopy plots for PLLA and PDLLA**

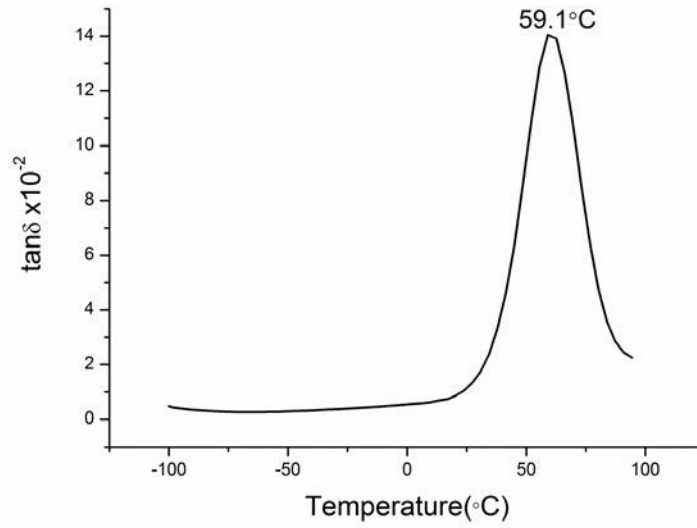Figure S4: Temperature dependence of tanδ measured for PLLA at 10^5Hz by Broadband Dielectric Spectrometer.

Figure S5: Temperature dependence of tanδ measured for PDLLA at 10^5 Hz by Broadband Dielectric Spectrometer.

Error estimation in T_g detection:

Repeated measurements show good coherence in the measured T_g for both polymers. A PT-1000 class A temperature sensor was used for measuring the temperature. The maximum uncertainty of the sensor within the temperature range used is ±0.35°C. COMSOL simulation was made to investigate the difference in measured temperature and the actual temperature on the strings due to finite heat conductivity and radiation loss. The error due to the finite size of the mesh is less than 0.1 %. For the simulation some literature values were assumed for the thermal conductivity and emissivity of the substrate and the polymer. An assumption of uncertainty of the material constants of ±20% leads to an uncertainty in the simulated temperatures of up to ±1°C. Finally to detect dynamic T_g the lowest point in the plot of Quality Factor vs. Temperature (Figure 1b and 2b) was considered. Since the peak is broad so an error of ±1°C is expected.

In summary the source of dominating error is from the material constants assumed for simulation which is ±1°C. So, the final error in T_g including both the material constants and the uncertainty due to a broad peak of Q can be ±2°C.

Paper III

Micromechanical fast quasi-static detection of α- and β-relaxations with nanograms of polymer

Micromechanical fast quasi-static detection of α- and β-relaxations with nanograms of polymer

Sanjukta Bose[1][*], Silvan Schmid[1], Tom Larsen[2], Stephan S. Keller[1], Anja Boisen[1] and Kristoffer Almdal[1]

[1]Department of Micro- and Nanotechnology, Technical University of Denmark, DTU Nanotech, DK-2800 Kongens Lyngby, Denmark

[2]Department of Mechanical Engineering, Stanford University, Stanford, CA, USA

ABSTRACT: Micromechanical string resonators are used as a highly sensitive tool for detection of glass transition (T_g or α relaxation) and sub-T_g (β relaxation) temperatures of polystyrene (PS) and poly (methyl methacrylate) (PMMA). The characterization technique allows for a fast detection of mechanical relaxations of polymers with only few nanograms of sample in a quasi-static condition. The polymers are spray coated on one side of the silicon nitride (SiN_x) microstrings which are pre-stressed suspended structures clamped on both sides on a silicon (Si) frame. Resonance frequency of the microstrings is detected with simultaneous increase in temperature. The change in slope of the resonance frequency curve directly relates to the change in mechanical contribution of the polymer on the static tensile stress of the microstring. α and β relaxation temperatures are estimated from the local slope maxima of the resonance frequency versus temperature. T_gs of PS and PMMA are detected at 91.3°C and 113.8°C respectively. The results match well with the glass transition values of 93.6°C and 114.5°C obtained from Differential Scanning Caloriemetry (DSC) of PS and PMMA respectively. The β relaxation temperatures are detected at 30.1°C and 32.5°C for PS and PMMA which is in accordance with values reported in literature.

INTRODUCTION

Over the years, relaxation processes in amorphous polymers have been widely studied. The glass transition temperature (T_g) also known as the α-relaxation is the characteristic temperature for a polymer where the long-range segmental motion starts when a polymer is heated. The α-relaxation temperature of a polymer is an important parameter for processing and end-use applications. Below the α-relaxation temperature, a considerable amount of local motions in the form of simple bond rotation or conformational changes inside groups is present corresponding to secondary relaxation processes like β relaxations.[1] These secondary chain motions respond to the applied stress and thus the process of β relaxations can impart toughness to some polymers.[2] Common techniques used to determine the relaxation temperatures of polymers are differential scanning calorimetry (DSC), thermomechanical analysis (TMA), dynamic mechanical analysis (DMA) and dielectric spectroscopy (DES). Among these, DSC is the most common method for detecting α-relaxation temperatures of polymers. For relaxations with low calorimetric effects like in some pharmaceutical products, proteins[3] or β relaxations where the associated change in heat capacity is too small, DSC is not suitable. In such cases measuring mechanical or electrical properties of the samples like in TMA, DMA or DES are more applicable. TMA can be used to detect α-relaxations of polymers but it is not recommended for detecting weak β-relaxation.[4] Whereas, both DMA and DES can be successfully used to detect α- and β-relaxation in polymers. DES is preferred in most cases due to its high sensitivity and wide dynamic range.[5,6] Nevertheless all these above mentioned state of the art techniques have their own advantages and disadvantages. Like in case of DSC, higher heating rate increases instrument sensitivity at the cost of the broadening of the shape of the DSC curves and shifting of T_g to higher temperatures. On the other hand in TMA, discrepancies in result may arise due to probe loading conditions. Moreover for precise measurements by TMA, a low heating rate (1-5° C/min) should be maintained and a minimum sample thickness of ~0.5 mm is required.[7] Glass transition is a kinetically controlled second order transition that depends on the applied oscillation frequency in case of DMA and frequency of the applied alternating current in case of DES. In particular for DES, the sample should also possess moderate to strong polarizability.[7] For comparison with transition values obtained from other thermal methods, DMA and DES are often run at low frequency (~1 Hz) and low heating rate (~2°C/min) which in turn adds on to the total experimental time.[4,7] Thus

1

there is a need for a new characterization tool that can assemble the advantages of both DSC where experiments are conducted in static conditions that eliminate the frequency dependency of T_g and DES, which is more sensitive in measuring α and β relaxations on a single platform. Micro sized beam resonators have been developed as highly sensitive sensors for sensing chemicals, humidity, mass or temperature[8–12]. In our previous work[13] it was shown that silicon nitride (SiN$_x$) microstrings can be used as a new analytical tool now named as microstring thermal analyzer (MTA) for detecting the α-relaxation of polymers with only few nanograms of sample. This is six orders of magnitude less sample as is required for DSC. Furthermore, there is no need for bulk samples, as they have to be prepared for TMA, DMA or DES. The small sample mass on the microstrings attains fast thermal equilibrium and thus higher heating rates can be used without affecting the transition temperatures, thereby reducing the experimental timeframe. Microstrings are doubly-clamped pre-stressed SiN$_x$ beams on a silicon (Si) frame. Minute changes of the tensile stress in the microstring can be detected with high sensitivity due to the mechanical resonance frequency detuning. When these strings are coated with polymers and subjected to heating cycles, the heating-related expansion and softening of the polymer causes a net change in the static tensile stress. The mechanical relaxations of the polymer under test can be detected from the slope maxima of the resonance frequency versus temperature. A comparison between the conventional techniques discussed above and our new tool MTA is presented in Table 1.

Table 1. Summary of different techniques used to determine α- and β-relaxations of polymers[4,7,13]

Tool	α	β	Frequency dependency	Heating rate (°C/min)	Sample size
DSC	✓	✗	✗	5-10	3-10 mg
TMA	✓	✗	✗	1-5	Bulk
DMA	✓	✓	✓	~2	Bulk
DES	✓	✓	✓	~2	Bulk
MTA	✓	✓	✗	15-30	5-10 ng

In this work, the potential of MTA to quasi-statically detect the more subtle β-relaxation of nanograms of polymer is evaluated. For this purpose polystyrene (PS) and poly (methyl methacrylate) (PMMA) are spray coated onto the microstrings. Temperature induced changes in the resonance frequency of the strings are monitored and compared with corresponding measured DSC results and literature reference values.

EXPERIMENTAL

The used PS (M_w 20,000 g/mol) was synthesized by anionic polymerization in cyclohexane at 30°C using sec-butyl lithium as initiator.[14] PMMA (M_w 35,000 g/mol) was purchased from Scientific Polymer Products, Inc., USA and used as received. SiN$_x$ microstrings used in this study were fabricated by standard microfabrication techniques from low-stress silicon-rich silicon nitride.[8] 0.5 wt% of PS and PMMA polymer solutions in chloroform (Sigma Aldrich) was prepared. Spray coating[15] on one side of the strings was done with an Exacta Coat Ultrasonic Spraying System (Sonotek, USA). Figure 1 shows clean reference and PMMA coated microstrings.
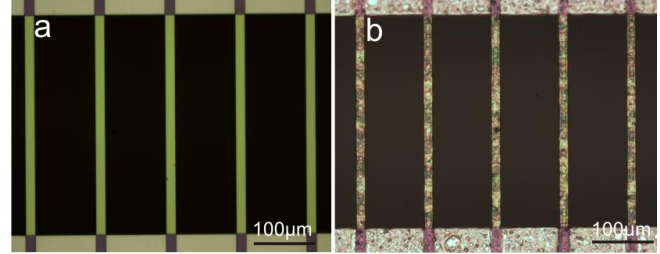

Figure 1. Optical microscope images of (a) reference and (b) PMMA coated SiN$_x$ microstrings.

From white light interferometry, a thickness of ~ 1 μm was obtained for PMMA. From the polymer layer thicknesses and the dimensions of the strings used, a rough estimate of the total PS and PMMA mass of 11.1 ng and 5.1 ng, respectively, was made, assuming a mass density of 1050 kg/m^3 for PS and 1180 kg/m^3 for PMMA. The resonance frequencies of the strings before and after coating as well as during the temperature sweeps were measured with a laser-Doppler vibrometer (MSA-500, Polytec GmbH, Germany). The temperature sweep data was fitted with a polynomial curve and differentiated to identify the slope changes. The experimental set up is the same as described in the previous publication.[13] The silicon chip comprising the microstrings was placed on a copper block attached to a Peltier element used for heating and cooling. A resistance temperature detector (PT-1000) was embedded inside the copper block for measuring the temperature which was controlled by a LabVIEW based PID controller. The microstrings were measured in high vacuum at a pressure below 3×10^{-5} mbar. The strings were actuated with an external piezoelectric element glued to the copper block. For the PS coated string the temperature was varied from 10 °C to 110 °C and from 10 °C to 120 °C for PMMA coated string at a heating rate of up to 30 °C /min. Finite element method (FEM) simulations (Comsol 4.2) were conducted to investigate the difference in measured temperature and the actual temperature on the strings due to heat loss to the surroundings through radiation. All the temperatures reported are corrected accordingly. For the FEM simulations, thermal conductivities[16,17] of Si, SiN$_x$, PS and PMMA were considered to be 130, 3.2, 0.15 and 0.2 W/(m K), respectively. Emissivities[18,19] of 0.01, 0.95, 0.82 and 0.9 were assumed for Si, SiN$_x$, PS and PMMA respectively. The polymer coated strings were subjected to repeated heating-cooling cycles in order to

remove the thermal history prior to each measurement. DSC studies of PS and PMMA were performed with a Discovery DSC from TA Instruments with heat-cool-heat cycles from 20 °C to 150 °C at a heating and cooling rate of 10 °C /min.

RESULTS AND DISCUSSION

PS and PMMA were spray coated to form a thin film on one side of the strings. Coating inhomogeneity has a negligible effect as it only affects the absolute resonance frequency of the microstrings but not the relative temperature-dependent change from which the relaxation temperatures are extracted.[13]

It is a common valid assumption that the deflection induced change in tensile stress during vibration of the microstrings is negligible[20] since the strings have a very high static pre-stress of ~190 MPa. When the temperature is ramped up, the microstrings show an increase in resonance frequency due to a heat induced static stress change. Figure 2a shows the change in resonance frequencies of a blank (f_{blank}) and PS coated (f_{coated}) microstring. The derivative plot of f_{coated}, with respect to the temperature (T), is shown in Figure 2b.

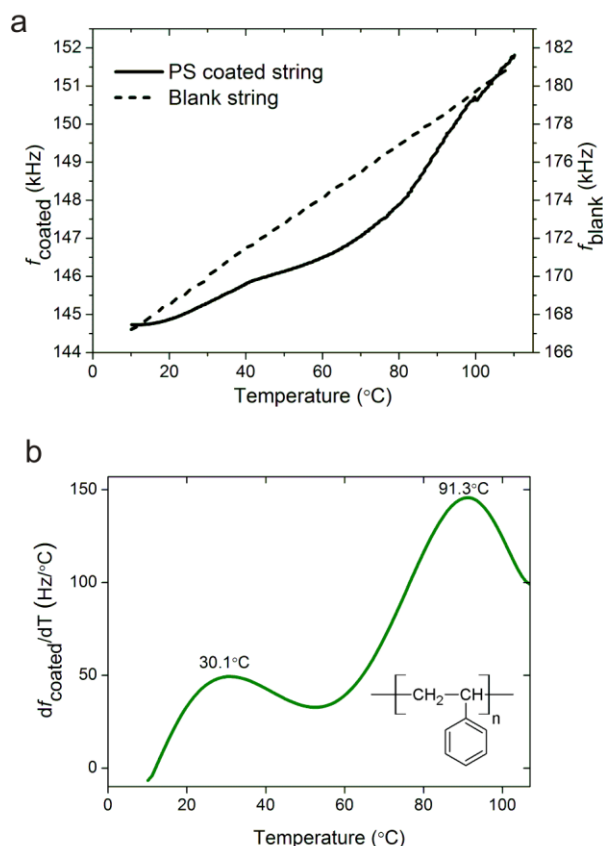Figure 2. Thermal analysis of PS coated on a 759 μm long, 14 μm wide and 340 nm thick SiN_x microstring. (a) Resonance frequency change reflecting static stress change. (b) The derivative plot of the resonance frequency and two peaks indicating the α and the β relaxations. The chemical structure of PS is shown.

From Figure 2a, it is observed that the resonance frequency of the blank microstring (dotted line) increases linearly with temperature. The Si frame has a higher thermal expansion, 2.6 ppm/K, compared to SiN_x microstrings, 1.25 ppm/K, and thus the frame expands more than the microstrings. As a result, the tensile-stress in the microstrings increases which is reflected by an increase in resonance frequency. The PS coated microstring in contrast (Figure 2a, solid line) shows a lower absolute resonance frequency than the reference microstrings due to the added mass. When the PS coated string is heated, the resonance frequency increases with a varying slope over the measured temperature range. At the higher temperatures, the resonance frequency seems to increase linearly behaving similarly as the reference SiN_x microstrings. This is expected due to the drastic drop of Young's Modulus of PS above T_g.[2] The mechanical relaxations of the polymer film correspond to the temperatures of maximal frequency change. From Figure 2b, it can be seen that there is a small broad peak at 30.1°C followed by a sharp peak at 91.3°C. The maximum peak at 91.3° C matches well with the DSC results of 93.6°C, as shown in Figure 3, and thus it is confirmed as the α relaxation peak of PS.
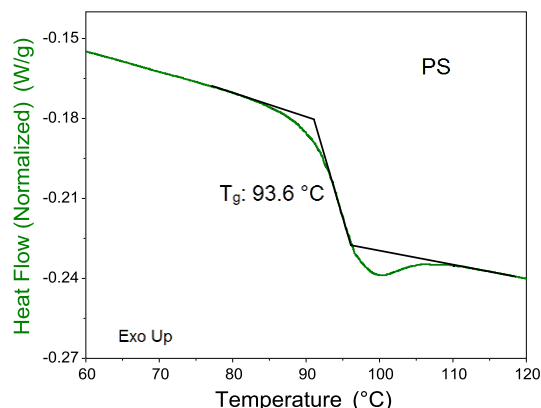

Figure 3. DSC thermogram of PS showing the midpoint of the endothermic shift as T_g.

From several sources in literature,[1,21–24] it has been observed that the β relaxation of PS appears in between 27-37°C, measured both by DES and DMA. Thus, the small broad peak at 30.1°C seems to represent the β relaxation peak of PS. β relaxation peaks are normally detected at lower frequencies[23] and become less pronounced[22,25] when measurement is carried out at higher frequencies in DES or DMA. Due to the negligible deflection of the strings, it can be assumed that this detection method operates in the quasi-static regime, which allows for the detection of a pronounced β-relaxation peak. The rotational motion of the phenyl rings on the PS backbone (Figure 2, inset) may contribute to the β relaxation process[26] but this still remains an open discussion.

To confirm our finding with PS, we repeated the experiments with PMMA coated microstrings. The change in resonance frequency of a blank and PMMA coated strings

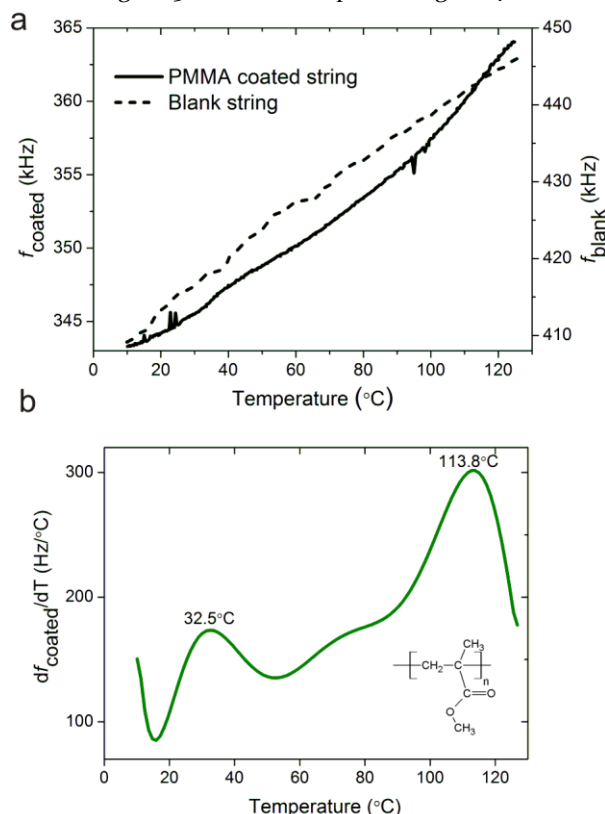and the derivative plot of the resonance frequency are shown in Figure 3 and the DSC plot in Figure 4.

Figure 3. Thermal analysis of PMMA deposited on a 311 μm long, 14 μm wide and 340 nm thick SiN_x microstring. (a) Resonance frequency change reflecting static stress change (b) The derivative plot of the resonance frequency with two peaks indicating the α and the β relaxations. The chemical structure of PMMA is shown.
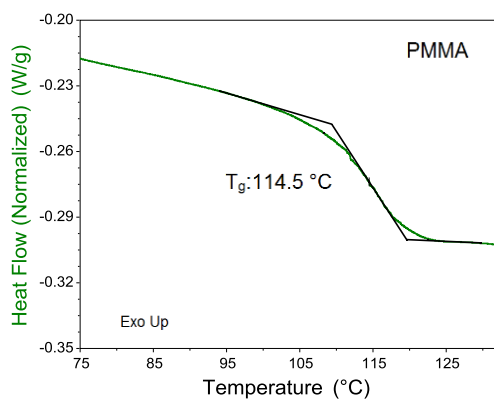

Figure 4. DSC thermogram of PMMA showing the midpoint of the endothermic shift as T_g.

The overall two peak behavior seen for the PS is also seen for the PMMA. The α relaxation appears at 113.8°C which matches well with the 114.5°C obtained from the DSC measurement shown in Figure 4. The local segmental motion coupled with side-group relaxation[27] in PMMA give rise to the β peak at 32.5°C which is very well match-

ing the reported T_β at 35 °C. [25] These experiments were repeated three times to confirm the reported data. An error of ±2°C was estimated in the extraction of the relaxation temperatures coming mainly from the uncertainty in the actual temperature of the microstrings.

CONCLUSION

Silicon nitride microstrings were successfully utilized to determine α and βrelaxation in PS and PMMA. The advantage of characterizing with MTA lies in its potential to measure both α and β relaxations with only few nanograms of sample in quasi-static conditions. The nanogram sample size reaches fast thermal equilibrium and measurements can thus be conducted in less time than conventional techniques with no effect of frequency dependency. Highly sensitive tools like microstrings can now also be employed to measure low calorimetric transitions shown by some drugs or proteins along with polymers. E.g. the molecular mobility determines the physical and chemical stability of amorphous pharmaceutical drugs and the knowledge of the mechanical relaxations of such samples is crucial to determine their stability.

ASSOCIATED CONTENT

Supporting Information

AUTHOR INFORMATION

Corresponding Author
 *Email: sbos@nanotech.dtu.dk.

Author Contributions

All authors have given approval to the final version of the manuscript.
Notes
The authors declare no competing financial interest.

ACKNOWLEDGMENT

REFERENCES

(1)   Yano, O.; Wada, Y. *J. Polym. Sci. Part A-2 Polym. Phys.* **1971**, *9*, 669–686.

(2)   Sperling, L. H. *Introduction to Physical Polymer Science*; Fourth.; John Wiley & Sons, Inc.: New Jersey, USA, 2005.

(3)   Reddy, R.; Chang, L. ' L. '; Luthra, S.; Collins, G.; Lopez, C.; Shamblin, S. L.; Pikal, M. J.; Gatlin, L. A.; Shalaev, E. Y. *J. Pharm. Sci.* **2009**, *98*, 81–93.

(4)   Foreman, J.; Sauerbrunn, S.; Marcozzi, C. Exploring the sensitivity of thermal analysis techniques to the glass

transition Document reference: TA082
http://www.tainst.com (accessed Aug 20, 2014).

(5)   Sengers, W. G. F.; van den Berg, O.; Wübbenhorst, M.; Gotsis, a. D.; Picken, S. J. *Polymer* **2005**, *46*, 6064–6074.

(6)   Jakobsen, B.; Niss, K.; Maggi, C.; Olsen, N. B.; Christensen, T.; Dyre, J. C. *J. Non. Cryst. Solids* **2011**, *357*, 267–273.

(7)   Chartoff, R. P.; Menczel, J. D.; Dillman, S. H. *Thermal Analysis of Polymer Fundamental and Applications*; John Wiley & Sons, Inc.: New Jersey, USA, 2009.

(8)   Schmid, S.; Dohn, S.; Boisen, A. *Sensors* **2010**, *10*, 8092–8100.

(9)   Lang, H. P.; Baller, M. K.; Berger, R.; Gerber, C.; Gimzewski, J. K.; Battiston, F. M.; Fornaro, P.; Ramseyer, J. P.; Meyer, E.; Güntherodt, H. J. *Anal. Chim. Acta* **1999**, *393*, 59–65.

(10)   Schmid, S.; Kühne, S.; Hierold, C. *J. Micromech. Microeng.* **2009**, *19*, 065018.

(11)   Larsen, T.; Schmid, S.; Grönberg, L.; Niskanen, a. O.; Hassel, J.; Dohn, S.; Boisen, A. *Appl. Phys. Lett.* **2011**, *98*, 121901.

(12)   Larsen, T.; Schmid, S.; Villanueva, L.; Boisen, A. *ACS Nano* **2013**, *7*, 6188–6193.

(13)   Bose, S.; Schmid, S.; Larsen, T.; Keller, S. S.; Sommer-Larsen, P.; Boisen, A.; Almdal, K. *ACS Macro Lett.* **2014**, *3*, 55–58.

(14)   Ndoni, S. *Rev. Sci. Instrum.* **1995**, *66*, 1090 – 1095.

(15)   Bose, S.; Keller, S. S.; Alstrøm, T. S.; Boisen, A.; Almdal, K. *Langmuir* **2013**, *29*, 6911–6919.

(16)   Sultan, R.; Avery, a. D.; Stiehl, G.; Zink, B. L. *J. Appl. Phys.* **2009**, *105*, 043501.

(17)   Yu, S.; Hing, P.; Hu, X. *Compos. Part A Appl. Sci. Manuf.* **2002**, *33*, 289–292.

(18)   Ravindra, N. M.; Abedrabbo, S.; Tong, F. M.; Nanda, A. K.; Speranza, A. C. *IEEE Trans. Semicond. Manuf.* **1998**, *11*, 30–39.

(19)   Babrekar, H. a.; Kulkarni, N. V.; Jog, J. P.; Mathe, V. L.; Bhoraskar, S. V. *Mater. Sci. Eng. B* **2010**, *168*, 40–44.

(20)   Magnus, K., Popp, K. In *Schwingungen*; Teubner: Stuttgart, 2005.

(21)   Miwa, Y.; Urakawa, O.; Doi, A.; Yamamoto, K.; Nobukawa, S. *J. Phys. Chem. B* **2012**, *116*, 1282–1288.

(22)   Pathmanathan, K.; Johari, G. P.; Faivre, J. P.; Monnerie, L. *J. Polym. Sci. Part B Polym. Phys.* **1986**, *24*, 1587–1595.

(23)   Struik, L. *Polymer* **1987**, *28*, 1869–1875.

(24)   Robertson, C. .; Wilkes, G. . *Polymer* **2000**, *41*, 9191–9204.

(25)   McCrum, N.; Read, B.; Williams, G. *Anelastic and dielectric effects in polymeric solids*; Dover Publications: New York, 1991.

(26)   Chung, C. I.; Sauer, J. A. *J. Polym. Sci. Part A-2 Polym. Phys.* **1971**, *9*, 1097–1115.

(27)   Gross, S.; Camozzo, D.; Di Noto, V.; Armelao, L.; Tondello, E. *Eur. Polym. J.* **2007**, *43*, 673–696.
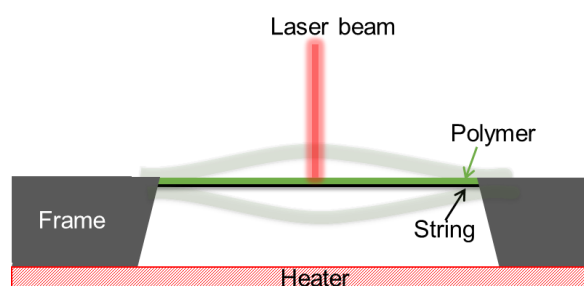
5

Paper IV

Microcantilever Sensors for Fast Analysis of Enzymatic Degradation of Poly (D, L-lactide)

Microcantilever Sensors for Fast Analysis of Enzymatic Degradation of Poly (D, L-lactide)

Sanjukta Bose, Stephan S. Keller, Anja Boisen and Kristoffer Almdal*

Department of Micro- and Nanotechnology, Technical University of Denmark, DK-2800 Kongens

Lyngby, Denmark

ABSTRACT

In this work we have performed a detailed analysis on enzymatic degradation of amorphous poly (D, L-lactide) (PDLLA) by measuring the resonance frequencies of the polymer coated microcantilevers before and after degradation. The miniaturized cantilever system provides a fast analysis of the biodegradation rate of PDLLA with a minute amount of sample and without the need of thermal and chemical acceleration. The degradation rate of the polymer has been estimated by multilayer cantilever theory and model simulation. A bulk degradation rate of 0.24 µg mm^{-2} hour^{-1} is estimated which agrees well with values reported in literature. The role of enzyme concentrations, pre-hydration in buffer, surface morphologies of PDLLA films and adsorption time of enzymes on the rate of degradation has been investigated. An increase in degradation rate is observed with an increase in enzyme concentration and after pre-hydration in buffer. A polymer film with a non-uniform surface degrades faster than the uniform one due to the preference of enzyme attack at film defects. A threshold time of around 3 hours is estimated for irreversible enzyme adsorption on the polymer surface after which degradation can proceed even in buffer solution in the absence of enzyme.

INTRODUCTION

In recent years a lot of research has focused on polymers obtained from natural resources or having capability to degrade in natural environment and physiological conditions[1]. A number of polymers such as poly(lactide) (PLA), poly(glycolic acid) (PGA), poly(lactide-co-glycolides) (PLGA), polyhydroxyalkanoates (PHAs), poly(caprolactone) (PCL), and poly(butylene succinate) (PBS) have come up as biocompatible and biodegradable candidates with wide spread applications in the biomedical field[2,3]. Among these biodegradable polymers PLA has gained a lot of importance due to the efficient production of its raw material, lactic acid, from sugars and starchy materials[4,5]. PLA has been used in various applications. For example, coatings on stents induce biocompatibility and eliminate immune response[6,7]. In controlled drug delivery, the therapeutic agent is incorporated into biodegradable polymeric carriers and as the polymer degrades the drug is released continuously. Therefore, the drug release kinetics can be tailored precisely by knowing the degradation profile of the polymer used[8]. Furthermore, biodegradable polymer implants and scaffolds for tissue engineering provide long term biocompatibility and eliminate the need for surgical removal[9,10]. This underlines the need for a thorough analysis of the degradation behavior of biodegradable polymers used in clinical applications.

Hydrolytic degradation plays a major role in all these applications. Hydrolytic degradation of the three stereo forms of PLA: poly(L-lactide) (PLLA), poly(D-lactide) (PDLLA), and poly(DL-lactide) (PDLLA) has been studied and reported extensively over the past decades[4,5,11–16]. These PLAs are members of the family of aliphatic polyesters and their ester groups are hydrolytically degraded in the presence of water according to the following reaction[10]:

$$-COO- + H_2O \rightarrow -COOH + OH- \qquad (1)$$

3
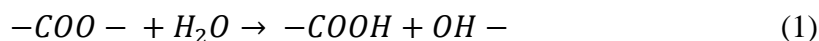
Hydrolysis reactions may be catalyzed by acids, bases, salts, or enzymes[10,15,17–20]. Williams first reported that hydrolysis of PLLA is catalyzed by proteinase K from *Tritirachium album*[21]. Later on, Ashley and McGinity confirmed the enzymatic degradation of PDLLA by proteinase K[22]. Thereafter enzymatic degradation of both the amorphous and the semi-crystalline form of PLA has been studied extensively[7,17]. PDLLA has been frequently used as drug delivery film for implants and temporary scaffold for tissue engineering[10]. Degradation of PLA with proteinase K occurs typically via four steps[23]: (1) diffusion of proteinase K from the bulk solution to the PLA surface, (2) adsorption of the enzyme on the substrate, (3) catalysis of the hydrolysis reaction i.e. the cleavage of the ester bond of PLA, and (4) diffusion of the soluble lactic acid as degradation product from the PLA substrate to the solution. Most of the studies have used conventional methods like measuring weight loss by gravimetry, size-exclusion chromatography (SEC), differential scanning calorimetry (DSC) and X-ray diffraction (XRD) for measuring degradation of PLA. In general degradation studies require a long time[24–26] ranging from several hours to a few months and are often performed at harsh conditions of high/low pH and elevated temperatures to accelerate the experiments[27]. As biodegradable polymer films are used in many emerging biomedical applications[10,19] there is a growing need for a fast analysis of degradation behavior of polymer films at the microscopic level. In the last decade, atomic force microscopy (AFM)[28], surface plasmon resonance (SPR)[29] and quartz crystal microbalance (QCM)[7] have shown new approaches to detect biodegradation of PLA in the micro scale. Microcantilevers have already been demonstrated to be highly sensitive sensors for mechanical and thermal characterization of polymers [30]. Keller *et al.* first showed the potential of using a cantilever based sensor as a tool to study PLLA degradation by proteinase K[31]. Both QCM and the micro cantilevers use the change in resonance frequency as an indicator of the degradation of a polymer film deposited on their surfaces. However, QCM measurements on polymers are typically limited to the thin film regime[7,32,33] (thickness less than

1μm) and characteristics exhibited by thin polymer films often strongly differ from bulk material properties[10,34]. Furthermore, QCM analysis shows some limitations for inhomogeneous polymer layers[35]. Compared to that micro cantilevers are capable of characterizing polymer films with thicknesses of several microns and varied surface morphologies thus allowing probing macroscopic properties on a microscopic platform.

In this study we have used micrometer sized cantilevers as to perform a detailed analysis of enzymatic degradation of thin biopolymer coatings by measuring the resonance frequency of the cantilevers before and after degradation. The miniaturized sensor system is highly sensitive towards biodegradation of minute amounts of polymer, resulting in a fast analysis of the degradation behavior without the need of thermal and chemical acceleration. Amorphous PDLLA is spray coated to form films on one side of the cantilevers which are then immersed for degradation in proteinase K in Tris-HCl buffer solution. The change in resonance frequency measured by a Laser Doppler vibrometer and the optical microscope images taken at regular time intervals reveal how the degradation of PDLLA proceeds in different conditions. The influence of varied enzyme concentrations, pre- hydration and of the time allowed for surface adsorption of enzyme on the enzymatic degradation of PDLLA is studied. By changing the spray coating parameters[36] both uniform and non-uniform PDLLA films are deposited on the silicon cantilevers and the biodegradation of films with different surface morphologies is investigated. Image analysis of the optical microscope images is conducted to monitor the dimensions of the PDLLA coating during degradation. Iterative finite element method (FEM) analysis is then carried out on a simulated cantilever model. Here, the resonance frequencies after degradation were used to determine the thickness of the polymer film, which allowed the calculation of the degradation rate.

EXPERIMENTAL

Materials

PDLLA (M_w 16,000g/mol), Trizma base, Trizma HCl and dichloromethane (b. p. 40°C, ρ 1.33 g/ml at 20°C) were purchased from Sigma Aldrich. Proteinase K was obtained from Roche Diagnosis GmbH, Germany and used as received. Arrays of 8 silicon cantilevers on one chip (Octo500D), each with length L=500±4 μm, width w=90±2 μm and thickness t=5±0.3 μm were purchased from Micromotive GmbH (Mainz, Germany).

Methods

Spray Coating

0.5 wt% PDLLA solution in dichloromethane was used for spray coating in an Exacta Coat Ultrasonic Spraying System (Sonotek, USA) equipped with an AccuMist nozzle operated at a frequency of 120 kHz with a generator power of 1.3 W. The cantilever arrays were mounted onto a chip holder to ensure no movement of the cantilever chip during spraying. Spray coating of PDLLA was only done on the top surface of the cantilevers. The spray coating parameters were optimized to prepare uniform and non-uniform coating on the cantilever surface[36]. For preparing uniform film, the nozzle-substrate distance was 15 mm with 10 spray-passes while for non-uniform film the nozzle-substrate distance was 45 mm with 20 spray-passes. Speed of spray of 10 mm/s, substrate temperature of 20 °C, infusion rate of PDLLA solution 0.1 ml/min and compressed nitrogen at 0.03 bar were maintained for both film types. The initial film thickness was in between 3-5 μm.

Enzymatic degradation

For degradation studies, each chip was placed in a petridish filled with 5 ml of 0.05 M Tris-HCl buffer solution (pH 8.6 at 23°C) containing various concentrations of proteinase K at 37°C. Resonance frequency measurement and optical microscope imaging were performed at intervals of 3 hours. For this, the chips were removed from the media, washed thoroughly with Milli-Q water to

remove residues of soluble degraded products, enzymes, salts and other impurities and dried in vacuum. After characterization the chips were placed in fresh enzyme solution to restore the original condition of degradation. Alternatively, measurements were also conducted with 24 hours immersion of the cantilever chips in the degradation media. An enzyme activity assay was performed with Chromozym PL (Roche Diagonistics GmbH, Germany) to confirm no alteration of enzyme activity of proteinase K in the experimental time frame.

Measurement of resonance frequency

The resonance frequency (f) of the fundamental mode of a cantilever depends on the effective mass m_{eff} and the effective stiffness k_{eff}[31,37] :

$$f = \frac{1}{2\pi}\sqrt{\frac{k_{eff}}{m_{eff}}} \qquad (2)$$

From (2), it is clear that the resonance frequency of the cantilever changes when a polymer layer is applied due to the change in the k_{eff}/m_{eff} ratio. In a similar way, removal of the PDLLA coating due to degradation results in a shift of f towards the reference value measured for the cantilevers before coating. For experiments performed in vacuum and assuming small cantilever deflections, the resonance frequency of a multi-layered cantilever can be approximated by[31,37]

$$f = \frac{1}{2\pi}\frac{\lambda^2}{L^2}\sqrt{\frac{\Sigma_i E_i I_i}{w \Sigma_i \rho_i t_i}} \qquad (3)$$

where, L and w are the length and width, and E_i, I_i, ρ_i and t_i the Young's modulus, the area moment of inertia, the density and the thickness of the i'th layer of the cantilever. For the first flexural mode λ=1.8751.

The resonance frequency of the first mode of the cantilevers was measured with a Laser Doppler Vibrometer (MSA-500, Polytec GmbH, Germany). The cantilever chips were placed on a piezoresistively actuated stage mounted in high vacuum at a pressure below 3×10^{-5} mbar. The measured initial resonance frequencies of the blank cantilevers were 30±5 kHz. The large deviation

was due to dimensional variations of the cantilevers. Therefore in all the experiments, each cantilever was characterized individually before and after coating with PDLLA to obtain the reference resonance frequencies of blank (f_b) and coated (f_c) devices respectively. For comparison of the initial shift in resonance frequency due to spray coating of polymer on the cantilevers and to accommodate for their dimensional variations, the relative resonance frequency shift (δ_0) was calculated by the following equation:

$$\delta_0 = \frac{f_b - f_c}{f_b} \times 100 \ [\%] \qquad (3)$$

δ_0 is used as relative frequency shift at degradation time, $t_{deg} = 0$ hour in all the plots presented in this paper. Similarly, after immersion in the degradation media, at specific time intervals, the resonance frequency f_t was measured. For comparison of the shift in resonance frequency at different degradation conditions with respect to f_b, the relative resonance frequency shift (δ_t) is reported by the following equations:

$$\delta_t = \frac{f_b - f_t}{f_b} \times 100 \ [\%] \qquad (4)$$

The subscript t stands for the time of degradation i.e., $t_{deg} = 3, 6, 9$ hours etc. All the frequency measurements were repeated three times and the average of the data is reported.

Image Analysis

The surface texture of the coated cantilevers before and after degradation was observed with an optical microscope (OM) (Zeiss, Germany) in bright field mode. Image J software was then used on the OM images to measure the dimensions of the cantilever and the change in lengths and widths of the PDLLA coatings during degradation.

FEM simulation

The thickness of the PDLLA coatings on the micro cantilevers was calculated with an iterative

finite element method using COMSOL 4.4[38]. For the FEM simulation, mass densities and Young's modulus of silicon and PDLLA are considered to be 2329 Kg/m^3, 1240 Kg/m^3 (taken from manufacturer's data sheet) and 170 GPa, 3.2 GPa[10] respectively. It was assumed that both the modulus and the densities remain constant throughout the experiment. The eigenfrequency of a silicon cantilever with a polymer layer on the top surface was simulated for a certain estimated thickness of the polymer film. The obtained eigenfrequency was then compared to the measured resonance frequency and the thickness of the polymer coating was iteratively adjusted until the difference of the computed and measured frequency values were below 0.1% compared to the measured frequency. The change in width and thickness was then used to determine the degradation rates of PDLLA in proteinase K for a particular degradation condition.

RESULTS AND DISCUSSION

The resonance frequencies of a coated cantilever after immersion in degradation media for various time are shown in Figure 1 and compared to the one of the initially blank cantilever.
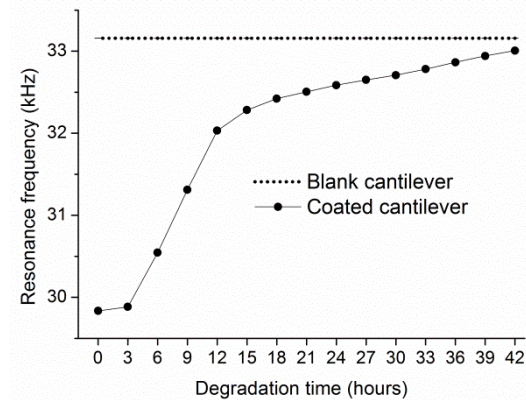

Figure 1. Resonance frequencies of an initially blank cantilever and a PDLLA coated cantilever during degradation in 50µg/ml proteinase K at 37°C.

When the cantilever is coated with polymer the resonance frequency drops from 33.3 kHz to 30.1 kHz (Figure 1) due to the addition of mass on one side of the cantilever (equation (2)). When

this cantilever is immersed in an enzyme solution of 50μg/ml proteinase K at 37°C, the amount of polymer on the cantilever surface decreases due to the onset of degradation and the frequency starts to increase until it approaches the initial resonance frequency of the blank cantilever.

Concentration of enzyme solution

The effect of varying concentrations of proteinase K on the degradation behavior of PDLLA is shown in Figure 2.
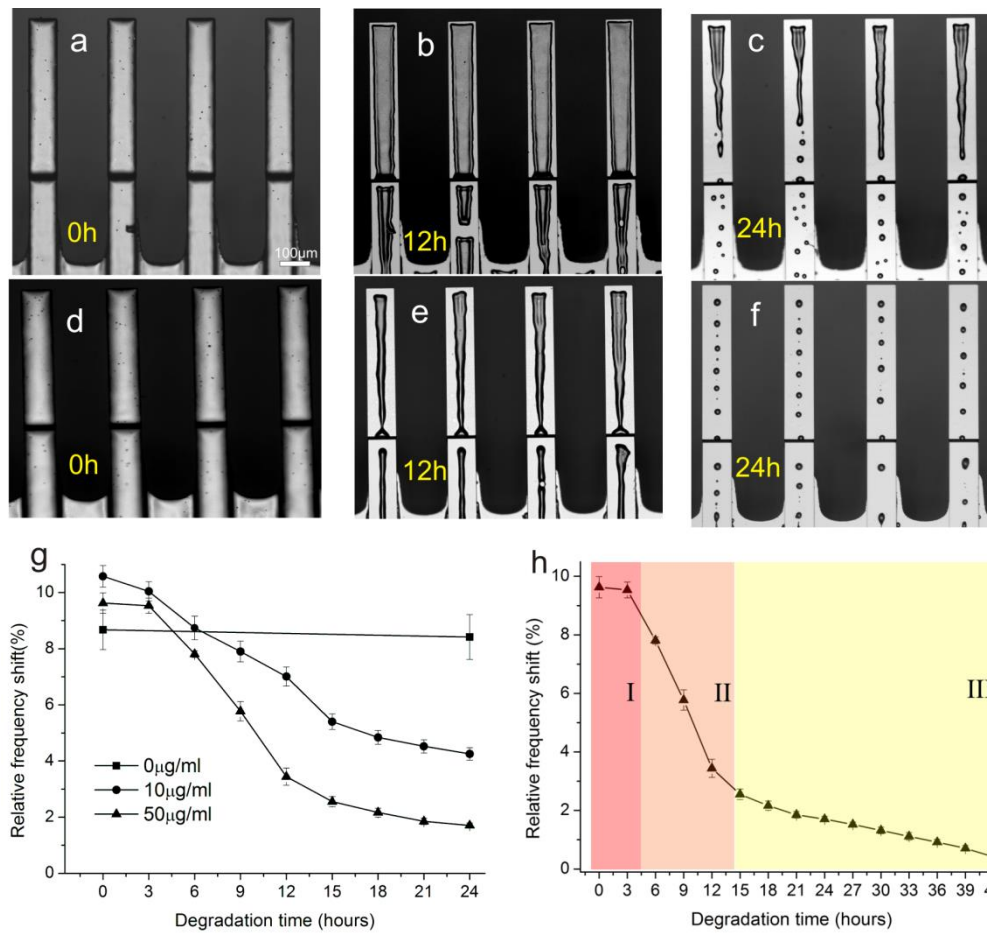
Figure 2. OM images of coated cantilevers (a-c) in 10 μg/ml proteinase K and (d-f) in 50 μg/ml proteinase K at 37 °C. Plots are shown for (g) relative frequency shift (δ_t) of coated cantilevers at different enzyme concentrations and (h) to illustrate the different regimes of degradation at 50 μg/ml enzyme concentration The scale bar shown in (a) is valid for all the OM images.

Figure 2 shows OM images of the PDLLA coated cantilevers at specified time intervals of degradation. Comparing Figure 2 (a-c) with Figure 2 (d-f) it is clearly observed that more PDLLA in removed from the cantilever surface in the same time interval when increasing the enzyme concentration from 10 µg/ml to 50 µg/ml. This is also reflected in the faster change in relative resonance frequency shift for the cantilevers (Figure 2g) exposed to 50 µg/ml of proteinase K compared to the ones exposed to 10 µg/ml. In the control experiment, without enzyme (0 µg/ml) in the degradation media, there is no change in frequency. The higher the concentration of enzyme in the degradation media the higher is the amount of enzyme available to catalyze the ester hydrolysis step and hence a faster change in frequency is observed[7,32]. Figure 2h shows that three main regimes can be identified for the measurement with 50 µg/ml of proteinase K at 37 °C.

For the first few hours of the experiment (regime I) the change of resonance frequency is very slow. It is then followed by an almost linear and relatively fast change of the resonance frequency up to ~12 hours (regime II). Then the change in frequency again slows down (regime III) and continues until the end of the measurement time frame. In regime I, the polymer coated chip is exposed to degradation media for the very first time. The polymer surface is hydrophobic and it is possible that the enzyme adsorption on the PDLLA surface before the initiation of the degradation reaction is hindered resulting in a very slow change in frequency. In regime II, a rapid decrease in the relative frequency shift indicates that the degradation is propagating very fast removing most of the polymer coating. In regime III, the polymer coating becomes discontinuous and eventually breaks into small islands of polymer (Figure 2c and 2f). Thereby the total coated area available for enzyme attack is reduced which in turn decreases the rate of relative shift in resonance frequency.

Regime I: Pre-hydration effects

To investigate the initial delay in regime I, coated cantilevers are immersed in Tris-HCl buffer solution for 3 hours (defined as prehydrated henceforth) before immersion in 50 µg/ml proteinase K solution.

Figure 3 shows a comparison between the relative shift in resonance frequency observed for PDLLA with and without pre-hydration in buffer solution before enzymatic degradation.
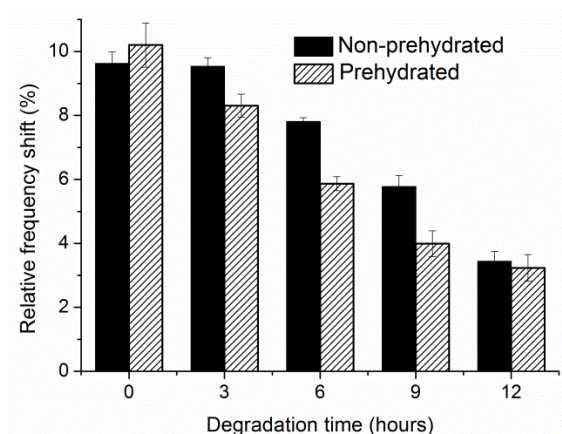
Figure 3. Relative frequency shift of prehydrated and non-prehydrated cantilevers when degraded in 50 µg/ml proteinase K at 37 °C.

From Figure 3, it is clearly observed that the cantilevers subjected to pre-hydaration are showing a faster decrease in relative frequency shift (hatched columns) than the devices that are directly immersed in enzyme solution (solid columns). The result is more prominent when the first data points after 3 hours are compared in Figure 3. It can be seen that there is almost no change in relative frequency shift for non-prehydrated cantilevers while there is a considerable decrease for the prehydrated ones.

Surface hydrophilicity is considered to be one of the important factors controlling the hydrolysability of biodegradable polymers. Surface modifications like alkaline treatment, coating, and surface grafting have been used as effective methods to control the biodegradability of polymers without affecting the bulk physical properties[10,39,40]. For alkaline treatment of PLLA prior

to enzymatic degradation, mostly NaOH solution (pH 12) has been used and it is reported that the cleavage of ester groups increases the number of hydrophilic hydroxyl and carboxyl groups on the surface thus increasing the surface hydrophilicity. In this study, most likely the pre-hydration for 3 hours in Tris-HCl buffer solution (pH 8.6) has modified the surface hydrophilicity of the PDLLA coating on the cantilevers which facilitates the enzyme attack when exposed to proteinase K solution. This might explain the initial delay in regime I (Figure 2h) when the cantilevers were directly subjected to enzymatic solution without pre-hydration.

Regime II: Estimation of degradation rate

The steep linear decrease in resonance frequency shift in regime II which is used to estimate the degradation rate of PDLLA in 50 µg/ml proteinase K at 37 °C. From OM images, the length and width of the coating is measured during degradation and FEM simulation is performed to estimate the thickness of the polymer layer as described earlier. The change in the measured width and calculated thickness of the PDLLA layer is shown in Figure 4.
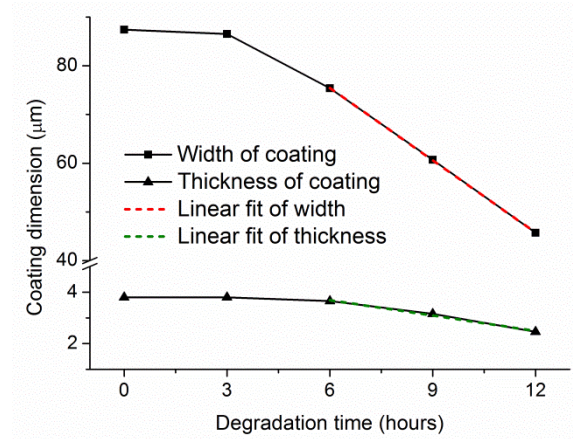
Figure 4. Change of dimension of PDLLA coatings on cantilevers during degradation with 50 µg/ml proteinase K at 37 °C.

From Figure 4, it is seen that both the width and thickness of the PDLLA coating are changing simultaneously but at different rates. The dimensional change is almost negligible in regime I. In regime III, the continuity of the film is lost and simulation was omitted. The degradation rates are calculated from the slope of the curve showing the change in width and thickness in regime II .

Two different rates are observed in this study: i) A lateral degradation rate corresponding to the change in width of the film which is also visible from the OM images in Figure 2 and ii) a vertical degradation rate corresponding to the change in thickness of the film. The lateral degradation rate is found to be ~2.5µm/hour whereas the vertical degradation rate is ~ 0.2µm/hour as calculated from the slope of the thickness plot against degradation time. The vertical degradation of the PDLLA coating is considered equal to the bulk degradation of the polymer. When calculated in terms of mass loss, the bulk degradation rate is $0.24\,\mu g\,mm^{-2}\,hour^{-1}$. This agrees well with a rate of $0.28\,\mu g\,mm^{-2}\,hour^{-1}$ for proteinase K degradation of PLA with 50% L-lactyl content i.e., PDLLA reported by Reeve $et\ al$[41]. for their specimen of dimension $2.5cm\times 1cm\times 0.06mm$ and is also in range with rates reported by others[42].

Studies have shown that in enzymatic degradation, the enzymes prefer to attack at the structural defects present on the substrate, i.e. at the edges, or in cracks and holes of the polymer films or lipid monolayers[43–46]. In our case, the enzymes seem to start fast degradation at the interface between the silicon cantilevers and the PDLLA film at the edge of the cantilevers. For small features such as in stents coated with biocompatible polymer, this lateral degradation can play a major role too. The vertical degradation rate of biodegradable polymer film is of great importance in applications in the biomedical field. Drug release kinetics can be tailored knowing the degradation rate of the polymer matrix used in drug delivery systems.

Surface morphology

The observation of high degradation rates at edges and defects indicates that the surface morphology of the PDLLA coating might have a major influence on the degradation rate. Therefore, enzyme degradation of PDLLA coatings with different surface morphologies was investigated. For this purpose, the spray coating parameters were modified to produce both uniform and non-uniform PDLLA coatings on cantilevers. Figure 5 shows the OM images and relative shift in resonance frequency with respect to the blank cantilevers for both types of coatings.
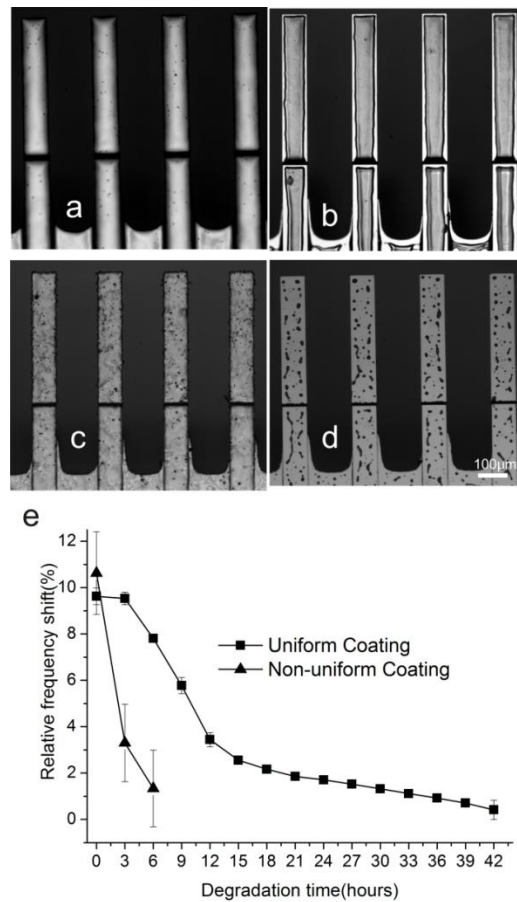
Figure 5. OM images of uniformly coated cantilevers at (a) 0 hr, (b) 6 hrs and non-uniformly coated cantilevers at (c) 0 hr and (d) 6 hrs and the relative frequency shift (e) upon degraded in 50 µg/ml proteinase K at 37 °C. The scale bar shown in (d) is valid for all the OM images.

It is seen from Figure 5 that after 6 hours there is almost a complete removal of PDLLA from non-uniformly coated cantilevers (Figure 5d) when subjected to degradation in 50 µg/ml proteinase K. Compared to that, the uniformly coated cantilevers (Figure 5b) are still mostly covered by PDLLA exposed to the same enzyme concentration for the same time. This observation is also confirmed by the almost 6x faster shift in the resonance frequency for the non-uniformly coated devices compared to the ones coated uniformly in Figure 5e.

This confirms that enzymes show preferential attack on edges or defects in the polymer films as discussed earlier. For the non-uniform coating, the surface of the PDLLA film (Figure 5c) is favorable for enzyme attack compared to the very smooth and intact film on the uniformly coated cantilevers (Figure 5a). In case of the uniformly coated cantilevers, degradation mainly propagates at the interface between the PDLLA film and the silicon cantilever surface at the edges of the cantilevers which acts as a defect at which the enzymes show higher ingression.

Influence of enzyme adsorption time

All the experiments discussed so far are conducted at the same time intervals and identical degradation conditions. Here, a new set of experiments is conducted varying the conditions for enzymatic degradation to study the influence of enzyme adsorption time. Degradation experiments are performed to find out the effect of different experimental conditions on the degradation during 24 hours as shown by the OM images and the relative frequency shift in Figure 6. Condition '24h E' (Figure 6) is when a PDLLA coated cantilever chip is immersed in enzyme solution and incubated continuously for 24 hours. Condition '3h E+21h E' and condition '1h E+23h E' (Figure 6) are coated cantilever chips immersed in enzyme solution for 3 hours and 1 hour respectively and then transferred without washing to buffer solution for 21 hours and 23 hours respectively to see the effect of the time available for surface adsorption of enzyme on the

degradation of the PDLLA film. Condition '24h B' (Figure 6) is a control experiment where a coated chip is immersed in buffer solution for 24 hours to see the effect of eventual hydrolytic degradation only.
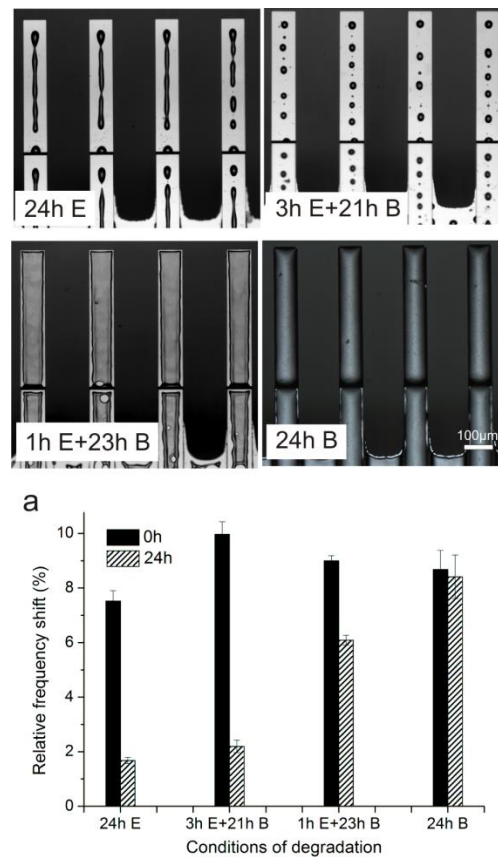
Figure 6. OM images and (a) relative frequency shift of coated cantilevers at different degradation conditions. The scale bar shown in 24h B is valid for all the OM images.

From Figure 6a comparing the shift in relative frequency, conditions '24h E' and '3h E+21h E' have reached regime III (Figure 2h). Condition '1h E+23h E' is still in regime II and condition '24h B' shows an almost negligible frequency shift in 24 hours. OM images of different conditions in Figure 6 showing the PDLLA left on the cantilever surface at the end of 24 hours confirm the frequency shift findings.

Yamashita *et al*. reported the irreversible adsorption of proteinase K on the surface of PLLA films and observed that when the enzyme solution was replaced with buffer solution the PLLA film was

hydrolyzed completely without a decrease in the degradation rate[7]. Li *et al.* confirmed the observation of adsorption of enzyme on PLLA but observed no enzyme attachment on PDLA[47]. In our study, when the PDLLA coated cantilevers are exposed to enzyme solution for 3 hours followed by immersion in only buffer solution for 21 hours (Condition '3h E+21h B', Figure 6) , degradation reaction continues uninterrupted as reported by others. But for condition '1h E+23h B' when the PDLLA coated cantilevers are exposed to enzyme solution for only 1 hour followed by immersion in only buffer solution for 23 hours (Figure 6) , degradation reaction continues for few hours but ultimately stopped unlike the previous. This indicates that in the initial phase, the enzymes require some time to adsorb on the entire PDLLA layer on the cantilever surface. 1 hour as in case of condition '1h E+23h B' is too short and thus the enzymatic degradation stops after sometime. In 3 hours the enzymes have suffciient time to attach well to the PDLLA surface and continue to degrade the biopolymer when transferred to buffer solution. Condition '24h B' shows negligible effect of buffer solution on degradation of the polymer (Figure 6) proving the catalytic behavior of proteinase K in enzymatic degradation.

CONCLUSION

Enzymatic degradation of amorphous PDLLA has been investigated using microcantilevers. These devices are an excellent tool to do a detailed analysis of the degradation of thin PDLLA coatings by measuring the resonance frequency of the cantilever before and after degradation. The miniaturized cantilever system is highly sensitive towards biodegradation of minute amounts of polymer, resulting in a fast analysis of the degradation behavior without the need of thermal and chemical acceleration. Degradation rate of the polymer has been estimated by multilayer cantilever theory and finite element simulation where two different rates were observed for lateral and vertical degradation. Bulk degradation rate of 0.24 μg mm^{-2} hour^{-1} was estimated which agrees well with

other reported values where larger specimen size and longer degradation time were required. We have demonstrated that the enzyme concentration, pre-hydration in buffer, surface morphologies of PDLLA films and adsorption of enzymes influence the rate of enzymatic degradation. An increase in degradation rate is observed with an increase in enzyme concentration. It has also been concluded that pre-hydration in buffer favours the overall enzymatic degradation process. A polymer film with a non-uniform surface degrades faster than the uniform one due to the preference of enzyme attack at film defects. This suggest that surface uniformity is important in biomedical applications. It was also concluded that a threshold time of around 3 hours is required for enzyme adsorption on the polymer surface after which degradation can proceed even in buffer solution. Our study helps to improve the understanding of the degradation behavior of polymer coatings. The approach can be applied to other biopolymers in different degradation conditions for a fast estimation of degradation rate.

AUTHOR INFORMATION

Corresponding Author

*Email: Kristoffer.Almdal@nanotech.dtu.dk

Author Contributions

The manuscript was written through contributions of all authors. All authors have given approval to the final version of the manuscript.

Notes

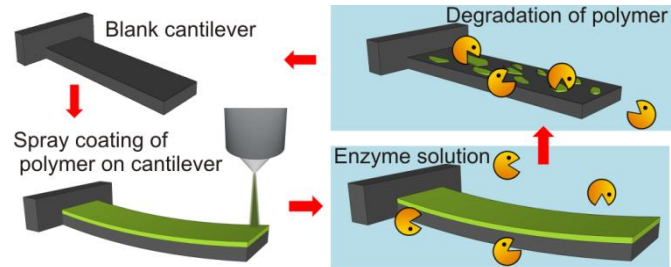The authors declare no competing financial interest

REFERENCE

(1)   Henton, D.; Gruber, P.; Lunt, J.; Randall, J. In *Natural Fibres, Biopolymers, and Biocomposites*; 2005; pp. 527–578.

(2)   Ulery, B. D.; Nair, L. S.; Laurencin, C. T. *J. Polym. Sci. B. Polym. Phys.* **2011**, *49*, 832–864.

(3)   Hayashi, T. *Prog. Polym. Sci.* **1994**, *19*, 663–702.

(4)   Tokiwa, Y.; Calabia, B. P. *Appl. Microbiol. Biotechnol.* **2006**, *72*, 244–51.

(5)   Datta, R.; Henry, M. *J. Chem. Technol. Biotechnol.* **2006**, *81*, 1119–1129.

(6)   Dan, Scott Gilead, D., Ed.; Chapman & Hall: London, 1995.

(7)   Yamashita, K.; Kikkawa, Y.; Kurokawa, K.; Doi, Y. *Biomacromolecules* **2005**, *6*, 850–857.

(8)   Engineer, C.; Parikh, J.; Raval, A. *Trends Biomater. Artif. Organs* **2011**, *25*, 79–85.

(9)   Chen, Q.-Z.; Harding, S. E.; Ali, N. N.; Lyon, A. R.; Boccaccini, A. R. *Mater. Sci. Eng. R Reports* **2008**, *59*, 1–37.

(10)   Auras, R.; Lim, L.; Selke, S.; Tsuji, H. *Poly (lactic acid): synthesis, structures, properties, processing, and applications*; Rafael A. Auras, Loong-Tak Lim, Susan E. M. Selke, H. T., Ed.; John Wiley & Sons, Inc.: New Jersey, USA, 2011.

(11)   Kulkarni, R. K.; Moore, E. G.; Hegyeli, a F.; Leonard, F. *J. Biomed. Mater. Res.* **1971**, *5*, 169–181.

(12)   Kulkarni, A.; Reiche, J.; Lendlein, A. *Surf. Interface Anal.* **2007**, *39*, 740–746.

(13)   Lyu, S.; Untereker, D. *Int. J. Mol. Sci.* **2009**, *10*, 4033–4065.

(14)   Tsuji, H.; Mizuno, A.; Ikada, Y. *J. Appl. Polym. Sci.* **2000**, *77*, 1452–1464.

(15)   Tsuji, H.; Ogiwara, M.; Saha, S. K.; Sakaki, T. *Biomacromolecules* **2006**, *7*, 380–387.

(16)   Auras, R.; Harte, B.; Selke, S. *Macromol. Biosci.* **2004**, *4*, 835–64.

(17)   Li, S.; Tenon, M.; Garreau, H.; Braud, C.; Vert, M. *Polym. Degrad. Stab.* **2000**, *67*, 85–90.

(18)   Vasanthan, N.; Ly, O. *Polym. Degrad. Stab.* **2009**, *94*, 1364–1372.

(19)   Azevedo, H. S.; Reis, R. L. In *Biodegradable Systems in Tissue Engineering and Regenerative Medicine*; Reis, R. L.; Román, J. S., Eds.; CRC Press: Florida, USA, 2005; pp. 177–202.

(20)   Kikkawa, Y.; Abe, H.; Iwata, T.; Inoue, Y.; Doi, Y. *Biomacromolecules* **2002**, *3*, 350–356.

(21)   Williams, D. F. *J. Mater. Sci.* **1982**, *17*, 1233–1246.

(22)   Ashley, SL and McGinity, J. *Congr Int Technol Pharm* **1989**, *5*, 195–204.

(23)   Rahmouni, M.; Chouinard, F.; Nekka, F.; Lenaerts, V.; Leroux, J. C. *Eur. J. Pharm. Biopharm.* **2001**, *51*, 191–198.

(24)   Södergård, A.; Selin, J.-F.; Näsman, J. H. *Polym. Degrad. Stab.* **1996**, *51*, 351–359.

(25)   Tsuji, H.; Ikada, Y. *J. Polym. Sci. Part A Polym. Chem.* **1998**, *36*, 59–66.

(26)   Cam, D.; Hyon, S.; Ikada, Y. *Biomaterials* **1995**, *16*, 833–843.

(27)   Xu, L.; Crawford, K.; Gorman, C. B. *Macromolecules* **2011**, *44*, 4777–4782.

(28)   Kikkawa, Y.; Hirota, T.; Numata, K.; Tsuge, T.; Abe, H.; Iwata, T.; Doi, Y. *Macromol. Biosci.* **2004**, *4*, 276–285.

(29)   Sumner, C.; Krause, S.; Sabot, A.; Turner, K.; McNeil, C. J. *Biosens. Bioelectron.* **2001**, *16*, 709–714.

(30)   Boisen, A.; Dohn, S.; Keller, S. S.; Schmid, S.; Tenje, M. *Reports Prog. Phys.* **2011**, *74*, 036101.

(31)   Keller, S. S.; Gammelgaard, L.; Jensen, M. P.; Schmid, S.; Davis, Z. J.; Boisen, a. *2011 IEEE 24th Int. Conf. Micro Electro Mech. Syst.* **2011**, 457–460.

(32)   Yamashita, K.; Funato, T.; Suzuki, Y.; Teramachi, S.; Doi, Y. *Macromol. Biosci.* **2003**, *3*, 694–702.

(33)   Wolff, O.; Seydel, E.; Johannsmann, D. *Faraday Discuss.* **1997**, *107*, 91–104.

(34)   Reiter, G.; Napolitano, S. *J. Polym. Sci. Part B Polym. Phys.* **2010**, *48*, 2544–2547.

(35)   Vogt, B. D.; Soles, C. L.; Lee, H.; Lin, E. K.; Wu, W. *Polymer* **2005**, *46*, 1635–1642.

(36)   Bose, S.; Keller, S. S.; Alstrøm, T. S.; Boisen, A.; Almdal, K. *Langmuir* **2013**, *29*, 6911–6919.
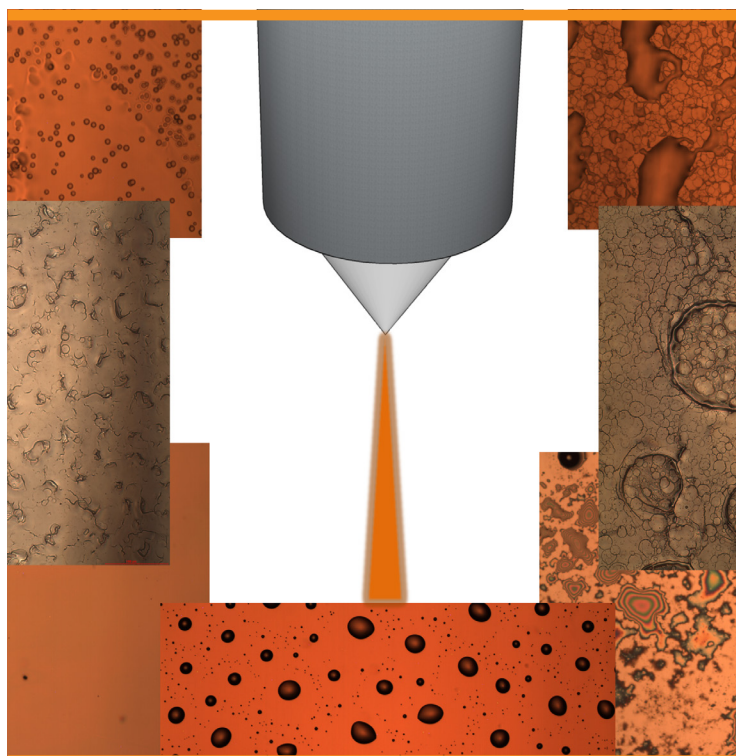
(37)   Sandberg, R.; Svendsen, W.; Mølhave, K.; Boisen, a *J. Micromechanics Microengineering* **2005**, *15*, 1454–1458.

(38)   Schmid, S. *Sci. reports Micro Nanosyst. Vol.6* **2009**, Der Andere Verlag, Zurich, Switzerland.

(39)   Tsuji, H.; Ishida, T.; Fukuda, N. *Polym. Int.* **2003**, *52*, 843–852.

(40)   Tsuji, H.; Nishikawa, M.; Osanai, Y.; Matsumura, S. *Macromol. Rapid Commun.* **2007**, *28*, 1651–1656.

(41)   Reeve, M. S.; McCarthy, S. P.; Downey, M. J.; Gross, R. A. *Macromolecules* **1994**, *27*, 825–831.

(42)   Tsuji, H.; Miyauchi, S. *Biomacromolecules* **2001**, *2*, 597–604.

(43)   Bikiaris, D. N.; Papageorgiou, G. Z.; Achilias, D. S. *Polym. Degrad. Stab.* **2006**, *91*, 31–43.

(44)   Liu, L.; Li, S.; Garreau, H.; Vert, M. *Biomacromolecules* **2000**, *1*, 350–359.

(45)   Balashev, K.; John DiNardo, N.; Callisen, T. H.; Svendsen, A.; Bjørnholm, T. *Biochim. Biophys. Acta* **2007**, *1768*, 90–99.

(46)   Balashev, K.; Jensen, T. R.; Kjaer, K.; Bjørnholm, T. *Biochimie* **2001**, *83*, 387–397.

(47)   Zhao, Z.; Yang, L.; Hua, J.; Wei, J.; Gachet, S.; El Ghzaoui, A.; Li, S. *Macromol. Biosci.* **2008**, *8*, 25–31.

Table of Contents (TOC)

DTU Nanotech
Department of Micro- and Nanotechnology